National Library
of Canada

Acquisitions and
Bibliographic Services Branch

395 Wellington Street
Ottawa, Ontario
K1A 0N4

Bibliothèque nationale
du Canada

Direction des acquisitions et
des services bibliographiques

395, rue Wellington
Ottawa (Ontario)
K1A 0N4

Your file Votre référence

Our file Notre référence

NOTICE

The quality of this microform is heavily dependent upon the quality of the original thesis submitted for microfilming. Every effort has been made to ensure the highest quality of reproduction possible.

If pages are missing, contact the university which granted the degree.

Some pages may have indistinct print especially if the original pages were typed with a poor typewriter ribbon or if the university sent us an inferior photocopy.

AVIS

La qualité de cette microforme dépend grandement de la qualité de la thèse soumise au microfilmage. Nous avons tout fait pour assurer une qualité supérieure de reproduction.

S'il manque des pages, veuillez communiquer avec l'université qui a conféré le grade.

La qualité d'impression de certaines pages peut laisser à désirer, surtout si les pages originales ont été dactylographiées à l'aide d'un ruban usé ou si l'université nous a fait parvenir une photocopie de qualité inférieure.

Canada

NUMERICAL EVALUATION OF WIND EFFECTS ON BUILDINGS

ZHOU, Yongsheng

A Thesis

in

The Centre

for

Building Studies

Presented in Partial Fulfilment of the Requirements

for the Degree of Doctor of Philosophy at

Concordia University

Montreal, Quebec, Canada

FEBRUARY, 1995

ABSTRACT

Numerical Evaluation of Wind Effects on Buildings

Yongsheng Zhou, Ph.D.

Concordia University, 1995

The wind environment around buildings and the wind pressures on building surfaces are studied by scale-model experiments in wind tunnels and confirmed by full scale measurements. Such experiments are often expensive and time consuming. Computational wind engineering as a new branch of computational fluid dynamics has been developed recently to evaluate the interaction between wind and buildings numerically. In the current study, a systematic examination of wind effects on buildings and wind flow conditions around buildings has been carried out numerically. Contrary to the usual numerical evaluations which were only performed on rectangular buildings, the current study evaluates the wind effects on buildings of different shapes such as L-shapes and Z-shapes. The steady state Reynolds averaged Navier-Stokes equations and the k-ε turbulence model have been adopted for the numerical studies. These equations have been solved with the SIMPLE method.

Some researchers declared that the discrepancies between the computed results with the k-ε model method and the experimental data on the flat roof of a rectangular building are caused by the coarse grid used. To check this, a systematic evaluation of the

k-ε model method in predicting the wind pressure on flat roofs has been attempted by using grids of various densities. Computations were made for a low building and a taller building. Both the advantages and limitations of this most widely used method in computing the wind pressure on flat roofs under normal and oblique wind conditions have been discussed. This study revealed that these discrepancies can be attributed not only to the coarse grid arrangement but also to the k-ε model itself.

To keep the advantages of k-ε model in representing the fully turbulent flow in the external region far from solid walls and to avoid its shortcomings for the near wall flows, a two-layer methodology combining the k-ε model in external flow region with either a one-equation model or a modified k-ε model in the near wall area has been adopted in this study to predict the wind conditions around a cubic building. The two-layer method based on the modified k-ε model has not been found effective. The two-layer method based on a one-equation model, however, has been proved very effective in predicting the separation above the roof surface and near the side walls of a cubic building which was not possible with the usual k-ε model method; as a result, the prediction of the wind pressure on the roof and side walls has also been apparently improved.

ACKNOWLEDGEMENT

My sincere thanks are given to my supervisor, Dr. **T. Stathopoulos**, for his consistent support and encouragement in the process of this work, for many helpful suggestions and stimulating discussions and also for his patient guidance when I was writing this thesis.

I would also like to give my sincere thanks to all the members of my thesis committee who have given me many constructive suggestions which have already been reflected in this thesis.

Sincere thanks are due to Dr. Hanqing Wu, Dr. H.D. Luchian and the technician Mr. Hans Obermeir for their very essential assistance in my wind tunnel experiments. Appreciation is also due to Mr. Sylvain Belanger for his assistance in dealing with issues related to the computing facilities.

Finally, I dedicate this thesis to my wife Yazhen Hu for her love, support, encouragement and understanding during the course of my degree.

TABLE OF CONTENTS

LIST OF FIGURES

Chapter 9

LIST OF TABLES

NOMENCLATURE

a	coefficient of discretized equations (Chapter 5);
a	half interval between two parallel plates (Chapter 7);
C_D, C_μ, C_μ, C_1, C_2, σ_k, σ_ε	turbulence model coefficients;
d	distance from a gridnode to the wall;
d_e	the distance from the edge of VSL to the solid boundary;
d_o	the grid interval adjacent to a solid boundary;
d_p	the distance between the first grid line and the solid boundary;
d_q	the distance between the second grid line and the solid boundary;
d_s	the distance from a point in VSL to the solid boundary;
e, w, n, s, t, b	subscripts denoting the neighbouring grid points of east, west north, south, top, bottom, half grid interval away from the reference point (Fig. 5.1);
E, W, N, S, T, B	subscripts denoting the neighbouring grid points of east, west north, south, top, bottom, one grid interval away from the reference point (Fig. 5.1);
E, C, C_1	wall function constants;
f_μ, f_1, f_2	damping functions;
H1, H2, H	height of buildings (Fig. 4.2);

k	turbulence kinetic energy;
k_e	turbulence intensity at the edge of VSL;
k_p	turbulence intensity on the first grid line near the solid boundary;
k_s	turbulence intensity in VSL;
L	length scale (Chapter 10);
l_m	mixing length;
L1, L2, L	length of buildings (Fig. 4.2);
p	pressure;
p'	pressure fluctuation;
P	augmented pressure;
$\overline{p}$	time averaged pressure;
P^*	production term in k- and ε-equation;
R_d	turbulence Reynolds number;
S_c, S_p, b	source term (Chapter 5);
t_2-t_1	time scale;
u_i	fluid flow velocity components along x_i direction;
u'_i	velocity fluctuation along x_i direction;
u^*	friction velocity;
U, V, W	velocity components along x, y, z directions (Chapter 5);
U_g	gradient velocity;
U_i	time averaged velocity component along x_i direction;

U^*, V^*, W^*, p^*, k^*, ε^*	guessed variables of U, V, W, p, k, ε (Chapter 5);
W1, W2, W3, W	width of buildings (Fig. 4.2);
x_i, x, y, z	Cartesian coordinate system;
x^*	dimensionless distance from reattachment point (Chapter 6);
Y^+	dimensionless distance;
z_g	gradient height;
z_o	roughness length;
α	power-law exponent;
ε	turbulence energy dissipation;
ε_e	turbulence energy dissipation at the edge of VSL;
ε_p	turbulence energy dissipation on the first grid line from the wall;
ε_s	turbulence dissipation in VSL;
ν	kinematic viscosity of the air;
ν_t	eddy viscosity;
μ	dynamic viscosity of the air;
ρ	density of the air;
δ_{ij}	kronecker delta;
ϕ	general dependent variable in convection equations;
Γ	transportation coefficient;
τ_i	shear stress component at wall along x_i direction;
τ_w	shear stress at wall;

κ	von Karman constant;
η	dimensionless distance;
β	underrelaxation factor.

Chapter 1

INTRODUCTION

Wind effects on buildings create an important class of problems that is embraced by the rapidly developing discipline of wind engineering (Cermak and Arya, 1970, Cermak, 1975 and Cermak, 1976). Wind pressures on building surfaces result in both steady and unsteady loading (Scruton, 1960 and Scruton and Rogers, 1971), while air motion over and around buildings transports heat, mass and momentum. Damage to main structural elements, rupture or dislodgment of cladding, breakage of glass, excessive building motion, movement of air, water and dust through openings and cracks and difficult operation of doors may result from wind pressures during strong winds. Recirculation of polluted effluent from stacks and vents into air-conditioning intakes, transport of automobile exhausts from adjacent streets into building ventilation systems, entrainment of dust and other debris at street level, drifting of snow, buffeting of pedestrians and aerodynamic noise may develop through action of wind movement around a building. A typical cladding failure caused by wind-induced pressures is shown in Fig. 1.1.

Although all of the foregoing wind effects are undesirable, favourable effects also exist in the form of building ventilation and transport of air pollutants away from a building. Design and planning of buildings to minimize adverse wind effects and to take

Figure 1.1 Cladding failure caused by wind-induced pressure, after Cook, 1985.

advantage of favourable conditions require detailed information on the aerodynamics of air flow over bluff bodies. Details of building aerodynamics depend upon both the building geometry and the characteristics of the wind flow around a building.

Conventionally, wind environmental conditions around buildings and wind-induced pressures on buildings are examined either in full-scale tests or in experiments carried out in boundary layer wind tunnels simulating the natural wind characteristics. Full-scale measurements provide the wind effects on real buildings under the natural wind conditions (Simiu and Scanlan, 1978). Due to the long duration and the high cost of the process to obtain data and, most importantly, due to the need to have built the structure or the building before the measurements can be carried out, this method is primarily used to validate the results from the wind tunnel tests or, more recently, from the numerical simulation.

Wind tunnel experiments are widely used to obtain information about the wind effects on buildings. Natural wind conditions are simulated by adopting the turbulent boundary layer type airflow in wind tunnels. Figure 1.2 shows the inside of a typical boundary layer wind tunnel for such purposes. However, the Reynolds numbers in wind tunnel tests based on the scale of small building models are usually much smaller than those for real buildings, and also the boundary effects of the wind tunnel are usually unavoidable.

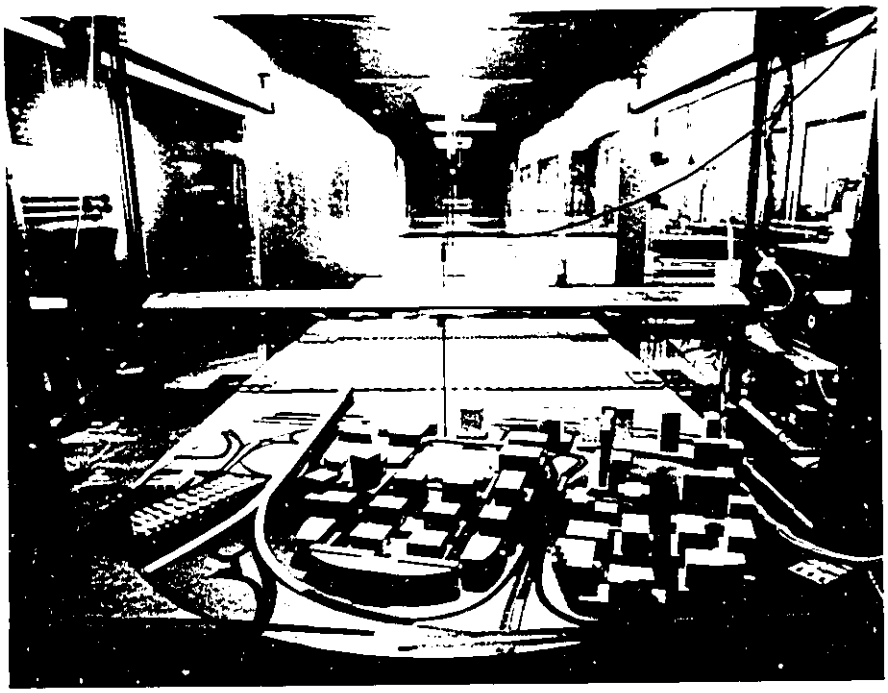

Figure 1.2 The inside-view of a boundary layer wind tunnel (Boundary Layer Wind Tunnel in Centre for Building Studies, Concordia University).

Computational wind engineering has been recently developed as a branch of computational fluid dynamics for the evaluation of wind effects on buildings. This method may be more efficient than the two methods described above and therefore, it has the potential to be used for optimization analysis of building shapes and arrangements of building locations. Although the application of this method for design purposes is limited, it will get more popularly used in construction industry along with the quick development of powerful computers and efficient, more accurate numerical techniques. The boundary effects can be avoided with the numerical wind tunnel and the computation can be carried out for any Reynolds numbers. However, since the wind flow is turbulent and its interaction with buildings is characterized by high Reynolds number of the order of 10^6-10^7, such numerical calculation in 3-D conditions is very complicated. The computation of the airflow fields around buildings requires the knowledge of both wind engineering and computational fluid dynamics. Different methods of treating turbulence effects and various techniques in choosing adequate boundary conditions are also needed.

There are many numerical methods available to deal with turbulent shear flows among which only the Reynolds averaged Navier-Stokes equations with the k-ε turbulence model and the large eddy simulation (LES) have been widely used in predicting the 3-D turbulent flow around obstacles. A detailed literature review will be given in Chapter 2. In the present study, the generation of an adequate grid system according to the building shape is explained in Chapter 3. The numerical methodology is discussed in Chapter 4. The boundary conditions, of either the air-to-air boundary or

the solid boundary, are given in Chapter 5. The code designed for the current study, which is named as RETWIST, has been validated by a bench mark problem of turbulent flow in Chapter 6. The wind effects on buildings of various shapes such as L-shapes and Z-shapes have been numerically evaluated by using this validated code (Chapter 7). The influence of proximity of grid point to the roof surface of a rectangular building has been examined (Chapter 8). Two-layer methods compiling the k-ε model in the external fully turbulent flow region with a near wall model in the inner areas have also been adopted to examine the wind conditions around a cubic building (Chapter 9).

Chapter 2

LITERATURE REVIEW

2.1 Introduction

There are many numerical methods available to deal with turbulent shear flows (Kline, Ferziger and Johnson, 1978 and Stanisic, 1988) among which only the Reynolds averaged Navier-Stokes (RANS) equations method and the large eddy simulation (LES) are widely used in predicting the 3-D turbulent flow over and around obstacles (Ferziger, Bardina and Allen, 1981, Ferziger, 1983 and 1990 and Zhou and Stathopoulos, 1993). These two methods are still the most feasible available at present although they are theoretically less accurate than the direct simulation method which calculates turbulent flow at all scales. The direct simulation method needs a very fine grid arrangement (Tamura, Krause, Shirayama, Ishii and Kuwahara, 1988, Tamura, 1990 and Ferziger, 1993), and is not an economically feasible approach especially for high Reynolds number flow. The storage capacity and the computational power needed for such fine grid calculations for a three-dimensional unsteady state problem are too large for the computers available to engineers now or in near future.

2.2 Applications of RANS Equations Method

Reynolds averaged Navier-Stokes (RANS) equations method is very frequently used in simulating wind conditions around buildings. In this method, the original Navier-Stokes equations are averaged over a time period. The additional terms introduced by this averaging from the nonlinear terms will be determined by turbulence models such as the k-ε model or the Algebraic Stress Model (ASM). The numerical studies for wind conditions around rectangular buildings adopting RANS equations and the k-ε turbulence model include Vasilic-Melling (1977), Paterson and Apelt (1986, 1990), Baskaran and Stathopoulos (1989), Stathopoulos and Baskaran (1990), Murakami (1990), Murakami and Mochida (1989), Baetke, Werner and Wengle (1990), Selvam and Paterson (1991), Stathopoulos and Zhou (1992a, 1992b, 1992c) and Qasim, Maxwell and Parameswaran (1991).

Vasilic-Melling (1977) has pioneered the numerical simulation of three-dimensional wind flow around a cube by using the k-ε turbulence model together with the Reynolds averaged Navier-Stokes (RANS) equations. However, the predicted mean pressure on the top surface of the cube did not agree well with the experimental results by Castro and Robins (1977) and this was attributed to the coarse grid arrangement used. Recent studies by Paterson and Apelt (1986, 1987 and 1990) have also addressed the numerical evaluation of wind pressure on the roof of a cubic building. Results compared fairly well with the experimental data by Castro and Robins (1977) except for the region

near the windward roof edge where suctions were overestimated by the computation.

Baskaran and Stathopoulos (1989) experimented with a modified k-ε model including curvature effect of streamlines to better predict the wind conditions around a rectangular building. However, the pressure coefficients on the roof did not show much difference from the results obtained with the standard k-ε model. Further modifications with respect to the solid boundary conditions of turbulence properties k and ε and the tangential flow velocities to account for the viscous effect in the immediate proximity of the solid boundaries were adopted by Stathopoulos and Baskaran (1990). This led to a better prediction of the mean pressures on the roof. However, the separation on the roof and beside the side walls is still not predicted properly probably due to the inadequacy of the model used in the inner region near the building envelope.

Murakami (1990) attempted the numerical simulation of the airflow around a cube by adopting the RANS equations for unsteady flow and the standard k-ε model. Numerical results from two different grid arrangements were compared with experimental data for a cubic building model. The numerical mean pressure coefficients over the top of a cube from a fine grid system agreed well with experimental data whereas such suctions obtained from a coarse grid arrangement showed apparent underestimation of the experimental data with distance from the first grid line to roof surface as big as 1.7 cm compared with the building height of 20 cm.

Baetke, Werner and Wengle (1990) also evaluated wind pressures numerically on the surface of a building with wind blowing at an oblique direction (45^{o}) as well as normal direction. Computed wind pressure for normal wind direction show reasonable agreement with experimental data by Castro and Robins (1977) as shown in Fig. 2.1. However, these data taken on the surfaces of a cubic building for oblique wind direction have only been presented for the case of uniform flow conditions while the natural wind flow is always turbulent.

The turbulent airflow around a three-dimensional high-rise rectangular building model was numerically studied by Fan, Wu and Jin (1989). Their results for ground surface pressure and velocity distributions agreed reasonably well with the experimental data by Melbourne and Joubert (1971) and Frank (1987). However, the wind pressures on the envelope of the building were not presented in this paper.

More recently, Selvam and Paterson (1991) and Selvam (1992a) simulated the three-dimensional wind flow around a low rise building for which both full-scale and wind tunnel data were available (Surry, 1989). They solved the RANS equations and the k-ε model by applying both staggered and non-staggered grid arrangements in their calculation. Results were presented along the central line of the roof for normal wind direction. Data from the computation with a staggered grid arrangement agreed fairly well with the wind tunnel results by Surry (1989), whereas the numerical results from the non-staggered grid failed to predict the pressure on the roof. An attempt to compute roof

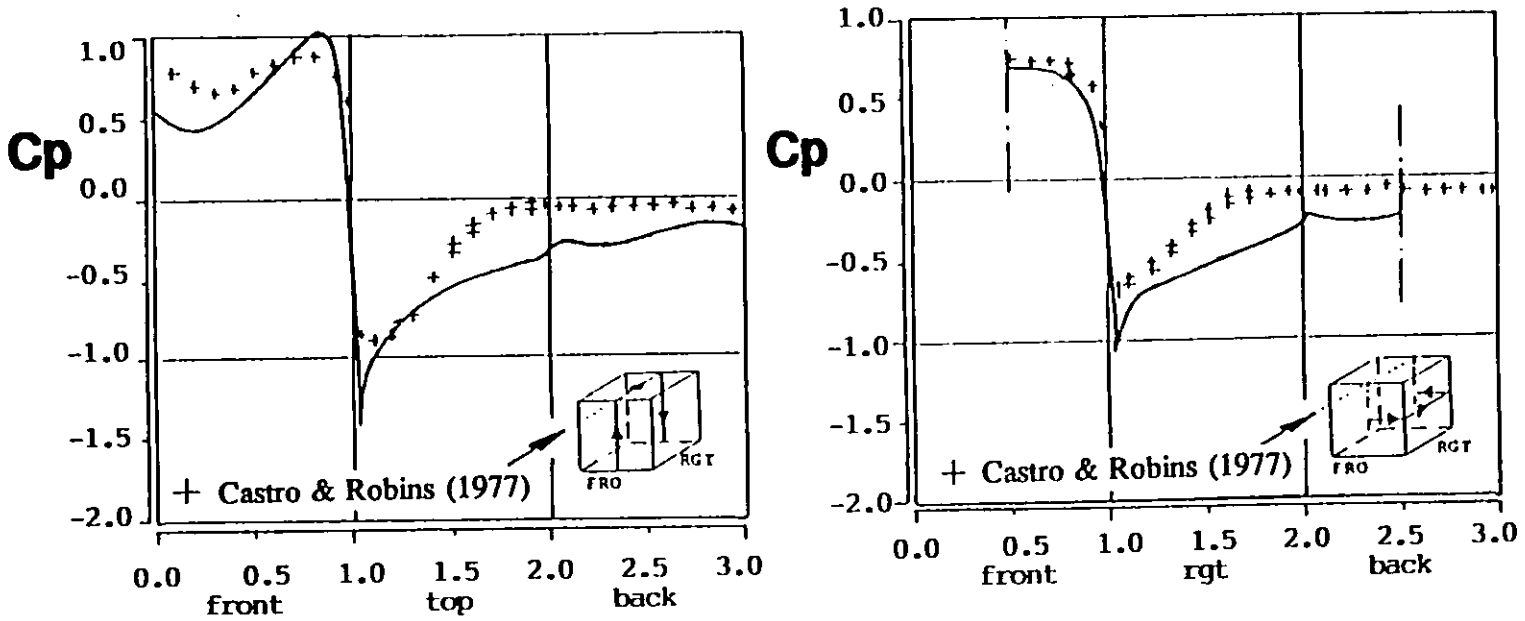

Figure 2.1 Pressure coefficients on the surface of a cube, after Baetke, Werner and Wengle (1990).

corner pressures for critical wind directions was not successful (Fig. 2.2) and this failure was attributed to coarse grid arrangement or the limitation of k-ε model by Selvam (1992b).

There have also been some numerical studies for the airflow conditions around buildings with shapes other than a single rectangular block. Majumdar and Rodi (1989) applied the cylindrical-polar grid and the k-ε model to the calculation of wind flow around a cylindrical structure. The numerical results show reasonably good agreement with the experimental data. The cylindrical-polar grid could be considered as a body-fitted grid for such structures. The general purposed body-fitted grid system is usually designed by using a body-fitted coordinate transformed from a Cartesian coordinate by an appropriate mapping function. However, with the exception of some simple geometries, the generation of transformation function from Cartesian coordinates to body-fitted coordinates is very complicated especially for three-dimensional problems.

Kot (1990) applied the body-fitted coordinate to simulate the stratified air flow around a three-dimensional hill. The Reynolds number of the wind flow is very small and prevents the development of turbulent flow conditions. The mapping function is found by the iterative method and assuming the hill (including the ground nearby) follows a fourth-order polynomial function. Similar numerical studies of two-dimensional airflow around one semicircular obstruction and two rectangular blocks were also attempted by Yeung and Kot (1985) and Kot and Yeung (1988) respectively.

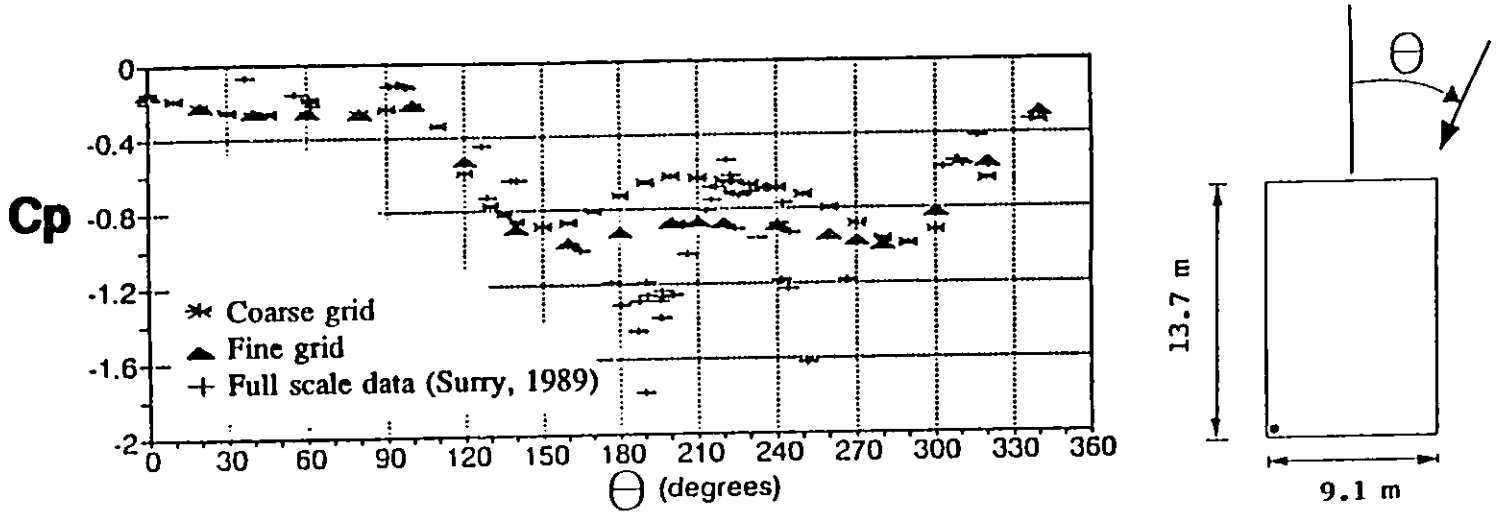

Figure 2.2 Pressure coefficients on a roof corner point, after Selvam (1992b).

By using body-fitted grid system and the k-ε turbulence model, Mouzakis and Bergeles (1991) studied the two-dimensional turbulent flow over a triangular ridge. However, their results in the separation region behind the ridge agrees with the experimental data only in quality. This implies that the standard k-ε turbulence model cannot adequately represent the turbulence properties in this separation region or that the simulation had other problems.

The body-fitted grid system was also adopted by Han (1989) to simulate the wind conditions around a vehicle-like body. The steady state k-ε model and RANS equations were solved numerically with a very dense grid arrangement. Reasonable agreement between the computed drag coefficients and the wind tunnel data has been found for small slant angles (the angle representing the slope of the upper surface of the rear end) while large discrepancies exist for big slant angles. Similar studies were also tested by Parameswaran, Kiris, Sun and Gleason (1993) by numerically solving the unsteady state RANS equations and the k-ε turbulence model. However, large discrepancies have been found between the computed drag and the experimental data which was attributed to the grid non-orthogonality near the forebody by the authors. The airflow around a vehicle has also been simulated by solving the Navier-Stokes equations by Himeno and Fujitani (1993) with body-fitted coordinate method and by Kanayama, Toshigami, Tashiro, Tabata and Fujima (1993) with finite element method. Other examples for the calculations of fluid flow around different bodies by applying body-fitted coordinates can be found in Deng, Piquet, Queutey and Visonneau (1991) and Deng, Piquet and Queutey (1990) for

a prolate spheroid.

To avoid the inconvenience of using body-fitted grid system, Paterson and Holmes (1992) adopted the usual rectangular grid system to simulate the wind conditions around an arched roof building by carefully arranging the grid nodes near the curved surface. However, this approach cannot be evaluated due to the inadequate comparison with experimental data.

When the k-ε model is used for the closure of the RANS equations, the Reynolds stresses are assumed to be isotropic. This assumption is not valid especially when the flow is curved (Leschziner, 1990). The Algebraic Stress Model (ASM) method has been proposed (Rodi, 1976) in order to include this anisotropy of Reynolds stresses. For this model, all the equations of Reynolds stress components are solved numerically together with the k, ε and RANS equations.

Murakami (1992) has adopted the ASM method to study the wind conditions around a cubic building. Results thus obtained were compared with those from the k-ε model method and with the experimental data. Some modest improvement was found in this study.

A similar experiment was also made by Kawamoto, Kawabata and Tawahashi (1992) by using finite element method (FEM). Their results obtained from the k-ε model

computation show apparent discrepancies with the experimental data of Castro and Robins (1977) whereas the results from Differential Stress Model (DSM), which is a variation of the ASM agree well with the experimental data as shown in Fig. 2.3. The results from DSM were also similar to those from the ASM simulation by Murakami (1992) who applied the finite difference method (FDM).

The wind conditions around a rectangular building under different attacking angles have also been studied numerically with the k-ε turbulence model by Mikkelsen and Livesey (1993). The numerically predicted wind pressures on the building envelope showed good agreement with the experimental data on the front and lee walls, whereas apparent discrepancies were found on the roof and the side walls. The turbulent flow around a two-dimensional square block was numerically simulated by Durao, Heitor and Pereira (1987). The RANS equations and the k-ε turbulence model were adopted for the computation. In order to take into account the effect of the streamline curvature, a streamline curvature modification proposed by Leschziner and Rodi (1981) was adopted in the study. The prediction of the recirculation region behind the block is improved when this curvature modification is introduced. Such studies on the turbulent flow around obstacles of various geometries have been tested by Djilali, Gartshore and Salcudean (1987 and 1991) for a front step, by Antoniou and Bergeles (1988) for a rectangular block and by Mouzakis and Bergeles (1991) for a triangular block.

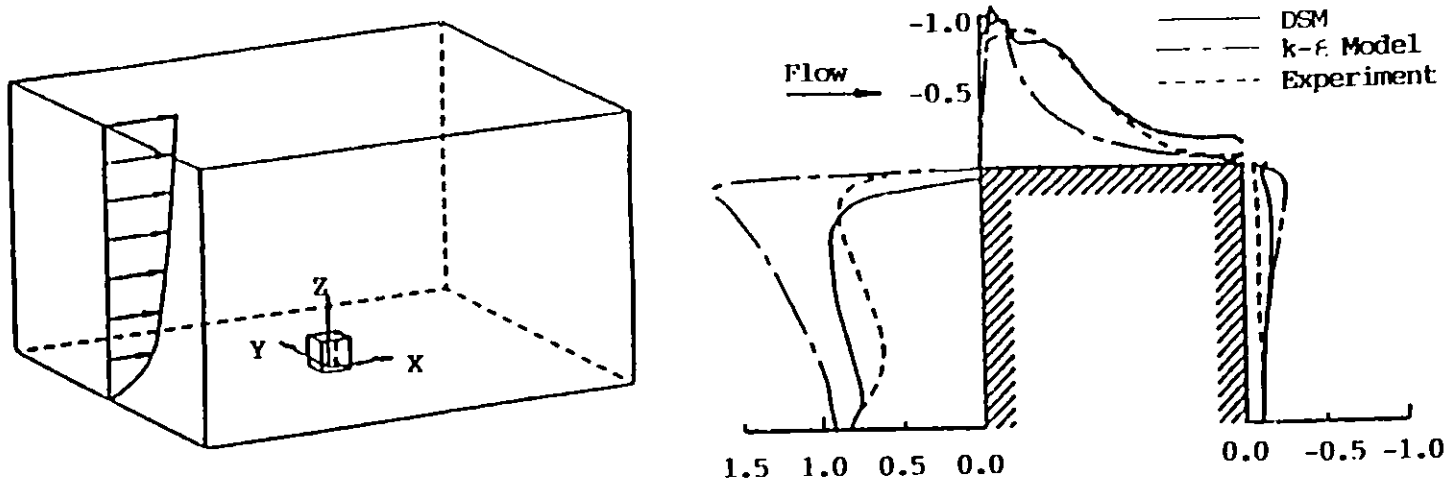

Figure 2.3 Pressure coefficients on the surface of a cube, after Kawamoto, Kawabata and Tawahashi (1992).

2.3 Application of LES

The Large Eddy Simulation (LES) is a higher level simulation method than the RANS equations method. This method can provide detailed information about the time-dependent large scale motion of turbulent air flow. The application of this method to the airflow around a cubic building has been attempted by Murakami and his group (Murakami, Hibi and Mochida, 1990; Murakami, Mochida and Hayashi, 1990) and He and Song (1990).

By using the LES method and the ABMAC computation procedure (Viecelli, 1971), Murakami, Hibi and Mochida (1990) have studied the wind conditions around a cubic building model set in a group of uniformly distributed buildings of the same geometry. The wind conditions around a single building have also been studied and compared with those from the k-ε model method for wind blowing normal to a building wall. Results show that LES can predict the recirculation of mean flow after the separation at the roof surface while the pressure on roof surface still show apparent discrepancy with the experimental data (Murakami, Hibi and Mochida, 1990).

The numerical study of the airflow properties around a building under oblique wind directions has been attempted by Mochida, Ishida and Murakami (1993) by adopting the large eddy simulation method. However, the important information about the wind pressure on building surfaces which is of most interest to wind engineers was not

presented in this paper.

By solving the so-called weakly compressible fluid flow equations along with the Smagorinsky's subgrid-scale turbulence model, He and Song (1990) have attempted a similar study with the MacCormack's predictor-corrector explicit method as solution procedure. The computed results for normal wind directions show relatively good agreement with the experimental data by Castro and Robins (1977). Other similar studies using LES method include Frank and Mauch (1992). Hibi, Ueda, Wakahara and Shimada (1992) and Nicholls, Peilke and Meroney (1992).

One of the main advantages of LES over k-ε model method is that LES can predict the separation region in mean flow observed in experiments above roof surface and near side walls of a rectangular building while the k-ε model method cannot (Murakami, 1992 and Zhou and Stathopoulos, 1993). However, such separation can also be predicted with an adequately chosen two-layer method (Zhou and Stathopoulos, 1994) as will also be addressed in Chapter 9 of this thesis.

2.4 Application of an Equation Solver - PHOENICS

The PHOENICS (Parabolic, Hyperbolic Or Elliptic Numerical - Integration Code Series) equation solver (Spalding, 1981 and 1989) is a general purpose code system solving the Reynolds averaged Navier-Stokes equations with the standard k-ε model.

Some researchers have adopted this equation solver to achieve their objectives of simulating the wind conditions around buildings of different geometries.

By using this equation solver, Haggkvist, Svensson and Taesler (1989) have numerically simulated the wind flow around a small-scale gabled house, and Svensson and Haggkvist (1990) have studied the airflow around a canopy. The numerical results obtained agreed only qualitatively with experimental data by Wiren (1985) as shown in Fig. 2.4.

Richards and Hoxey (1991 and 1992) and Hoxey, Robertson and Richards (1989) have also used PHOENICS solver to study the wind conditions around the Silsoe Structure Building (Robertson and Glass, 1988). The computed mean pressures on the surfaces of this low rise building show reasonably good agreement with the experimental data by Robertson and Glass (1988). This code has also been used for wind conditions around rectangular prisms by Gadilhe and Fleury (1989), Richards, Shepard and Maharas (1989) and Lovgren (1986) with success in only some cases.

2.5 Other Attempts for the Simulation of Wind Conditions around Bluff Bodies

By solving the Navier-Stokes equations with an artificially high viscosity (10^3 times higher than that of the air viscosity) to avoid the fine grid needed for the computation without using turbulence models, Hanson, Summer and Wilson (1986) and

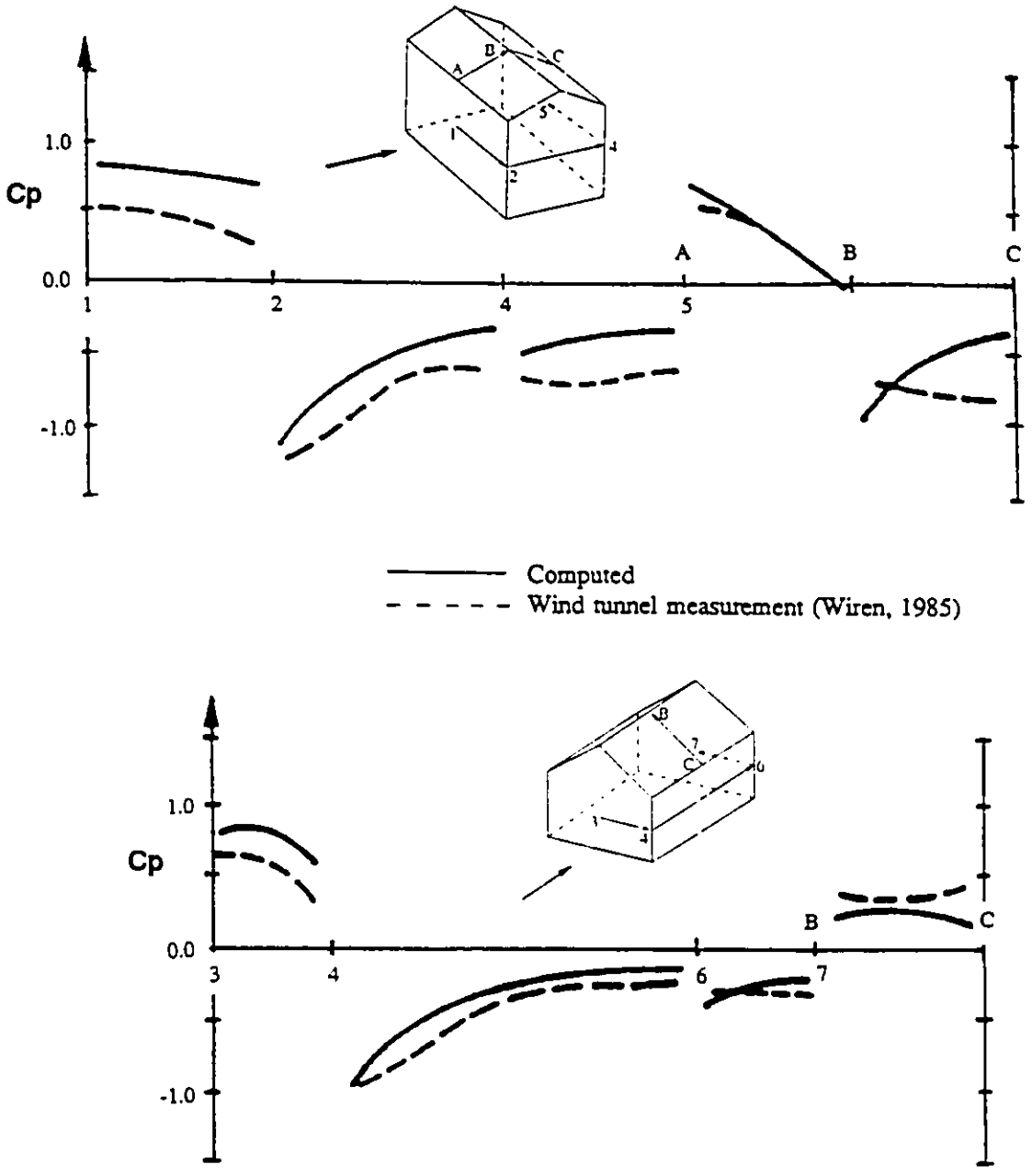

Figure 2.4 Pressure coefficients on the surface of a gabled house, after Haggkvist, Svensson and Taesler (1989).

Summer, Hanson and Wilson (1986) studied the wind conditions around two rectangular buildings and one single rectangular building respectively. Not surprisingly, the numerical results obtained show poor agreement with experimental data. The poor agreement comes from the inadequate model they adopted.

The laminar airflow around a two-dimensional bridge deck was computed by Onyemeluke and Bosch (1993) and Onyemeluke, Torkamani and Bosch (1992) by solving the Navier-Stokes equations. However, the accuracy of their results is questionable since the Reynolds number adopted is as large as 10^5 and turbulence will surely develop very quickly even if the initial air flow were laminar.

The Discrete Vortex Method (DVM) has been used by some researchers in studying the mechanisms of flow-induced vibration of a structure. Such studies include Inamuro (1992), Kawai (1990 and 1992), Sung, Kim and Hyun (1992) and Shirato, Matsumoto and Shiraishi (1992). This problem has also been attempted by Sakamoto, Murakami, Kato and Mochida (1992) with large eddy simulation method. The DVM is also used to evaluate the airflow effects on a bridge by Walther (1993). Other similar studies regarding fluid flow around bluff bodies include Bienkiewicz and Kutz (1990), Sarpkaya and Ihrig (1986), Sarpkaya and Kline (1982) and Turkiyyah, Reed and Yang (1994). The main advantage of this method is that less computer storage capacity and CPU time are needed for a two-dimensional problem since less equations are solved; and also this method is good in predicting the vortex shedding from a structure. However, this

method seems to be unable to give proper prediction of mean flow properties which are important information in wind engineering (Turkiyyah, Reed and Yang, 1994). When 3D problems are considered, this method is not adequate since more equations will have to be solved than the direct method.

2.6 Justification of the Present Study

In the current study, the steady state Reynolds averaged Navier-Stokes equations and the k-ε turbulence model have been solved with the well-known SIMPLE method (Patankar, 1980). A systematic examination of wind effects on buildings and wind flow conditions around buildings has been carried out numerically. Firstly, contrary to the usual numerical studies which were only performed on rectangular buildings, the current study evaluates the wind effects on buildings of different shapes such as L-shapes (either in vertical cross-section or plan view) and Z-shapes (see Chapter 7). Since many researchers (Selvam, 1992a, Murakami and Mochida, 1989) have declared that the discrepancies between the computed results with k-ε model method and the experimental data on the flat roof of a rectangular building is caused by the coarse grid used, a systematic evaluation of k-ε model method in predicting the wind pressure on the flat roofs has been attempted by using grids of various densities (Chapter 8). Both the advantages and limitations of this most widely used method in computing the wind pressure on flat roofs under normal and oblique wind conditions have been evaluated. The influence of the proximity of grid points to the roof surface has also been evaluated. In order to keep the

advantages of k-ε model in representing the fully turbulent flow in the external flow region far from solid walls and to avoid its shortcomings for the near wall flows, two two-layer methods combining either a one-equation model or a two-equation modified k-ε model in the near wall area with the k-ε model in the external flow region have been adopted in this study to predict the wind conditions around a cubic building (Chapter 9).

The present study did not choose to utilize a commercial code, such as PHOENICS, for the following reasons:

i) The unsuccessful use of this code in predicting the wind pressures on the surfaces of a cubic building by Gadilhe and Fleury (1989) and in evaluating the wind pressures on the surfaces of a gabled house by Haggkvist, Svensson and Taesler (1989), as shown in Fig. 2.4, and Svensson and Haggkvist (1990) discourage researchers from using it.

ii) PHOENICS is a black box from which no idea can be obtained about the internal structure of the equation solver of the program. Using it will only make a user a code operator rather than a CFD researcher - a person who is able to develop a code. The fact that the PHOENICS code is a black box accounts for many unsuccessful applications of this code. Many users cannot even get convergent solutions after working on the code for a significant period of time.

iii) The general purpose PHOENICS code is too much and too general for the present case of limited objectives which deals only with one-phase, incompressible, Newtonian fluid flow.

Consequently, it was decided that the program named TWIST (Baskaran, 1990) developed in the Centre for Building Studies, Concordia University would be adopted, modified and, for some key parts, redesigned for the current study.

Chapter 3

GRID GENERATION AND BUILDING GEOMETRIES

3.1 Choice of the Grid Arrangement

The finite difference method (FDM) has been used in this study. The discretization scheme used is the rectangular staggered grid system (see Fig. 3.1). Although the non-staggered grid system is a little easier to use, the staggered grid system has been used since it avoids the evaluation of the boundary conditions for pressures (Patankar, 1980). In fact the pressures near solid surfaces can be obtained directly without the extrapolation necessary for non-staggered grids (Peric, Kessler and Scheuerer, 1988).

3.2 Building Geometries

The routine for grid generation is designed to be applicable to any arbitrarily-shaped building composed of two rectangular blocks (Stathopoulos and Zhou, 1993a). This general building configuration set in a computational domain is shown in Fig. 3.2. The building shape and size is defined by the values of L1, L2, W1, W2, W3, H1 and H2, whereas the size of the computational domain which should be relevant to the building size is determined by the magnitudes of UD, DD, DS1, DS2 and DT. For example, the stepped-roof building studied in the present study (Chapter 7) is specified by setting W1=W3=0 and H1=25 mm, H2=50 mm, W2=100 mm and L1=L2=75 mm.

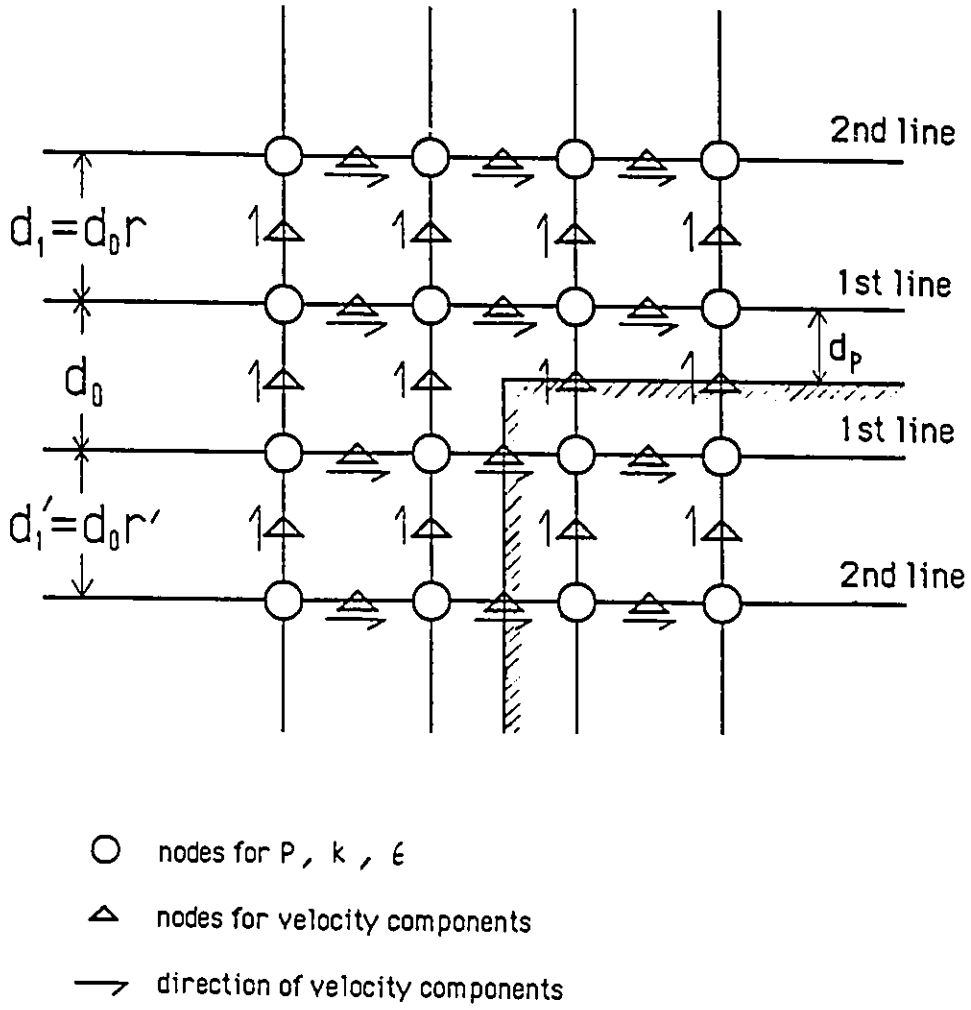

Figure 3.1 Staggered grid arrangement.

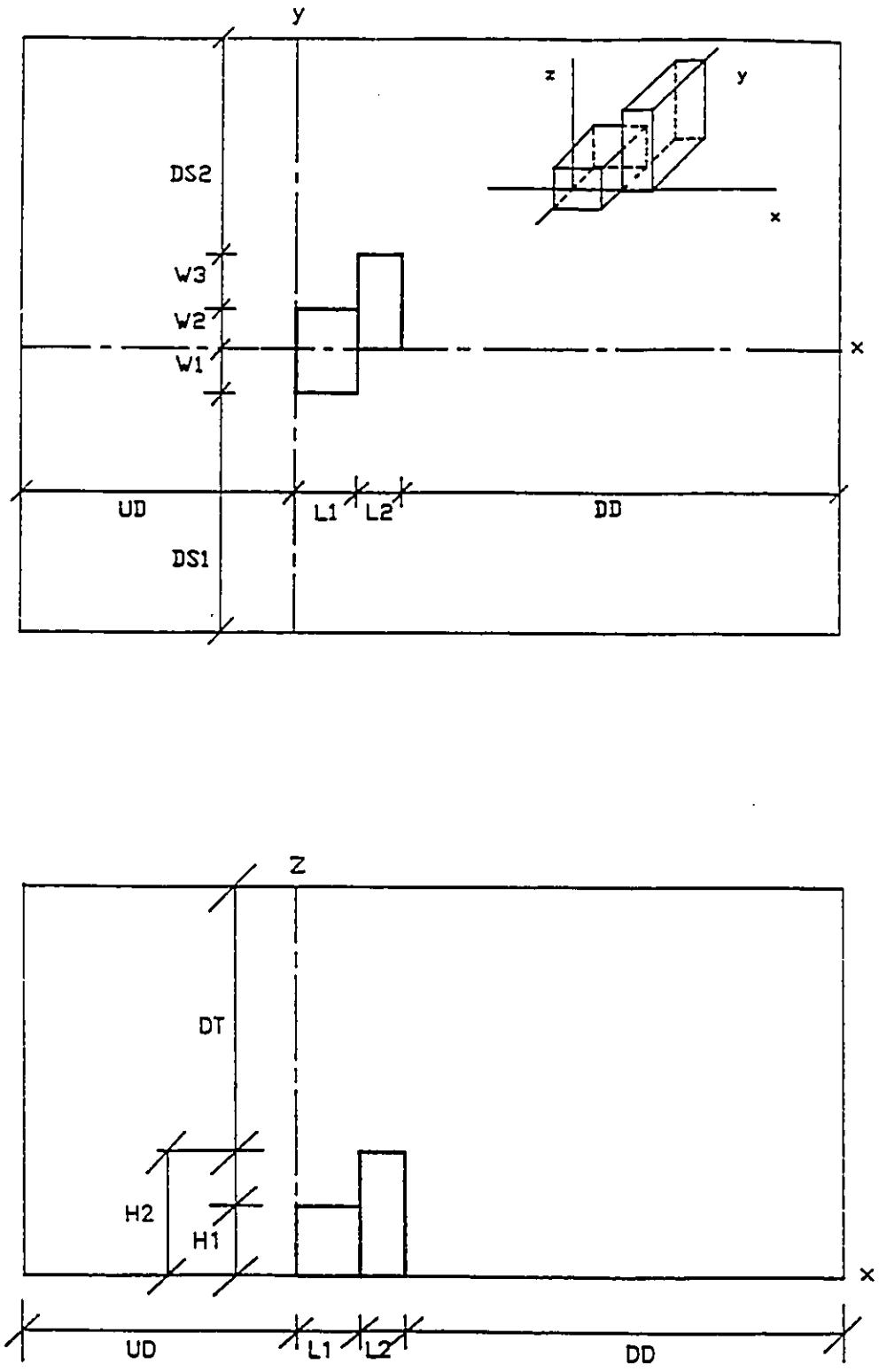

Figure 3.2 Building configurations and computational domain.

This building corresponds to a 1:400 scaled model of a full-scale building with H1=10 m, H2=20 m, W2=40 m, L1=L2=30 m. The plan view L-shaped building in the present calculation (also see Chapter 7) is defined by setting W3 to zero and L1=L2=W1=W2=75 mm, H1=H2=50 mm. The rectangular buildings studied in the present investigation (see Chapter 8) have the dimensions of 15.2cm x 15.2cm x 13.5cm (height) for a tall building and 15.2cm x 15.2cm x 3.0cm for a low building. A cubic building of 20 cm side has also been studied in Chapter 9. These buildings are specified by the program as a special building shape with zero length for the second block (L2=0).

3.3 Grid Generation

The numerical simulation of wind flow around an L-shaped building as well as a rectangular building needs special care in arranging the computational gridnodes especially those near the building surfaces. The gridnodes for normal wind velocity components are set on the solid boundary and the high density gridnodes are only used in the region where it is required, i.e. near the building envelope and near the ground. The algorithm generating the grid system takes into account the building shape and size specified by the user. This makes the use of this program easy by avoiding manual gridnode arrangement commonly used by other researchers, e.g. Murakami and Mochida (1989) for a building complex. When generating a grid system, the program first reads in the distance d_p ($=d_o/2$) between the first grid line and its respective solid boundary; then successive grid lines are generated at the specific expanding factor (r) defined for

each region starting from that solid boundary. Here, d_0 denotes the distance between the first grid lines on either side of the wall as shown in Fig. 3.1, in which a typical grid node arrangement near a building corner is presented. The expanding factor is defined as the ratio of the distance between the nth grid line and the (n+1)th grid line (d_n) to the distance between (n-1)th grid line and nth grid line (d_{n-1}), i.e.

$$r = \frac{d_n}{d_{n-1}} \qquad (3.1)$$

According to equation (3.1), the expanding factor (r) is then determined for each region by equalizing the sum of the grid intervals in the region to the length of the region (Lr) - an example of Lr is the distance from the front wall to the upwind free boundary. Grid systems are thus generated with dense grid lines near solid boundaries and relatively coarse grid lines far from solid boundaries. A typical grid system for the plan view L-shaped building case is shown in Fig. 3.3. The grid nodes included in this figure are those for augmented pressures (P) and turbulence properties (k and ε) only. The points where velocity components are stored are set between every two successive nodes because of the staggered grid used (see e.g. Patankar, 1980).

The simulation of oblique wind cases is achieved by rotating the flow field rather than the building itself to avoid the difficulty in re-arranging the gridnodes. The method used in this computation is easier to control and more suitable than body-fitted coordinate system for a building composed of rectangular blocks.

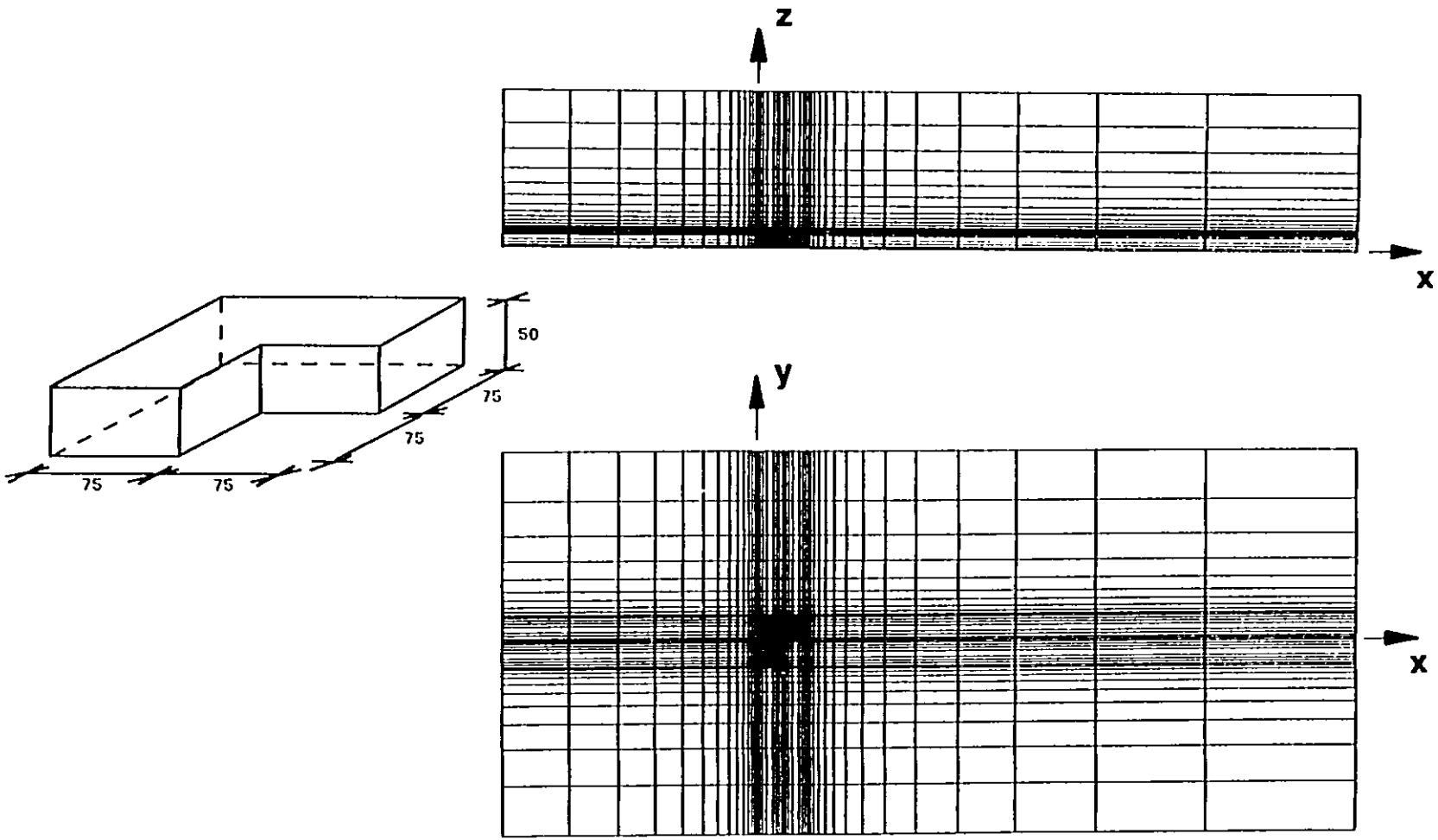

Figure 3.3 Grid system for the plan view L-shaped building model.

Chapter 4

NUMERICAL SOLUTION PROCEDURE

4.1 Governing Equations

In present study, the steady state RANS equations and the k-ε turbulence model are adopted as governing equations of the turbulent airflow around buildings. These equations are as follows (see Paterson, 1986):

$$\frac{\partial U_j}{\partial x_j}=0 \tag{4.1}$$

$$U_j\frac{\partial U_i}{\partial x_j}=-\frac{\partial P}{\partial x_i}+\frac{\partial}{\partial x_j}\left[(\nu_t+\nu)\frac{\partial U_i}{\partial x_j}\right]+\frac{\partial \nu_t}{\partial x_j}\frac{\partial U_j}{\partial x_i} \tag{4.2}$$

$$U_j\frac{\partial k}{\partial x_j}=\frac{\partial}{\partial x_j}\left[\left(\nu+\frac{\nu_t}{\sigma_k}\right)\frac{\partial k}{\partial x_j}\right]+\nu_t\left(\frac{\partial U_i}{\partial x_j}+\frac{\partial U_j}{\partial x_i}\right)\frac{\partial U_i}{\partial x_j}-\epsilon \tag{4.3}$$

$$U_j\frac{\partial \epsilon}{\partial x_j}=\frac{\partial}{\partial x_j}\left[\left(\nu+\frac{\nu_t}{\sigma_\epsilon}\right)\frac{\partial \epsilon}{\partial x_j}\right]+C_1\frac{\epsilon}{k}\nu_t\left(\frac{\partial U_i}{\partial x_j}+\frac{\partial U_j}{\partial x_i}\right)\frac{\partial U_i}{\partial x_j}-C_2\frac{\epsilon^2}{k} \tag{4.4}$$

where P is the augmented pressure defined by

$$P=\frac{p}{\rho}+\frac{2}{3}k \tag{4.5}$$

and eddy viscosity (ν_t) is represented by

$$\nu_t = C_\mu \frac{k^2}{\epsilon} \qquad (4.6)$$

The model constants C_1, C_2, C_μ, σ_k and σ_ϵ are equal to 1.44, 1.92, 0.09, 1.0 and 1.3 respectively (see e.g. Rodi, 1980).

4.2 Discretization Procedure

4.2.1 General equation

Equations (4.2) to (4.4) can be written in the following general form:

$$U_j \frac{\partial \phi}{\partial x_j} = \frac{\partial}{\partial x_j} \left(\Gamma \frac{\partial \phi}{\partial x_j} \right) + S_c + S_p \phi \qquad (4.7)$$

with ϕ, Γ, S_c and S_p corresponding to the variables shown in Table 4.1.

4.2.2 Discretization of the general equation

Since five of the six governing equations [i.e. Eq (4.2) which represents three equations, Eq (4.3) and Eq (4.4)] can be represented by equation (4.7), the discretization of these equations can be achieved by just discretizing equation (4.7). Clearly, equation (4.7) is composed of both convection terms and diffusion terms for which the SIMPLE method can be applied. The hybrid scheme developed by Spalding (1972) is used to discretize this equation. With the grid nodes for ϕ and its coefficients U_i and Γ being

Table 4.1 Variables in equation (4.7)

ϕ	Γ	S_c	S_p	
U_i	$\nu_t+\nu$	$-\partial P/\partial x_i+(\partial \nu_t/\partial x_j)(\partial U_j/\partial x_i)$	0	(4.2)
k	$\nu_t/\sigma_k+\nu$	$\nu_t P^*$	$-\varepsilon/k$	(4.3)
ε	$\nu_t/\sigma_\varepsilon+\nu$	$C_1 C_\mu k P^*$	$-C_2\varepsilon/k$	(4.4)

Note, in equations (4.3) and (4.4):

$$P^* = \left(\frac{\partial U_i}{\partial x_j}+\frac{\partial U_j}{\partial x_i}\right)\left(\frac{\partial U_i}{\partial x_j}\right) \qquad (4.8)$$

arranged staggered (Fig. 3.1), equation (4.7) is integrated over a three-dimensional control volume whose two-dimensional form is shown in Fig. 4.1, and is finally discretized into the following expression (see Patankar, 1980):

$$a_P\phi_P = a_E\phi_E + a_W\phi_W + a_N\phi_N + a_S\phi_S + a_T\phi_T + a_B\phi_B + b \qquad (4.9)$$

where

$$a_E = \max\left(\frac{1}{2}|F_e|, D_e\right) - \frac{1}{2}F_e$$

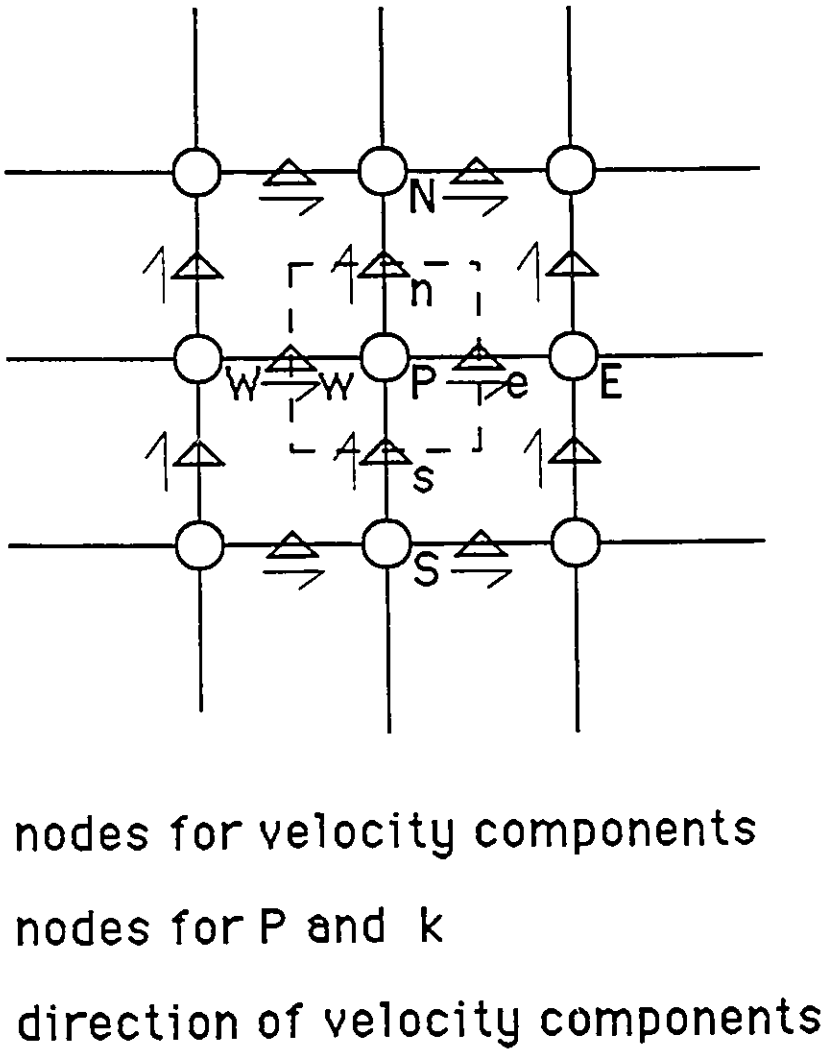

Figure 4.1 Control volume for equation (4.9).

$$a_W=\max\left(\frac{1}{2}|F_w|, D_w\right)+\frac{1}{2}F_w$$

$$a_N=\max\left(\frac{1}{2}|F_n|, D_n\right)-\frac{1}{2}F_n$$

$$a_S=\max\left(\frac{1}{2}|F_s|, D_s\right)+\frac{1}{2}F_s$$

$$a_T=\max\left(\frac{1}{2}|F_t|, D_t\right)-\frac{1}{2}F_t$$

$$a_B=\max\left(\frac{1}{2}|F_b|, D_b\right)+\frac{1}{2}F_b$$

$$b=S_c\Delta x\Delta y\Delta z$$

$$a_P=a_E+a_W+a_N+a_S+a_T+a_B-S_P\Delta x\Delta Y\Delta z \qquad (4.10)$$

where

$F_e=U_e\Delta y\Delta z$

$F_w=U_w\Delta y\Delta z$

$F_n=V_n\Delta z\Delta x$

$F_s=V_s\Delta z\Delta x$

$F_t=W_t\Delta x\Delta y$

$F_b=W_b\Delta x\Delta y$

$D_e=\Gamma_e\Delta y\Delta z/(\delta x)_e$

$$D_w=\Gamma_w\Delta y\Delta z/(\delta x)_w$$

$$D_n=\Gamma_n\Delta z\Delta x/(\delta y)_n$$

$$D_s=\Gamma_s\Delta z\Delta x/(\delta y)_s$$

$$D_t=\Gamma_t\Delta x\Delta y/(\delta z)_t$$

$$D_b=\Gamma_b\Delta x\Delta y/(\delta z)_b$$

In these equations, U, V and W are the velocity components along x, y and z directions; the subscripts e, w, n, s, t and b, representing east, west, north, south, top and bottom, indicate the positions where the velocity components and the diffusion coefficients are defined.

4.2.3 Discretization of the momentum equations

In the momentum equation, ϕ stands for the relevant velocity component, and Γ and S are to be given their appropriate meanings (Table 4.1). The adoption of the staggered grid does make the discretized momentum equations somewhat different from the discretization equation for the other ϕ's that are calculated for the main grid points. But this difference is not essential. It arises from the use of staggered control volumes for momentum equations.

A staggered control volume for the x-component momentum equation is shown in Fig. 4.2. If attention is focused on the locations for U only, there is nothing unusual

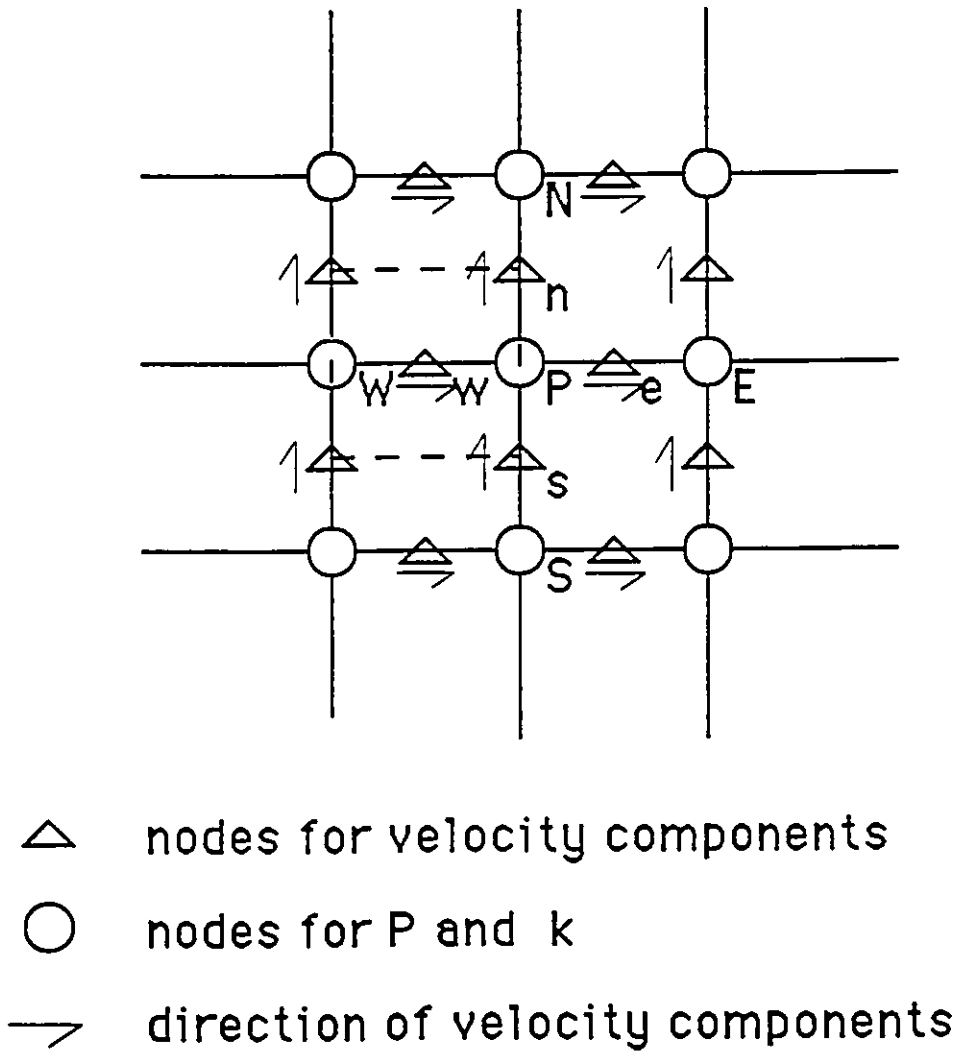

Figure 4.2 Control volume for equation (4.11).

about this control volume. Its faces lie between the point w and the corresponding locations for the neighbouring U's. The staggering is in the x-direction only, such that the faces normal to that direction pass through the main grid points P and W. This layout realizes one of the main advantages of the staggered grid, i.e. the difference p_W-p_P can be used to calculate the pressure force acting on the control volume for the velocity U so that the "checker-board effect" is avoided (Patankar, 1980)

The calculation of the diffusion coefficients and the velocity components at the faces of the U control volume shown in Fig. 4.2 would require an appropriate interpolation; but, essentially, the same formulation as described in section 4.2.1 would be applicable. The resulting discretized equation can be written as:

$$a_w U_w = \sum a_{nb} U_{nb} + b + (p_w - p_p)\,\Delta y \Delta z \qquad (4.11)$$

The subscription "nb" denotes the six neighbouring points around the point w on the surfaces of the control volume. Fig. 4.2 shows a two-dimensional situation for which there are only four such neighbouring points. The momentum equations for the other directions are handled in a similar manner so that the discretized equations for V_s and W_b can be obtained as:

$$a_s V_s = \sum a_{nb} V_{nb} + b + (p_S - p_p)\,\Delta z \Delta x \qquad (4.12)$$

$$a_b W_b = \sum a_{nb} W_{nb} + b + (p_B - p_p)\,\Delta x \Delta y \qquad (4.13)$$

Equations (4.11), (4.12) and (4.13) will be solved based on an estimated pressure field p^*. The velocity field thus obtained will be denoted as U^*, V^* and W^* respectively.

However, these velocity fields will not satisfy the continuity equation until the correct pressure field is found and used in the momentum equations. So the p^*, U^*, V^* and W^* fields need to be "corrected".

4.2.4 The pressure and velocity corrections

A method to improve the guessed values p^* and U^*, V^* and W^* is found by using the continuity equation:

$$(U_e-U_w)\Delta y\Delta z+(V_n-V_s)\Delta z\Delta x+(W_t-W_b)\Delta x\Delta y=0 \qquad (4.14)$$

If the corrected pressure and velocities p, U, V and W are denoted as

$$p=p^*+p'$$

$$U=U^*+U'$$

$$V=V^*+V'$$

$$W=W^*+W' \qquad (4.15)$$

where p′, U′, V′ and W′ are called the pressure correction and velocity corrections respectively, equation (4.11) with the guessed variables (U^*, p^*) can be subtracted from the same equation with the corrected variables (U, p). The resulted equation is:

$$a_w U'_w=\Sigma a_{nb}U'_{nb}+(p'_w-p'_p)\Delta y\Delta z \qquad (4.16)$$

Similarly, we can also get the equations for V′ and W′:

$$a_s V_s' = \Sigma a_{nb} V_{nb}' + (p_S' - p_P')\,\Delta z \Delta x \qquad (4.17)$$

$$a_b W_b' = \Sigma a_{nb} W_{nb}' + (p_B' - p_P')\,\Delta x \Delta y \qquad (4.18)$$

In SIMPLE method, the terms with Σ in equations (4.16), (4.17) and (4.18) are abandoned to make the solution procedure "simple", so that

$$U_w' = d_w (p_W' - p_P') \qquad (4.19)$$

$$V_s' = d_s (p_S' - p_P') \qquad (4.20)$$

$$W_b' = d_b (p_B' - p_P') \qquad (4.21)$$

where $d_w=\Delta y\Delta z/a_w$, $d_s=\Delta z\Delta x/a_s$, and $d_b=\Delta x\Delta y/a_b$.

The corrected velocities will then become:

$$U_w = U_w^* + d_w (p_W' - p_P') \qquad (4.22)$$

$$V_s = V_s^* + d_s (p_S' - p_P') \qquad (4.23)$$

$$W_b = W_b^* + d_b (p_B' - p_P') \qquad (4.24)$$

If equations (4.22), (4.23) and (4.24) are incorporated into equation (4.14), the following equation for pressure correction will be obtained:

$$a_P p'_P = \Sigma a_{nb} p'_{nb} + b \qquad (4.25)$$

where the subscript nb represents E, W, N, S, T and B etc, and a_{nb}, a_p and b are given as:

$$a_E = d_e \Delta y \Delta z$$

$$a_W = d_w \Delta y \Delta z$$

$$a_N = d_n \Delta z \Delta x$$

$$a_S = d_s \Delta z \Delta x$$

$$a_T = d_t \Delta x \Delta y$$

$$a_B = d_b \Delta x \Delta y$$

$$a_P = a_E + a_W + a_N + a_S + a_T + a_B$$

$$b = (U^*_w - U^*_e)\,\Delta y \Delta z + (U^*_s - U^*_n)\,\Delta z \Delta x + (U^*_b - U^*_t)\,\Delta x \Delta y \qquad (4.26)$$

4.2.5 Semi-Implicit Method for Pressure Linked Equations (SIMPLE) solution procedure

In order to obtain eddy viscosity, equations (4.3) and (4.4) for the turbulence kinetic energy (k) and its dissipation (ε) must also be solved. The computation procedure is as follows:

i) start from the initial pressure (p^*), eddy viscosity (ν_t^*), velocity field (U_i^o),

turbulence kinetic energy (k^*) and its dissipation (ε^*).

ii) use the pressure field, ν_t field and the velocities obtained from the previous iteration p^*, ν_t^* and U^o, V^o and W^o, to solve the momentum equations (4.11), (4.12) and (4.13) to obtain U^*, V^* and W^*;

iii) solve equation (4.25) for the pressure correction p';

iv) add p' to p^* to get new pressure field p;

v) calculate the new corrected velocity field by using equations (4.22), (4.23) and (4.24);

vi) solve equation (4.9) for k and ε;

vii) calculate new eddy viscosity by using equation (4.6);

viii) treat the corrected pressure field (p) as guessed pressure (p^*), new k and ε as k^* and ε^* and new eddy viscosity (ν_t) as ν_t^*, new velocity field as U^o, V^o and W^o for next iteration; return to the step ii).

This procedure will be repeated until some specified convergence criteria have been reached. The first iteration will be executed by adopting the initial conditions of p, ν_t, U, V and W etc. In the computation, underrelaxation is used to avoid divergence (Patankar, 1980) since equations (4.19), (4.20) and (4.21) were used instead of equations (4.16), (4.17) and (4.18) in this SIMPLE method. The underrelaxation factors (β) used in the current study which were determined through trial and error are shown in Table 4.2.

This solution procedure can be presented more clearly by the flow chart shown in Fig. 4.3.

Table 4.2 Underrelaxation factors

variables	U_i	p	k	ε	ν_t
β	0.5	0.3	0.7	0.7	0.7

4.2.6 Convergence criteria

In practice, the iterative process is terminated when some arbitrary convergence criterion is satisfied. An appropriate convergence criterion depends on the nature of the problem and on the objectives of the computation. A common procedure is to examine the most significant quantities given by the solution and to require that the iterations be continued until the relative change in these quantities between two successive iterations is smaller than a certain small number. This type of criterion can sometimes be misleading (Patankar, 1980). When heavy underrelaxation is used, the change in the dependent variables between successive iterations is intentionally slowed down. This may create an illusion of convergence although the computed solution may be far from being converged. Another method of monitoring convergence is to examine how perfectly the

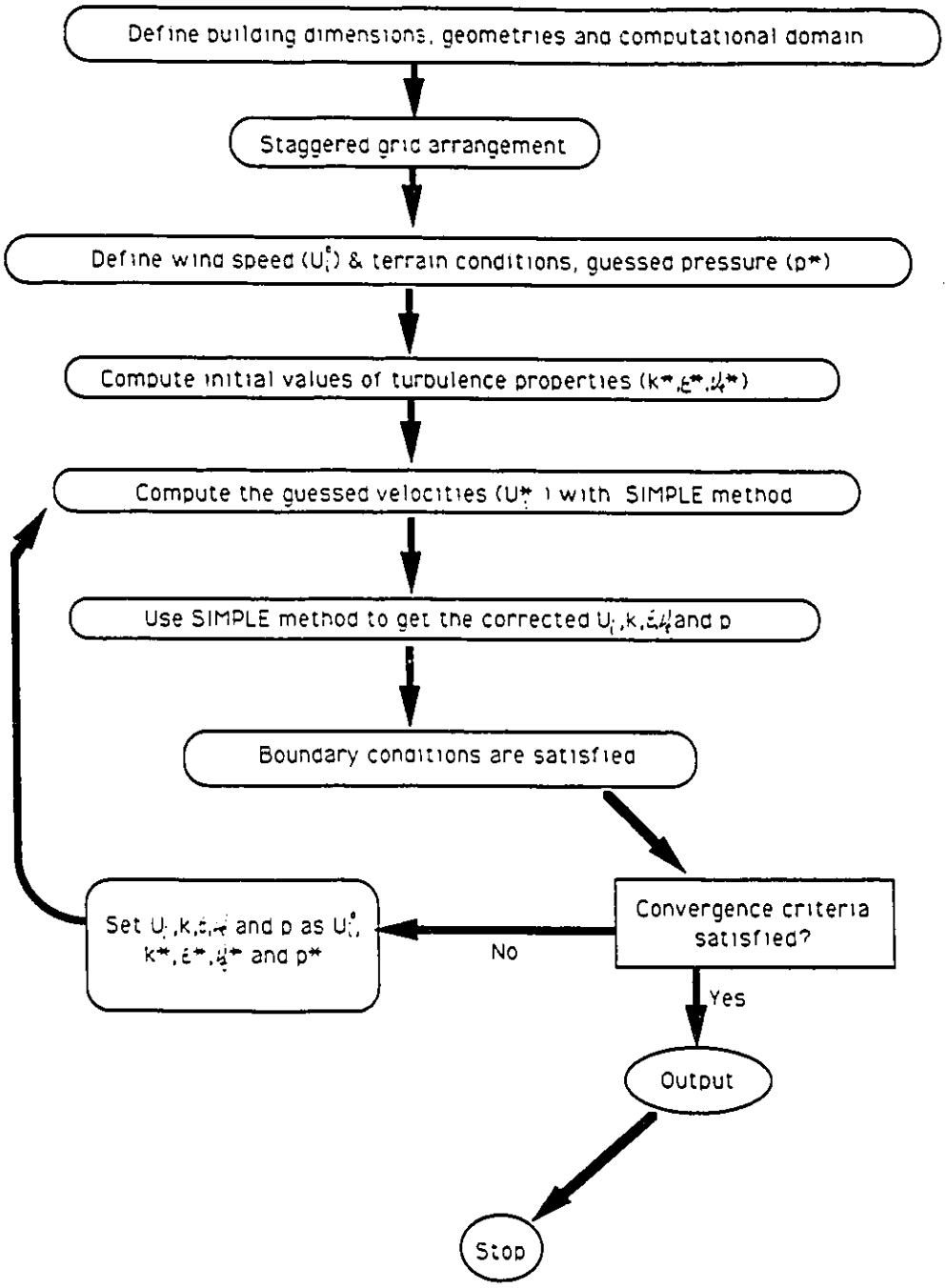

Figure 4.3 The flow chart of the SIMPLE solution procedure.

discretization equations are satisfied by the current values of the dependent variables. For each grid point, a residual R can be calculated from

$$R=\Sigma a_{nb}\phi_{nb}+b-a_p\phi_p \qquad (4.27)$$

Clearly, when the discretization equation is satisfied, R will be zero. A suitable convergence criterion requires that the largest value of $|R|$ or the sum of $|R|$ over the computational region be less than a certain small number. However, the residue thus defined depends on the magnitude of ϕ and the number of control volumes which vary in a large range especially for 3D computations. To avoid such short-comings, Doormaal and Raithby (1984) suggested to use the relative residue as the convergence criterion. The relative residue is defined as the ratio of the current residue $|R^n|$ to the residue after the first iteration $|R^1|$, i.e.

$$\gamma_n=\frac{|R^n|}{|R^1|} \qquad (4.28)$$

According to Doormaal and Raithby (1984), the optimal values of the relative residues are typically from 0.25 to 0.05. In the present study, the computation is considered convergent if the relative residues of all equations are less than 0.02. The difference between the results of two successive steps is also checked to ensure that the computation converges. Such check for the case of wind flow around a rectangular building shows that the maximum relative difference of all the variables (U_i, P, k, ε) is already less than 1% when this relative residue criterion has been satisfied. Such relative residue has also been used as a convergence criterion by Paterson (1986), Majumdar and Rodi (1989), Paterson and Apelt (1990) and Baskaran (1990).

Chapter 5

BOUNDARY CONDITIONS

5.1 Specification for Free Boundaries

5.1.1 Specification of the initial mean flow velocities

Since the SIMPLE solution procedure has been adopted in the present study to solve the steady state equations (4.1) to (4.4), iteration is needed for the computation. The initial distributions of mean flow velocity components (U_i), turbulence properties (k, ε and ν_t) and static pressure (p) are needed to start the iteration. The initial conditions are assumed to be those for mean wind flow in an open field. The initial mean flow velocity distribution is determined by the power-law velocity profile, i.e.

$$U(x,y,z) = U_g\left(\frac{z}{z_g}\right)^{\alpha} \tag{5.1}$$

$$V(x,y,z) = 0 \tag{5.2}$$

$$W(x,y,z) = 0 \tag{5.3}$$

where U, V and W are the mean flow velocity components along x, y and z directions; U_g is the gradient velocity (Simiu and Scanlan, 1978); z is the height above ground; z_g is the gradient height and α is the power-law exponent which is 0.15 for the application in Chapters 7 and 8 and 0.25 for that in Chapter 9.

5.1.2 Specification of the initial turbulence properties

Once the mean flow velocities are given, there will be a corresponding k and ε distribution. Since the initial mean flow velocity is pseudo-one-dimensional, its corresponding turbulence properties can also be assumed to be pseudo-one-dimensional. In other words, the conditions V = 0, W = 0, $\partial/\partial x = 0$ and $\partial/\partial y = 0$ will also be satisfied by k and ε equations. The simplified equations obtained from equations (4.3) and (4.4) under these conditions will be (Paterson, 1986):

$$\frac{\partial}{\partial z}\left[\left(\nu+\frac{\nu_t}{\sigma_k}\right)\frac{\partial k}{\partial z}\right]+\nu_t\left(\frac{\partial U}{\partial z}\right)^2-\varepsilon=0 \qquad (5.4)$$

$$\frac{\partial}{\partial z}\left[\left(\nu+\frac{\nu_t}{\sigma_\varepsilon}\right)\frac{\partial \varepsilon}{\partial z}\right]+C_1\frac{\varepsilon}{k}\nu_t\left(\frac{\partial U}{\partial z}\right)^2-C_2\frac{\varepsilon^2}{k}=0 \qquad (5.5)$$

Equations (5.4) and (5.5) are discretized and numerically solved by iteration with solid boundary conditions to be discussed in section 5.2.3. Free-slip conditions have been assumed on the air-to-air boundaries. The converged solutions for k and ε are used as the initial conditions of k and ε for the SIMPLE solution procedure. The k- and ε- profiles thus obtained together with the power-law initial velocity field are shown in Fig. 5.1. The initial eddy viscosity is obtained by using equation (4.6) in which k and ε are assigned their initial values.

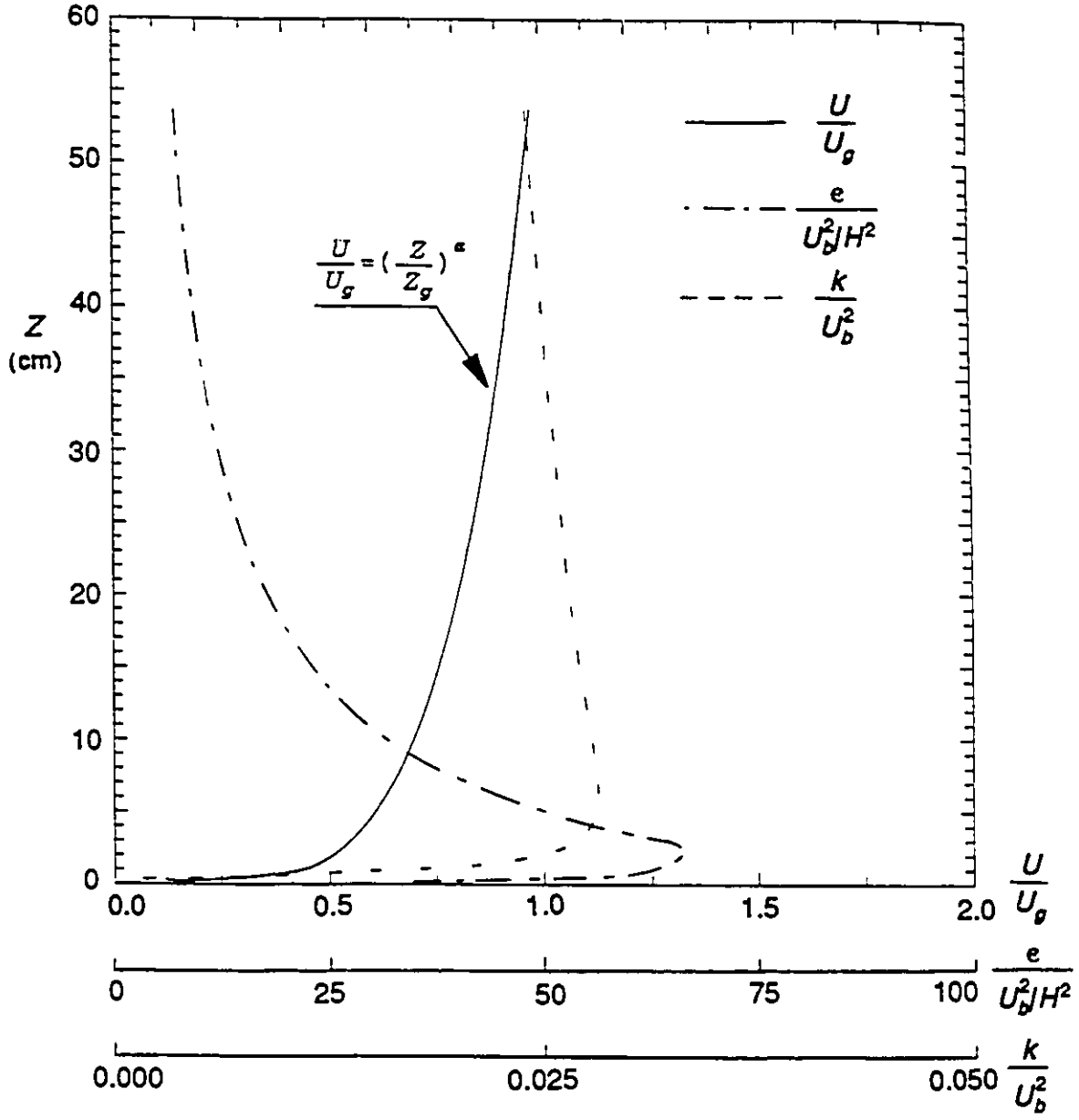

Figure 5.1 Initial conditions adopted in the current study.

5.1.3 Specification of the initial mean flow static pressure

The initial static pressure is assumed to be a constant everywhere. Since pressure only appears in the RANS equations in its differential form, this constant can be any value. It is noted that P in equation (4.2) is the augmented pressure which is represented by equation (4.5). So the initial augmented pressure P should be the initial static pressure divided by air densities plus the additional term (2/3k) in which k is the initial turbulence kinetic energy.

5.1.4 Specification of free boundary conditions

It is assumed that a small building model set in a large open field does not affect the mean wind flow conditions at the positions far enough from the building. Since the computational domain adopted is very large compared with the building model, the free boundary conditions of velocity, pressure and turbulence properties at air to air boundaries are fixed at the initial power-law velocity profile (section 5.1.1), the corresponding initial values of turbulence properties (section 5.1.2) and the initial uniform pressure distribution (section 5.1.3).

5.2 Specification for Solid Boundaries

The boundary conditions introduced in this section are those for one-layer k-ε

model method only. The special boundary conditions for two-layer methods will be explained in Chapter 9.

5.2.1 Derivation of log-linear-law wall functions

At a solid boundary, the no-slip condition can be applied to both mean and fluctuating velocity because of the viscosity of air. However, these conditions are seldom used in real computation. First, very steep gradients prevail in the viscous sublayer so that a lot of grid nodes have to be placed there and the computation becomes very expensive if not impossible. Second, viscous effects become very important in this layer so that the high Reynolds number turbulence models employed in most of the computations are not applicable there. Consequently, suitable boundary conditions for turbulent flow should be employed to get good predictions from numerical simulations.

The turbulent flow at a height y above a large smooth solid wall under zero pressure gradient along the flow direction necessarily depends upon the height y, the shear stress at the wall τ_w, and the fluid properties ρ and ν. Dimensional analysis gives (Bradshaw, 1976):

$$\frac{U}{u^*} = f_1(Y^*) \qquad (5.6)$$

and

$$\frac{dU}{dy} = \frac{u^*}{y} f_2(Y^+) \tag{5.7}$$

where $u^* = (\tau_w/\rho)^{1/2}$ is the friction velocity, $Y^+ = u^* y/\nu$ is the dimensionless height.

The function f_2 is almost a constant which is equal to $1/\kappa$ when Y^+ is large (see Bradshaw, 1976), so that equation (5.7) becomes:

$$\frac{dU}{dy} = \frac{u^*}{\kappa y} \tag{5.8}$$

Integrating equation (5.8) yields:

$$U = \frac{u^*}{\kappa} \ln y + C_1 \tag{5.9}$$

or

$$\frac{U}{u^*} = \frac{1}{\kappa} \ln Y^+ + C \tag{5.10}$$

where C = 5.5 and κ = 0.4 are constants determined by experiments (see Klebanoff, 1954). Another form of equation (5.10) is:

$$\frac{U}{u^*} = \frac{1}{\kappa} \ln EY^+ \tag{5.11}$$

where E = 9.0.

The log-law wall function has been confirmed by the experiments of Laufer (1954) for channel flow and of Klebanoff (1954) and Wieghardt (1944) for the flow over a flat plate as shown in Fig. 5.2. Clearly, when $Y^+ > 40$, the log-law wall function is valid in a wide range of Y^+.

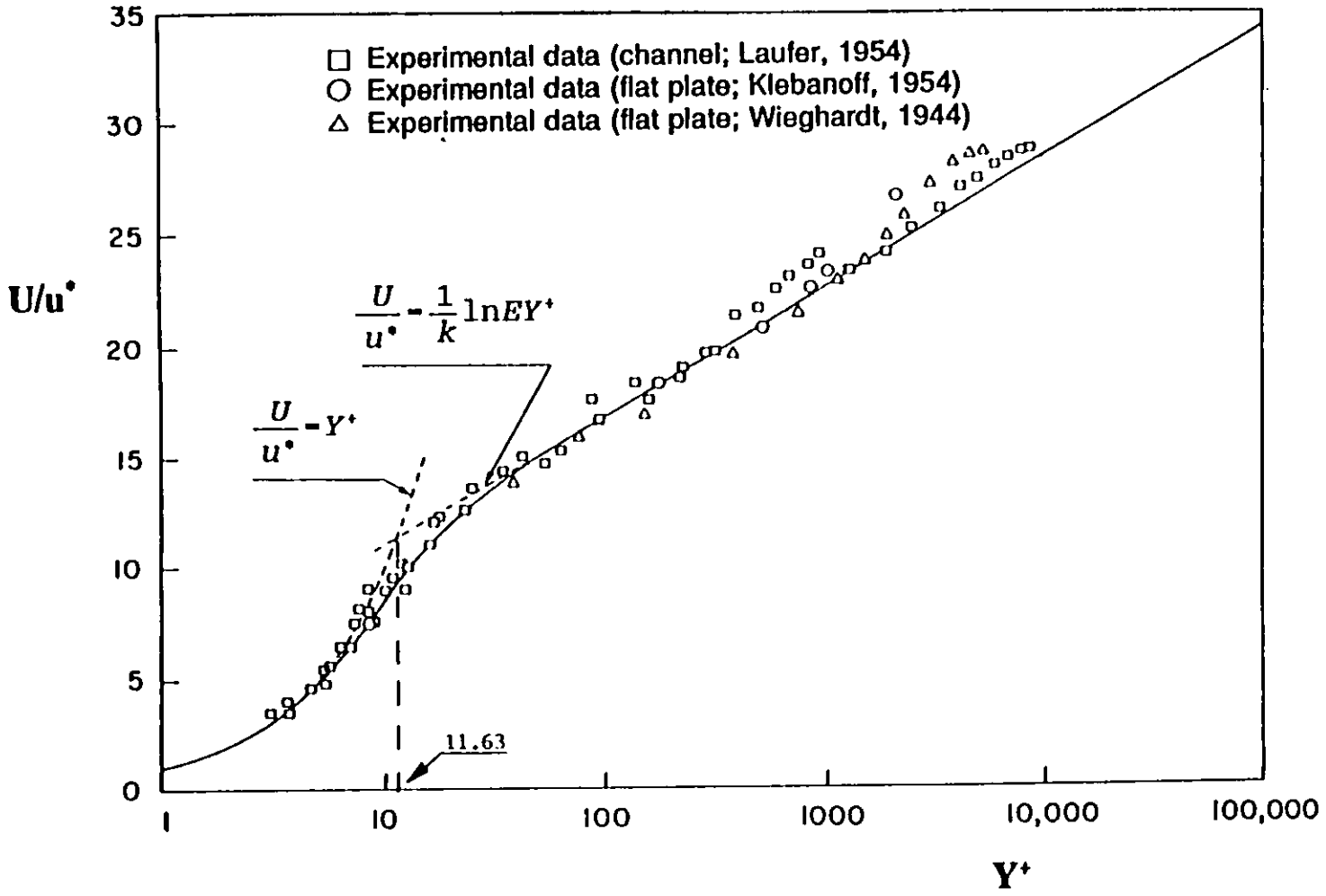

Figure 5.2 Linear-law and log-law wall functions, after Bradshaw (1976).

In equation (5.6), $f_1(0) = 0$ because the velocity components are zero at wall (no-slip). When Y^+ is very small, the viscous effect will prevail so that $f_1(Y^+)$ equals Y^+ and equation (5.6) becomes:

$$\frac{U}{u^*} = Y^+ \tag{5.12}$$

This is because that when Y^+ is very small,

$$\frac{\partial U}{\partial y} = constant = \frac{\tau_w}{\mu} \tag{5.13}$$

or

$$U = \frac{\tau_w}{\mu} y \tag{5.14}$$

Here, the boundary condition $f_1(0) = 0$ is already used. Rearranging equation (5.14) and noticing $u^*y/\nu = Y^+$ and $(\tau_w/\rho)^{1/2} = u^*$, equation (5.12) is obtained.

This linear form wall function near a solid wall is also confirmed by experiments (Klebanoff, 1954 and Laufer, 1954). Comparison of this function with experimental data is shown in Figure 5.2, which shows that the linear-law wall function is valid only in the region $Y^+ < 7$ which is called the viscous sublayer. The linear- and log-law wall functions are valid in viscous sublayer ($Y^+ < 7$) and the log-law region ($Y^+ > 40$) respectively. There is, however, an area where neither function is valid. This region defined approximately by $7 < Y^+ < 40$ is called the buffer layer (Bradshaw, 1976). As an approximation, the linear sublayer and the log-law area are extrapolated into the buffer region so that the turbulent boundary layer can be divided into two regions, namely linear

layer specified by $Y^+ < 11.63$ and log-law area defined by $Y^+ > 11.63$ as shown in Fig. 5.2.

It is noted that the standard log-law wall function is obtained from experiments under zero pressure gradient. It provides the mean flow velocity profile across the fully developed turbulent boundary layer over a very large smooth wall. These assumptions are certainly not generally valid, e.g. when strong second flows are extended into the sublayer (Iacovides, and Launder, 1987), or in separated flows (Rodi, 1991).

The velocity profile of the turbulent flow in the recirculation region behind a backward step (Fig. 5.3) was measured by Adams and Johnston (1988). The velocities were measured in a shear-layer whose thickness is defined by the bottom solid wall and the line connecting the locations of maximum back-flow velocity. The dimensionless velocities (U/u^*) were measured at different locations (x^*), where x^* is the dimensionless distance from the reattachment point normalized by the recirculation length (Fig. 5.3). These velocities versus the dimensionless distance above the bottom wall (Y^+) are presented in different symbols as shown in Fig. 5.4. It is clear that the measured velocity distribution deviates significantly from the logarithmic part of the wall function. The linear distribution, however, seems to be affected only very slightly. A similar measurement of velocity profiles in a recirculation region behind a normal plate and above a splitter plate (Fig. 5.5) was also made by Ruderich and Fernholz (1986). The results were presented in Fig. 5.6 in a similar format as Fig. 5.4. In particular, the

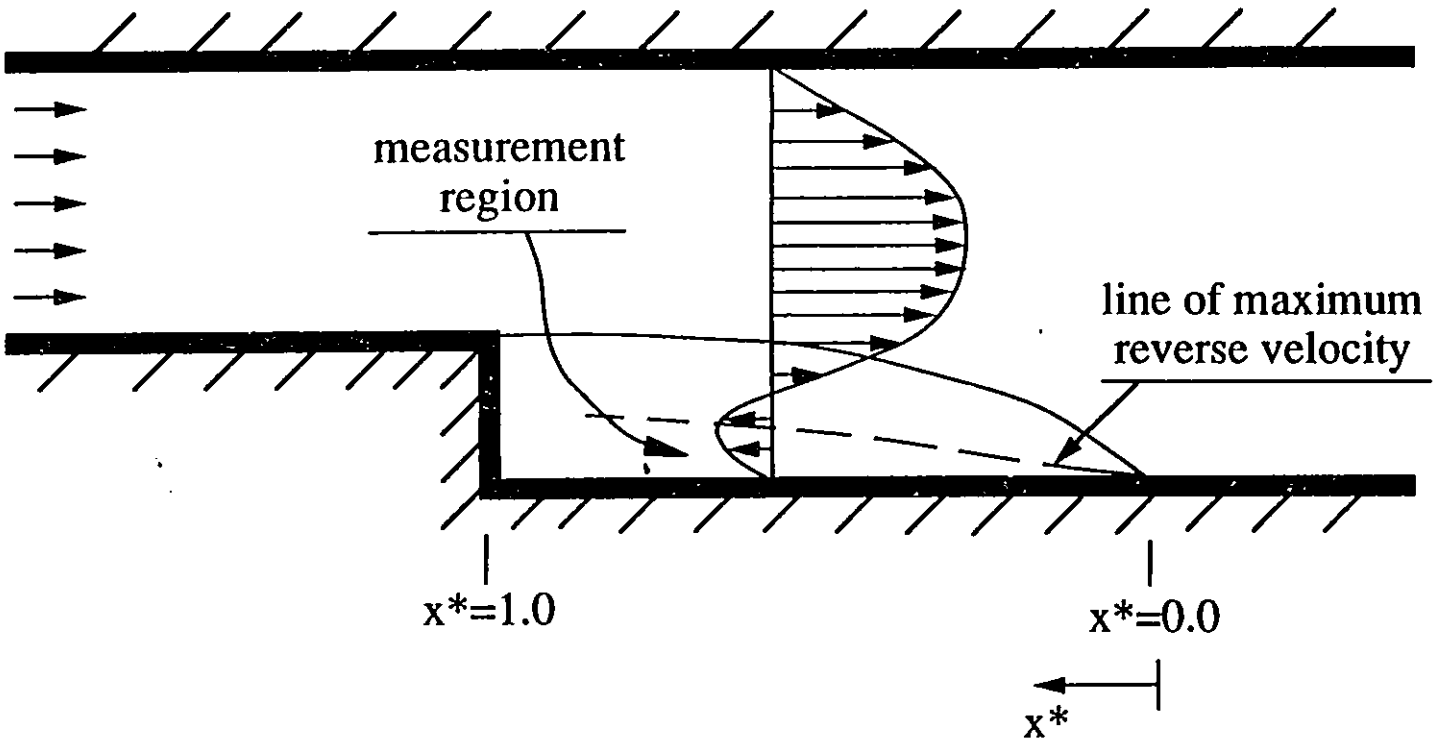

Figure 5.3 The shear-layer behind a step measured by Adams and Johnston (1988).

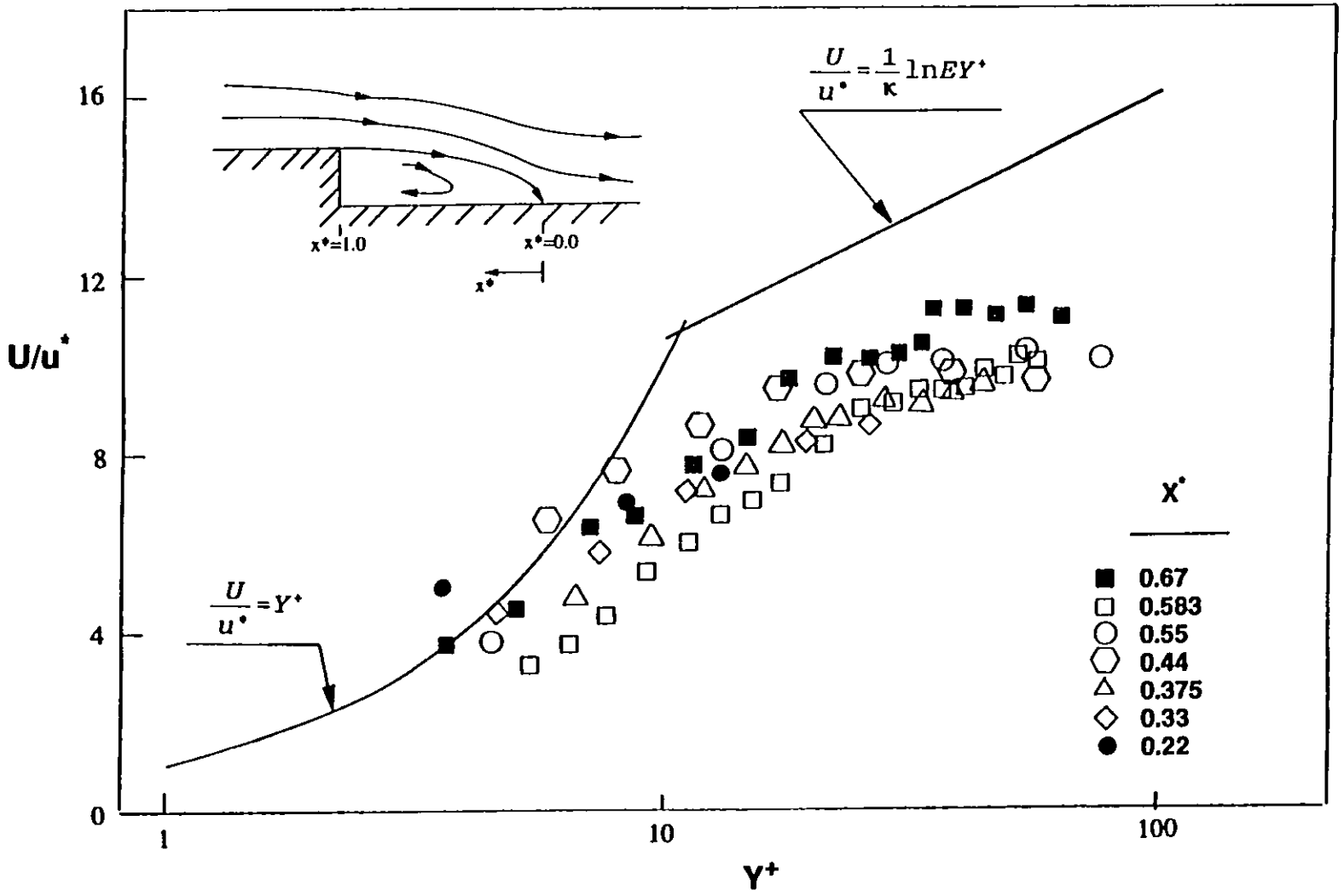

Figure 5.4 Mean flow velocity profiles behind a step at different locations, by Adams and Johnston (1988).

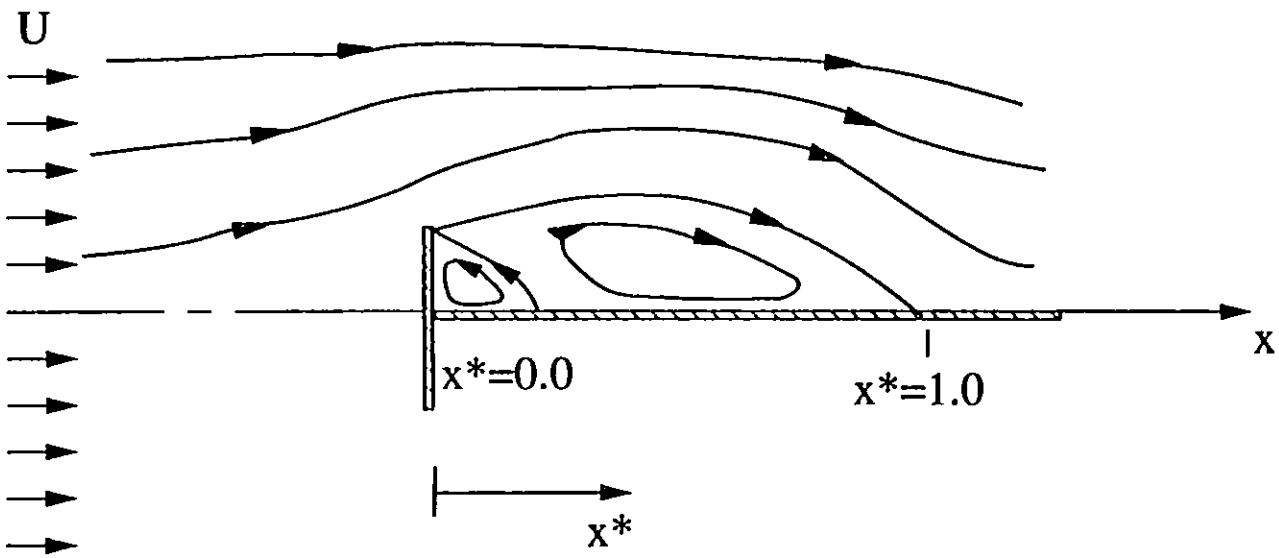

Figure 5.5 Flow behind a normal plate and above a splitter measured by Ruderich and Fernholz (1986).

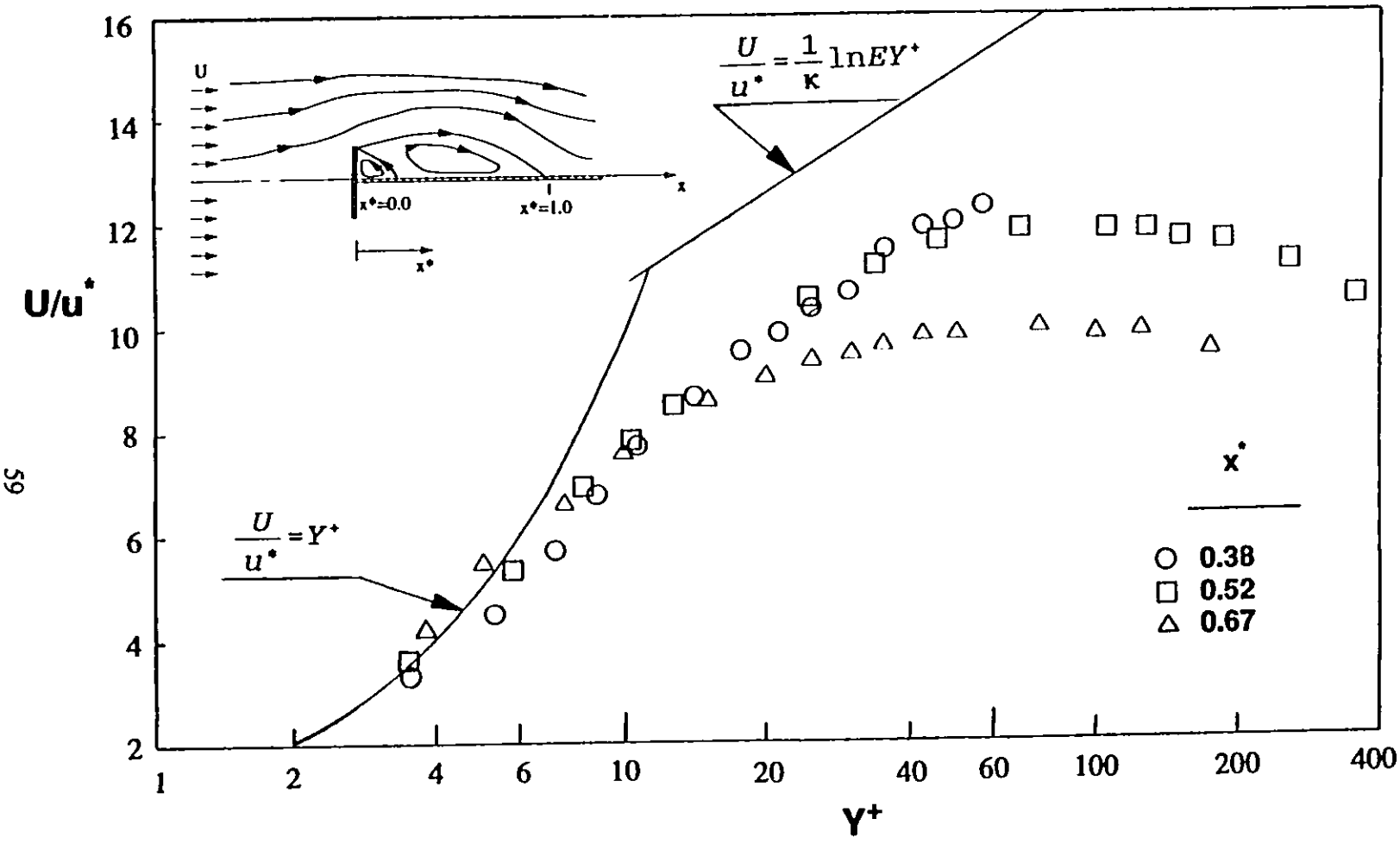

Figure 5.6 Mean flow velocity profiles behind a normal plate, by Ruderich and Fernholz (1986).

dimensionless distance (x^*) is measured from the corner point of the normal plate and the splitter plate. Again, the dimensionless velocity profiles in the area very close to the the wall at bottom, say $Y^+ < 7$, agrees well with the linear-law. In the region farther away from the wall, however, the velocity profiles deviate apparently from the log-law. This indicates that the log-law wall function should be used with care especially in the separation region. The understanding of the limitation of this widely used function is very important in correctly using this function as a solid boundary condition.

In the current study, as the first step, either the linear law or the log-law wall function is used depending on the dimensionless distance of the first grid line from the adjacent solid wall. This is compared with the usual studies (Paterson and Apelt, 1986 and Baetke, Werner and Wengle, 1990) which have only used the logarithmic law. To avoid the errors arising from the inadequate logarithmic law wall function in the near wall region, two-layer methods have been adopted in the present study in evaluating the wind effects on a cubic building as explained in Chapter 9.

5.2.2 Solid boundary conditions

It should be noted that equations (5.11) and (5.12) are valid for the flow of only one direction. For the present study of 3D turbulent flow, the component form of these equations are used. For the calculation of tangential velocity components on the first grid line near a wall, a correction in the source term of the discretized RANS equations is

needed to account for the friction effect from the wall (see e.g. Baetke, Werner and Wengle, 1990). This friction effect is evaluated by the well known wall functions which in their components form (see Murakami, Mochida and Hayashi, 1990) are as follows:

$$U_i = \frac{(\frac{\tau_i}{\rho}) \ln(EY^+)}{C_\mu^{1/4} k^{1/2} \kappa} \qquad (Y^+ > 11.6) \quad (5.15)$$

or

$$U_i = \frac{(\frac{\tau_i}{\rho}) Y^+}{C_\mu^{1/4} k^{1/2}} \qquad (Y^+ \leq 11.6) \quad (5.16)$$

where U_i represents the component of tangential velocity along x_i direction, τ_i is the corresponding shear stress on the wall, Y^+ is the dimensionless distance from the wall to the gridnode expressed as:

$$Y^+ = \frac{C_\mu^{1/4} k^{1/2} d}{\nu} \qquad (5.17)$$

in which d is the distance from the gridnode to the wall. For this case, $d=d_p$ is the distance of the first grid line from the wall. These equations are used to evaluate the components of the shear stress on the wall (τ_i) which will correct the source term of the discretized RANS equations for the calculation of tangential velocities on the first grid line near this wall.

Compared with Paterson and Apelt (1986) and Baetke, Werner and Wengle (1990) who have only adopted the logarithmic law, the current study uses either the logarithmic

law [equation (5.11)] or the linear law [equation (5.12)] to evaluate the wall friction according to the magnitude of the dimensionless distance (Y^+). The calculation of velocities farther away from solid walls uses the finite difference form of RANS equations without correction in the source terms.

5.2.3 Zonal treatment of k and ε

The zonal treatment method by Stathopoulos and Baskaran (1990) has been applied for the formulation of the conditions of turbulence properties (k and ε) near solid boundaries to bridge the flow properties in the turbulent field with those in the viscous sublayer near solid boundaries. According to this method, the wind flow near a solid boundary is composed of two regions. One is the fully turbulent flow region far from solid boundaries and the other is the viscous sublayer (VSL) near the walls and the ground. In the fully turbulent flow region, the k-ε model is applied to obtain the turbulence properties k and ε while in the viscous sublayer (VSL), the turbulence intensity k and its dissipation ε are determined by their values at the edge of the VSL, i.e.

$$k_s = k_{es}\frac{d_s^2}{d_{es}^2} \tag{5.18}$$

$$e_s = \frac{2\nu k_{es}}{d_{es}^2} \tag{5.19}$$

where k_{es} and k_s are the turbulence kinetic energy at the edge and within the VSL

respectively considered at the distances d_{es} and d_s from the solid boundary. The ε_s in equation (5.19) is the energy dissipation at the distance d_s from the wall and ν is the fluid viscosity.

Although the above-mentioned boundary conditions used are only valid for two-dimensional flow over large planes, they seem to work well for the case of a small wind tunnel building model. For the computation of airflow conditions around a full-scale size building, however, these boundary conditions should be represented by the usual wall function method since the distance between first grid line and solid boundary will normally be much larger than the viscous sublayer thickness.

All these boundary conditions are used for the k-ε model method. For the two-layer methods, these boundary conditions can also be used with only a slight change in the expressions as will be explained in Chapter 9.

5.3 Application

To apply the relevant boundary conditions, the program evaluates the position of each grid point according to the building geometries defined by the user. When the point is inside the building, the variables (velocities, pressures, turbulence properties etc) will be fixed at an almost zero value by using a very large number (i.e. Payne-Irons method, see Patankar, 1980) of the order 10^{22}. If this point is on a free boundary, the calculation

will be omitted to keep the initial values as free boundary conditions. If this grid point is on a solid wall, the velocity component normal to this wall will be set to zero (Fig. 3.1). If this point is on the first grid line near a solid boundary, the solid boundary conditions for velocity components, i.e. equation (5.15) or (5.16) will be used depending on the dimensionless distance Y^+. If this point is inside the VSL, equations (5.18) and (5.19) will be used to obtain k and ε.

These principles can be used for both rectangular and L-shaped buildings because the program developed is applicable to arbitrary buildings composed of either one or two rectangular blocks (see Fig. 3.2).

Chapter 6

VALIDATION OF THE CODE

6.1 The Code RETWIST

The current program RETWIST which is a REvised version of the program named TWIST designed in the Centre for Building Studies of Concordia University includes a subroutine generating the grid system automatically, a subroutine defining and calculating the initial values of the mean flow velocities (U_i) and the turbulence properties (k, ε and ν_t) and a subroutine specifying the boundary conditions for buildings of any arbitrary shape composed of two rectangular blocks. These currently designed subroutines are combined with the equation solver taken from TWIST which adopts the SIMPLE method (Chapter 4). The SIMPLEC method (Doormaal and Raithby, 1984) which avoids the underrelaxation required by SIMPLE method, has also been tested with little influence on computational time and numerical accuracy.

Unlike TWIST which can only be applied to the computation of the airflow around a single rectangular building with the k-ε model and the RANS equations, the new revised code named RETWIST (REvised TWIST) can be applied to the computation of the turbulent airflow around two buildings or one building composed of two blocks (see Fig. 3.2 in Chapter 3). The two-layer method adopting the modified k-ε model or one-equation model for the inner flow region near building walls and the k-ε turbulence

model for the external flow region (Chapter 9) can also be applied for the computation of wind flow around a rectangular building by the current program.

6.2 Validation of the Code with a Turbulent Flow Problem

6.2.1 Specification of the problem

One of the most often used problem for the validation of turbulence models is the turbulent flow in a two-dimensional channel (Deardorff, 1970, Rodi, 1980 and Chien, 1982) because of the abundant experimental data available and the simplicity of the problem which is also very typical. In the current validation, this typical problem has also been considered. With the exception of free boundary condition specifications, no other changes is required to the code to calculate this problem. By reading in zero heights of buildings (see Chapter 3), the problem is solved numerically with the present code which adopts the RANS equations and the k-ε model. The computational domain is 400 cm long by 120 cm wide by 7 cm high and the grid system used is 59 x 29 x 39. To save computational time and computer storage, only half channel height was considered. The experimental data for this geometry, i.e. a channel flow without a free surface, were available by Laufer (1951), see Fig.6.1.

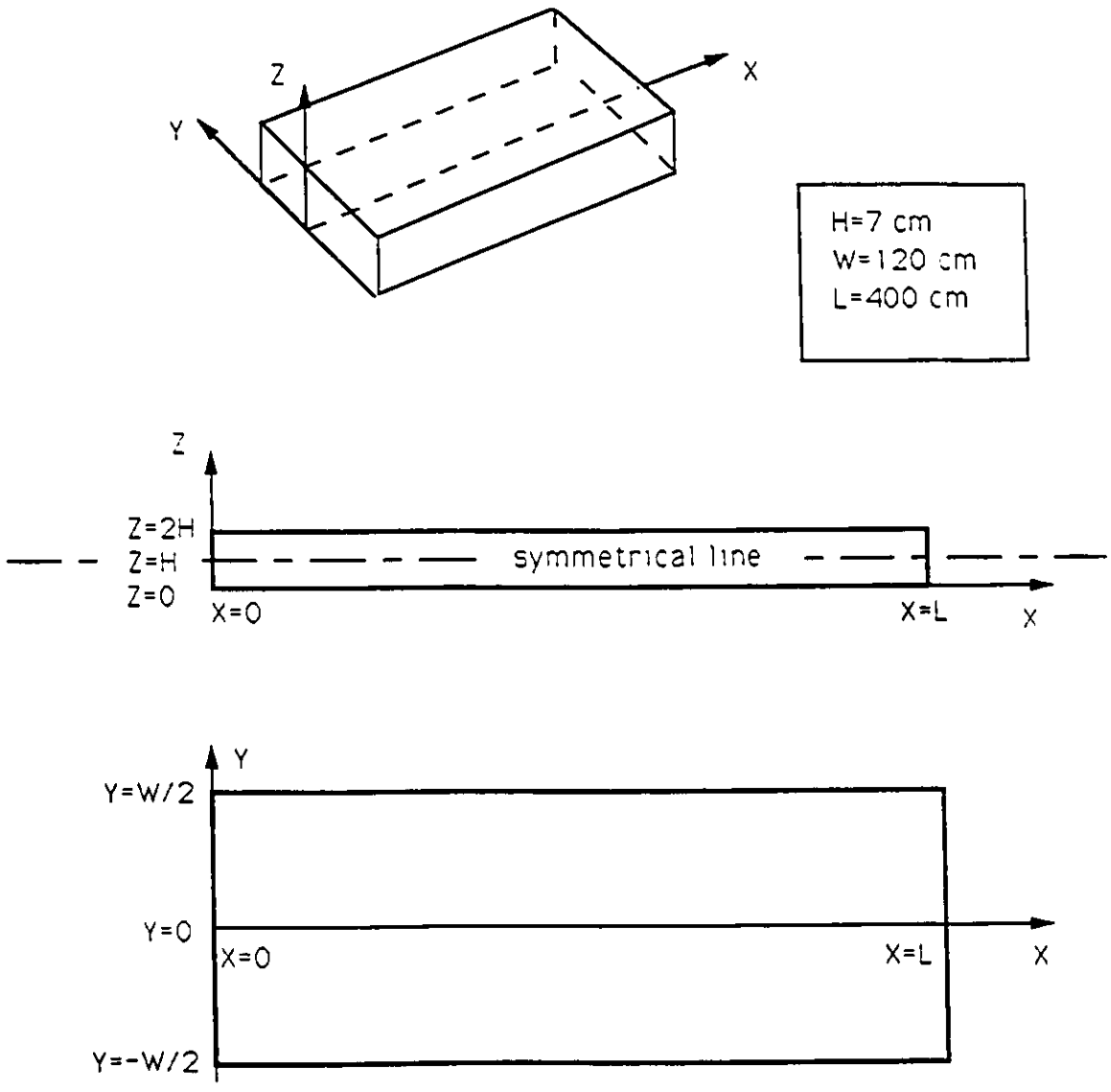

Figure 6.1 The computational region of the 2-D turbulent flow in a channel.

6.2.2 Boundary conditions

i) At the inlet, the mean flow is assumed to be uniform, i.e.

$$U=Const. \tag{6.4}$$

$$W=0 \tag{6.5}$$

except the first grid line above the ground where the velocity is assumed to follow the linear distribution. The turbulence properties corresponding to this given velocity distribution (Chapter 5) are used as the inlet boundary conditions of k and ε.

ii) At the outlet, the free-slip condition is used, i.e.

$$\frac{\partial U}{\partial x}=0 \tag{6.6}$$

$$W=0 \tag{6.7}$$

$$\frac{\partial k}{\partial x}=0 \tag{6.8}$$

$$\frac{\partial e}{\partial x}=0 \tag{6.9}$$

iii) On the top, symmetry condition is used, i.e.

$$\frac{\partial U}{\partial z}=0 \tag{6.10}$$

$$W=0 \tag{6.11}$$

$$\frac{\partial k}{\partial z}=0 \qquad (6.12)$$

$$\frac{\partial \epsilon}{\partial z}=0 \qquad (6.13)$$

The boundary conditions for pressure are as follows (Laufer, 1951):

a) at inlet:

$$\frac{P}{\rho}=0.18\left(\frac{U_o^2}{2}\right) \qquad (6.14)$$

where U_o is the fully developed velocity at the centre of the channel and 0.18 is the pressure drop coefficient estimated from Laufer's measured data.

b) at outlet:

$$\frac{P}{\rho}=0 \qquad (6.15)$$

c) on top, linear distribution of pressure along x-direction is assumed (Laufer, 1951 and Hussain and Reynolds, 1975).

The solid boundary conditions adopted are exactly the same as those discussed in Chapter 5. To ensure the two-dimensionality of the flow, the velocity component along y-direction has been fixed to an almost zero value by using the Payne-Irons method. The computation was terminated after 210 iterations when all the relative residues (Chapter 4) were below 0.02. The CPU time used was about 10 hours.

6.2.3 Results and discussion

The computed results for the fully developed turbulent flow in a channel have been compared with the experimental data by Laufer (1951). The Reynolds number based on the centreline velocity (U_0), the half-height of the channel (H) and the air viscosity (ν) is about 60,000 for both the computation and the experiment. Since the experimental results vary from different tests (Chien, 1982), another set of experimental data by Clark (1968) is also included for comparison purposes. Note that the Reynolds number in this case is about 50,000 while the general experimental conditions of Clark (1968) are very similar to those of Laufer (1951). The results presented are taken along a vertical line through the middle of the width of the channel and in a cross-section very close to the outlet (x=370 cm) where the flow is ensured to be fully developed and two-dimensional.

The computed fully developed mean flow velocity profile has been presented in Fig. 6.2 and compared with the experimental data by Laufer (1951) and Clark (1968). Results show that fairly good agreement is generally found.

The same comparison is also made for the turbulence kinetic energy (k) in Fig. 6.3. The turbulence kinetic energy presented here has been normalized by $\frac{1}{2}U_0^2$ for proper comparison with the experimental data by Laufer (1951) and Clark (1968). In both experiments, the turbulence intensity was presented as root mean square (r.m.s.) of the fluctuations of velocity components, i.e. $\sqrt{\overline{u'_i{}^2}}$; the k values in Fig. 6.3 have been obtained

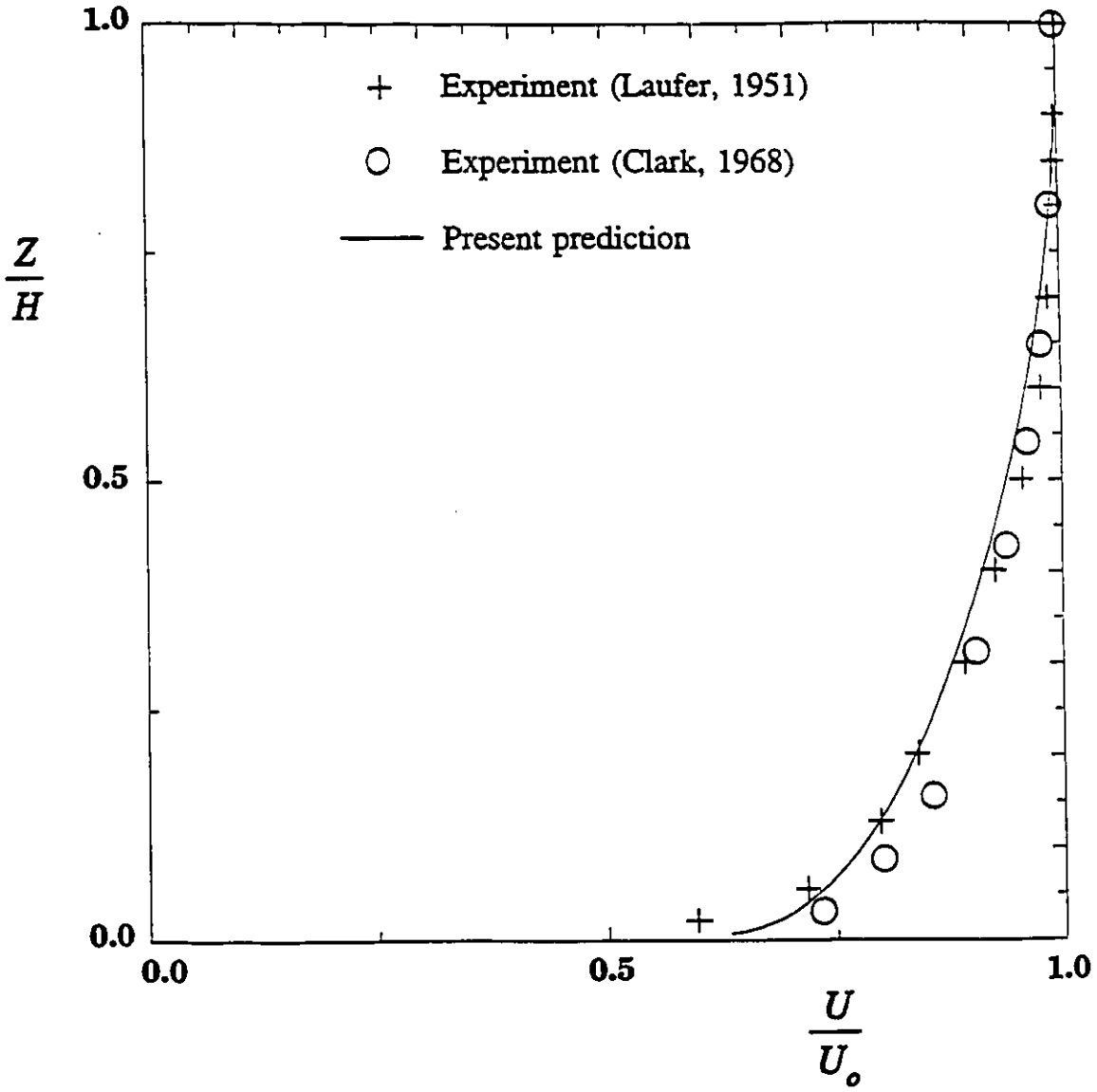

Figure 6.2 Mean velocity profile of a fully developed turbulent flow in a 2-D channel.

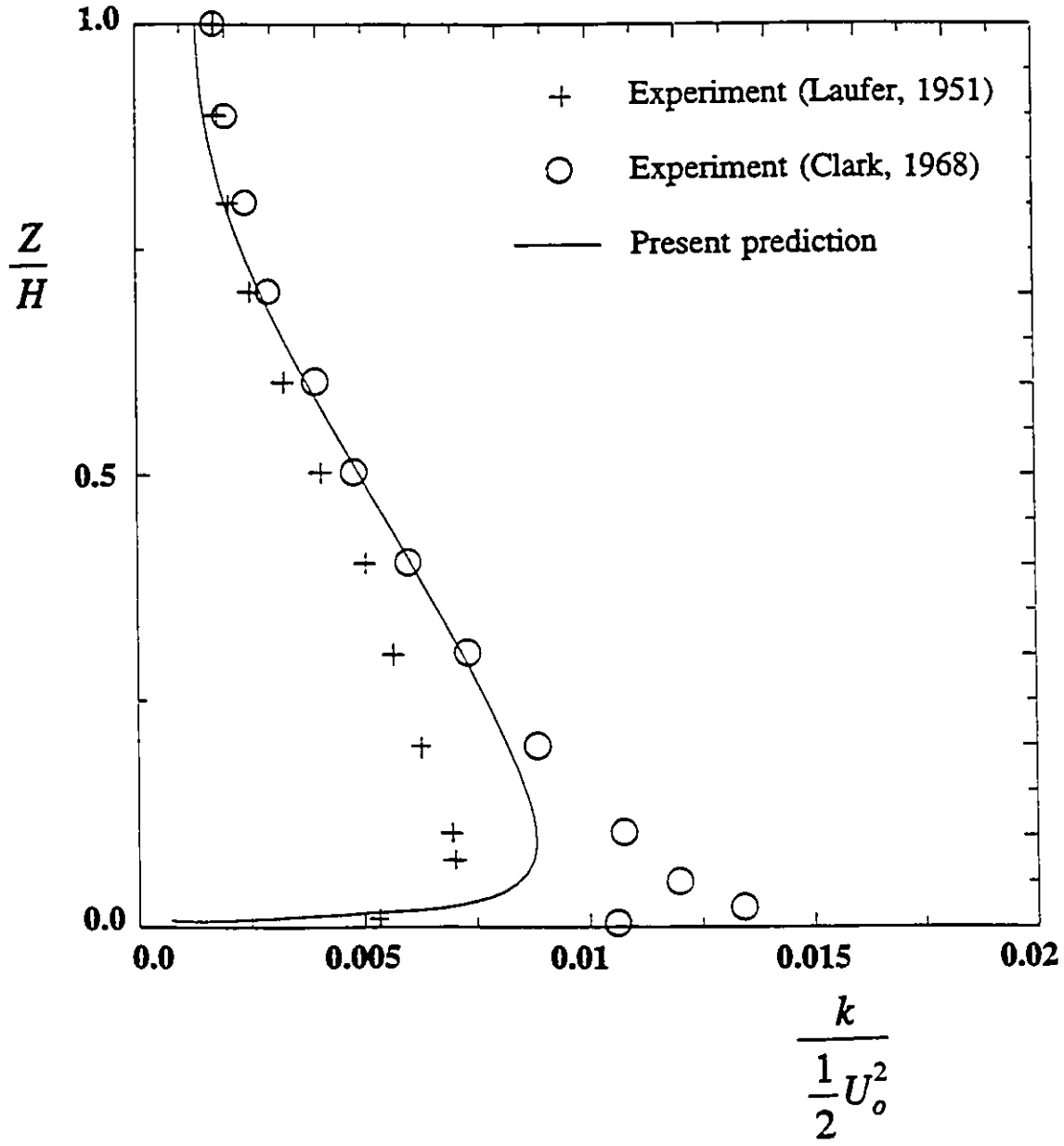

Figure 6.3 Turbulence kinetic energy profile of a fully developed turbulent flow in a 2-D channel.

from these r.m.s. values by

$$k=\frac{1}{2}\sum_{i=1}^{3}\overline{u'^2_i} \qquad (6.16)$$

Results have shown that the agreement between the experimental and the currently computed data is reasonably good regardless of the discrepancies that exist among the different experiments (Chien, 1982).

6.3 Conclusions

The validation of the present code RETWIST by computing the problem of two-dimensional turbulent flow in a channel has been carried out. The results have shown that the current program works well for turbulent flow as far as the mean velocity and the turbulence kinetic energy are concerned.

Chapter 7

COMPUTATION OF WIND CONDITIONS AROUND L- AND Z-SHAPED BUILDINGS

7.1 Introduction

Although the L-shape and Z-shape are common building geometries, there are no numerical results ever published for them while experimental data for buildings with such shapes and different wind directions are very limited. The present study has obtained numerical results for the wind conditions around a plan view L-shaped, Z-shaped, and a stepped-roof building (L-shaped in cross-section). The numerical results for the L-shaped building in cross-section have been compared with the experimental data obtained by Stathopoulos and Luchian (1990). Unfortunately, no experimental data were available for the plan-view L-shaped and Z-shaped buildings for comparison purposes. However, comparisons made with other cases have generated a fair degree of confidence in the present numerical work.

The stepped-roof building considered in the present study is specified by setting W1=W3=0 and H1=25 mm, H2=50 mm, W2=100 mm and L1=L2=75 mm (see Fig. 3.2). This building corresponds to a 1:400 scaled model of a full-scale building with H1=10 m, H2=20 m, W2=40 m, L1=L2=30 m. The plan view L-shaped building in the present calculation is defined by setting W3 to zero and L1=L2=W1=W2=75 mm, H1=H2=50

mm. Figure 7.1 shows both L-shaped building configurations considered in this study.

7.2 Methodology

The grid arrangement used for the present calculation is the rectangular grid system since this is the most "body-fitted" system for buildings composed of rectangular blocks and is easy to use. This rectangular grid system is generated through the procedure presented in Chapter 3.

Since the flow properties change drastically near the windward corners of building roof just because of the high vorticity behind them, very small distances from the first grid line to roofs and front walls have been chosen. Such distances for side walls and back walls are larger in order to save computational time and storage. In particular, compared with the usual values of 5 mm to 15 mm for this distance ($d_p=d_o/2$) - see e.g. Paterson and Apelt (1990), Murakami (1990) and Baskaran and Stathopoulos (1989) - the present study for L-shaped building cases has used d_p = 0.7 mm for roof, 1.5 mm for front wall, 3.5 mm for side and back walls and 3 mm for ground surface.

The governing equations used are the Reynolds-averaged Navier-Stokes equations and the standard k-ε turbulence model, i.e. equations (4.1), (4.2), (4.3), (4.4) and (4.6). These are nonlinear steady state equations solved by iteration. They are first integrated over appropriate control volumes on the staggered grid system (see Chapter 4 and Fig.

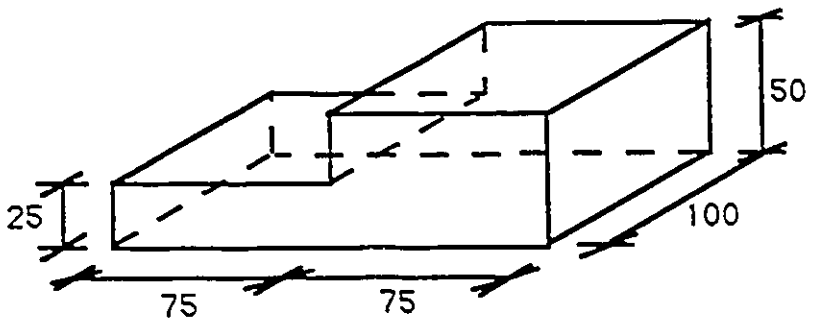

a) Stepped roof building

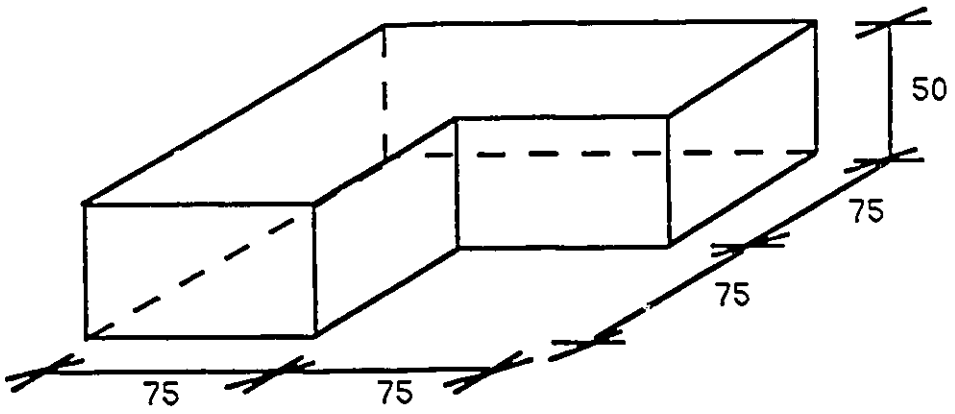

b) Plan-view L-shaped building

Figure 7.1 L-shaped buildings considered.

3.1, Fig. 4.1 and Fig. 4.2), and the discretized equations obtained are solved by the well known SIMPLE method (see Chapter 4 and also Patankar, 1980). Adequate boundary conditions outlined in Chapter 5 are also used in the calculation. Since the buildings considered are of complex shapes, special care should be taken in the computational process - see Chapters 3 and 5.

The extent of the typical computational domain for the stepped-roof building case is 2800 mm along x, 850 mm along y and 500 mm along z. Although this computational domain appears large for this building, it has been used to ensure power-law velocity profile free boundary conditions. The grid used has 47x31x29 nodes.

All the computations were carried out by using the VAX station 3100 model 76 system of the Centre for Building Studies, Concordia University. A typical run takes about 120 minutes CPU time.

7.3 Results and Discussion

7.3.1 Cross-section L-shaped building

The wind conditions around the L-shaped building in cross-section (stepped-roof building) and the plan view L-shaped building - see Fig. 7.1 - have been numerically simulated and the results are presented in this section. Pressures on building surfaces are

presented in terms of pressure coefficients, i.e. pressures normalized by the upstream dynamic pressure at roof height (the higher roof for the stepped-roof building) and compared with experimental data. The experimental results from Stathopoulos and Luchian (1990) have been re-arranged for the purpose of present comparisons.

Computations for the stepped-roof building have been attempted for different wind directions from 0° to 180°. Figure 7.2 shows the numerically predicted velocity vector field on the cross-section through the centre of the stepped-roof building for 0° azimuth. The recirculation flow region behind the building, the upward wind velocities near the windward corners and the reverse flow in front of the windward wall near ground are clearly predicted. However, the program failed to predict the reverse flow region after separation at the windward edges of both roof sections. This is possibly due to the inadequacy of the k-ε model for the flow in this high vorticity region and the two-dimensional nature of boundary conditions used in the simulation. However, since this reverse flow region is very small for the case of a low-rise building, the final results have not been affected significantly by this misrepresentation.

The numerically predicted pressures in the form of pressure coefficient contourlines on the building envelope are shown in Fig. 7.3. Results indicate that there is a zero pressure contourline normal to the wind direction in the centre of lower roof. This divides the lower roof into two parts: the upwind part with negative pressure and the downwind part with positive pressure. The latter is related to the high reduction in wind

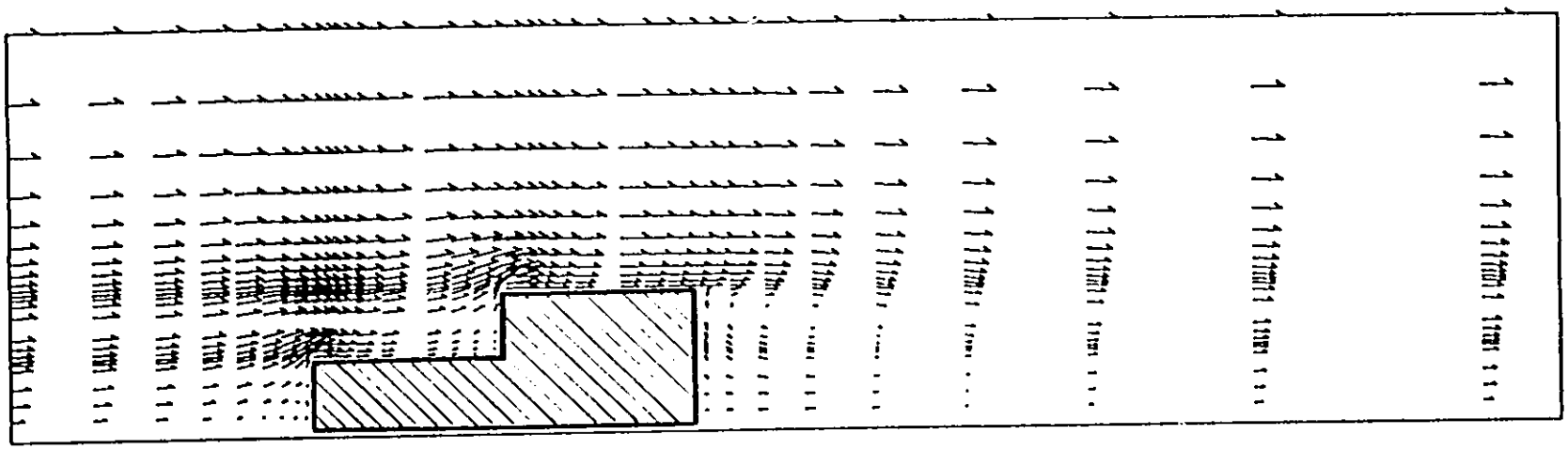

Figure 7.2 Mean flow velocity field on the cross-section of a stepped-roof building (0^0 azimuth).

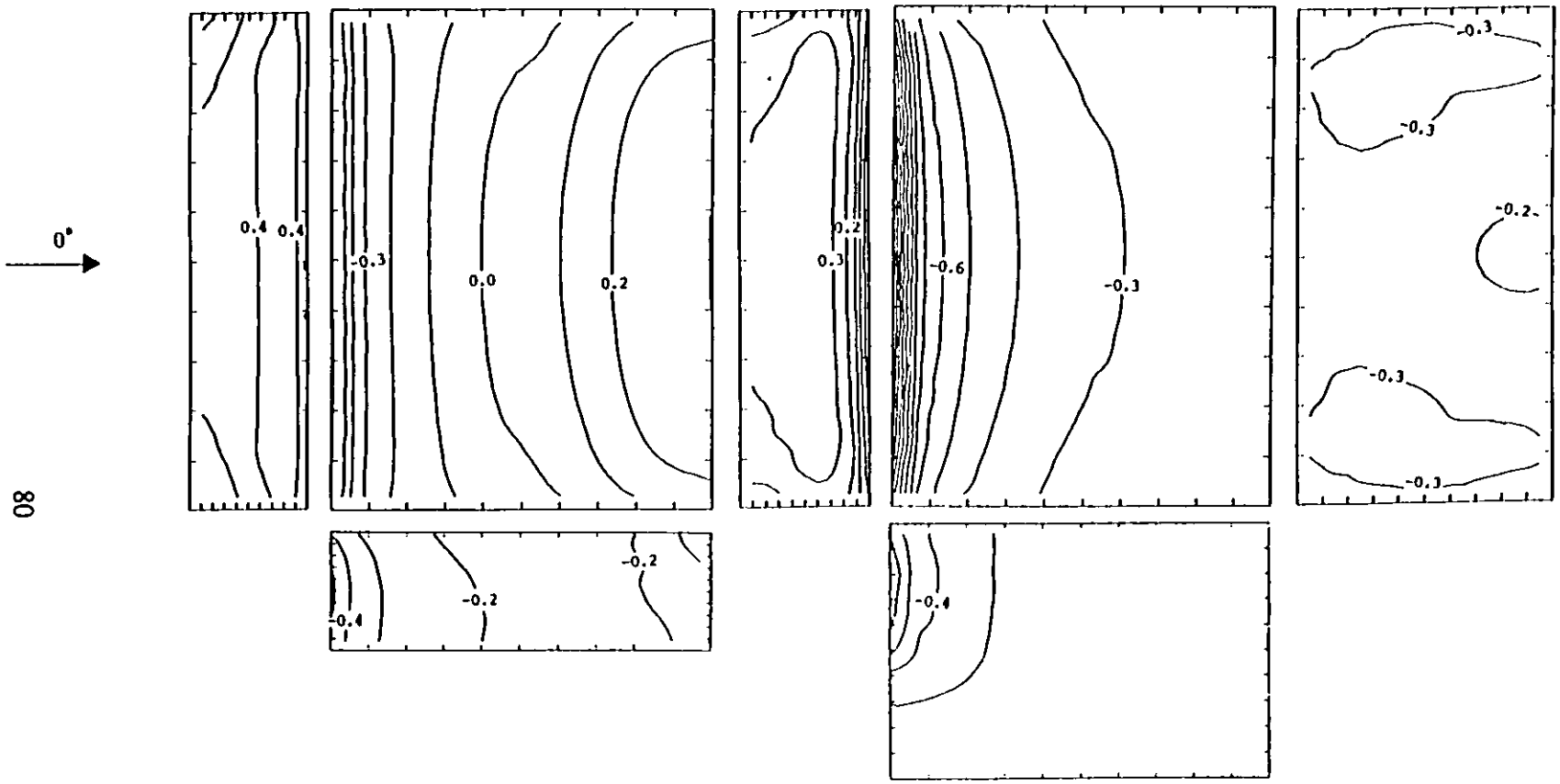

Figure 7.3 Contours of pressure coefficients on the envelope of the stepped-roof building (0^o azimuth).

velocity mainly caused by the roof step of the L-shaped buildings. Since the flow is symmetrical, the pressure coefficients on side walls are presented only for one side. Very dense pressure coefficient contourlines, indicating high pressure gradients, exist in the region near the windward edge of the higher roof as well as on the upper part of the higher front wall. Negative pressures on the back wall are uniformly distributed as would be expected in the wake region.

The profile of wind-induced pressure coefficients along the centreline and the edgeline of the roof is shown in Fig. 7.4, compared with the experimental data from Stathopoulos and Luchian (1990). The agreement between numerical results and experimental data is very good for the centreline with some underestimation of suction generally shown by the computed data along the edgeline. Figure 7.5 shows the variation of pressure coefficients along the centreline on the front and the back walls. The figure shows a reasonably good agreement between numerical results and the experimental data except for pressures on the top of the step where negative pressures were predicted by the computation. This may be due to the location of grid lines in this region. Recall that the first grid point is 1.5 mm upwind of the step and only 0.7 mm below the high roof section.

The results for 60^{0} azimuth have been presented and compared with experimental data as shown in Figs. 7.6 and 7.7 in the same format with Figs. 7.3 and 7.4. Figure 7.6 shows that the zero pressure contourline still exists on the lower roof but becomes very

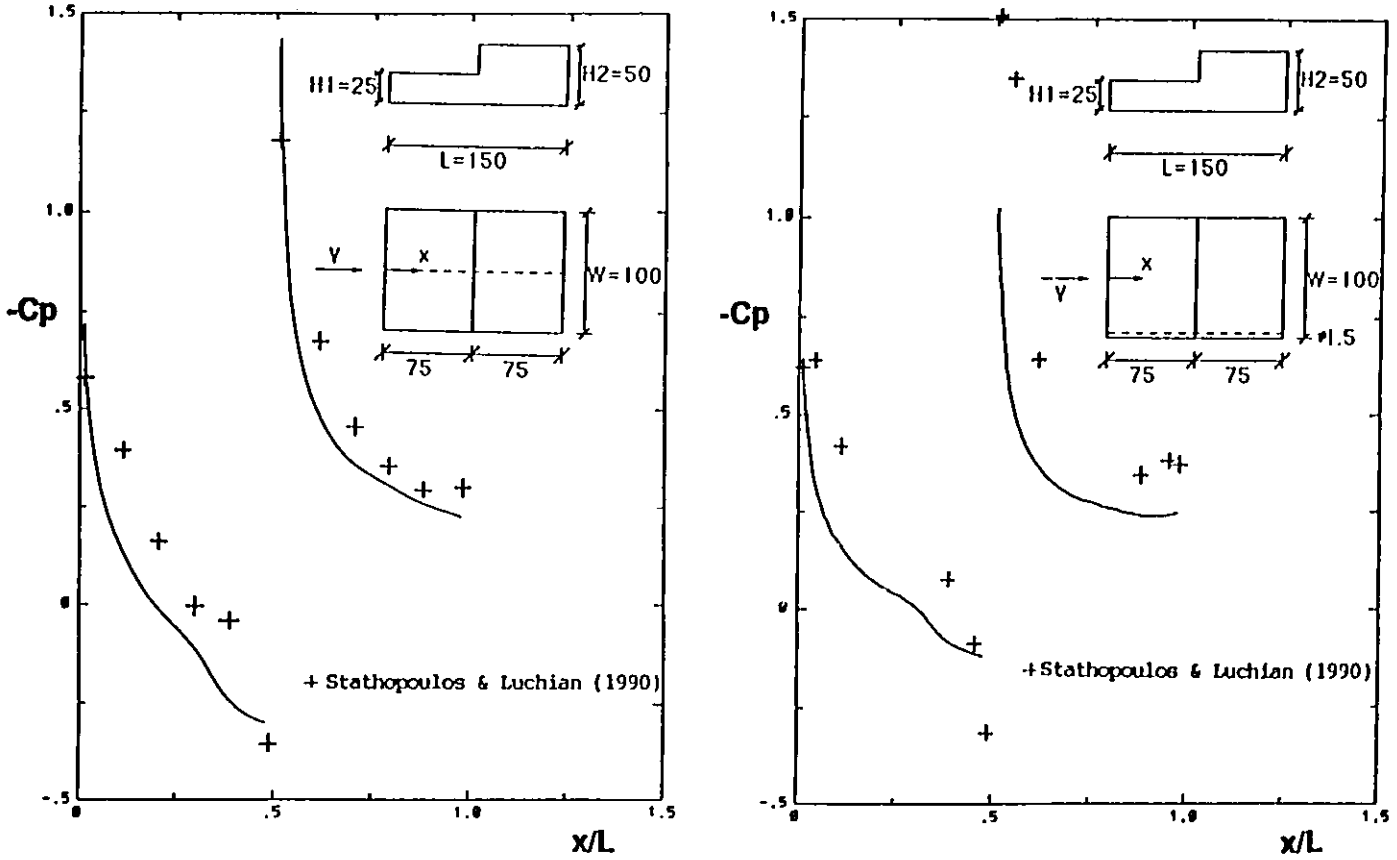

Figure 7.4 Pressure coefficients on the roofs of the stepped-roof building (0^0 azimuth).

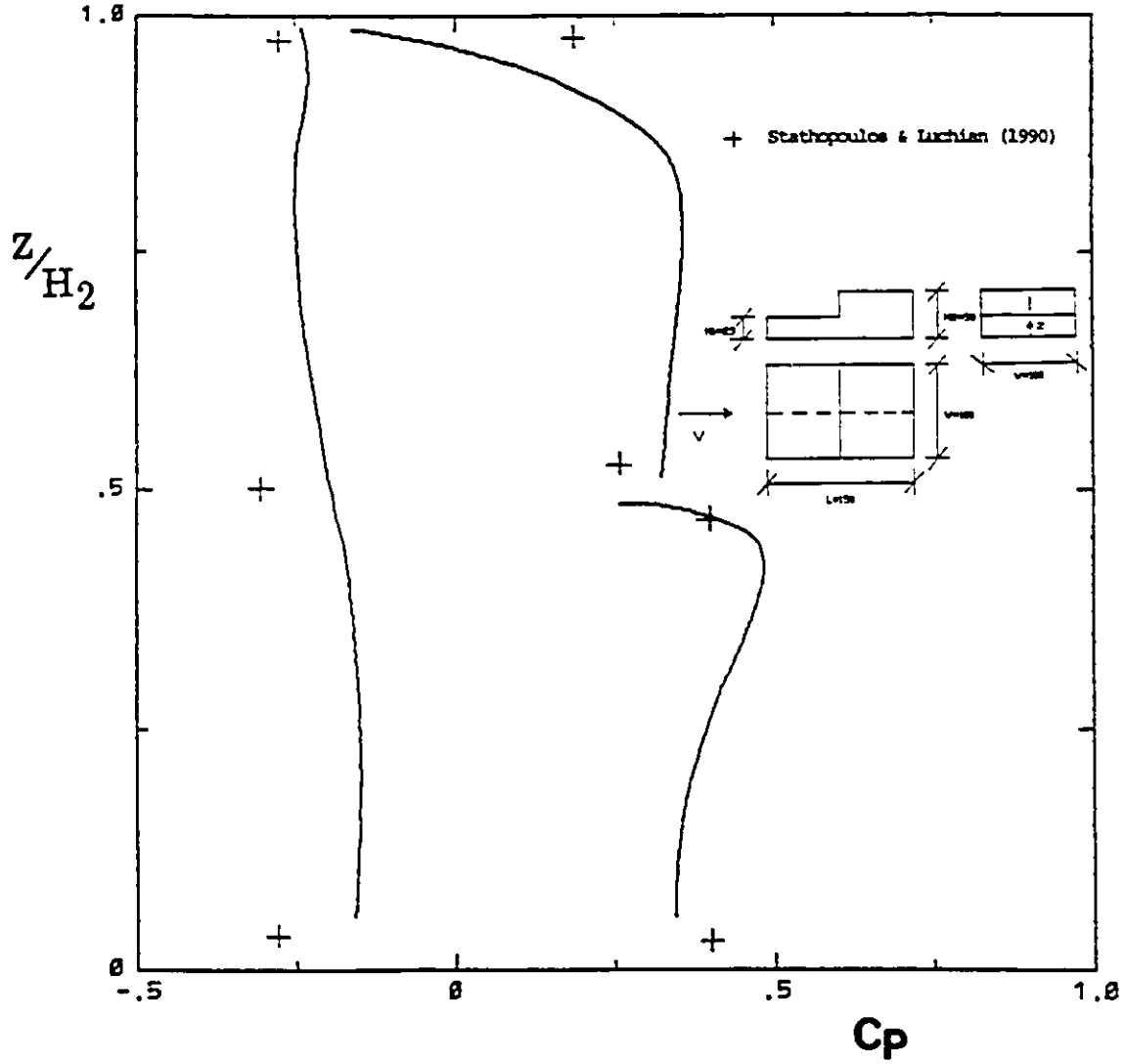

Figure 7.5 Pressure coefficients on the front and back walls (0° azimuth).

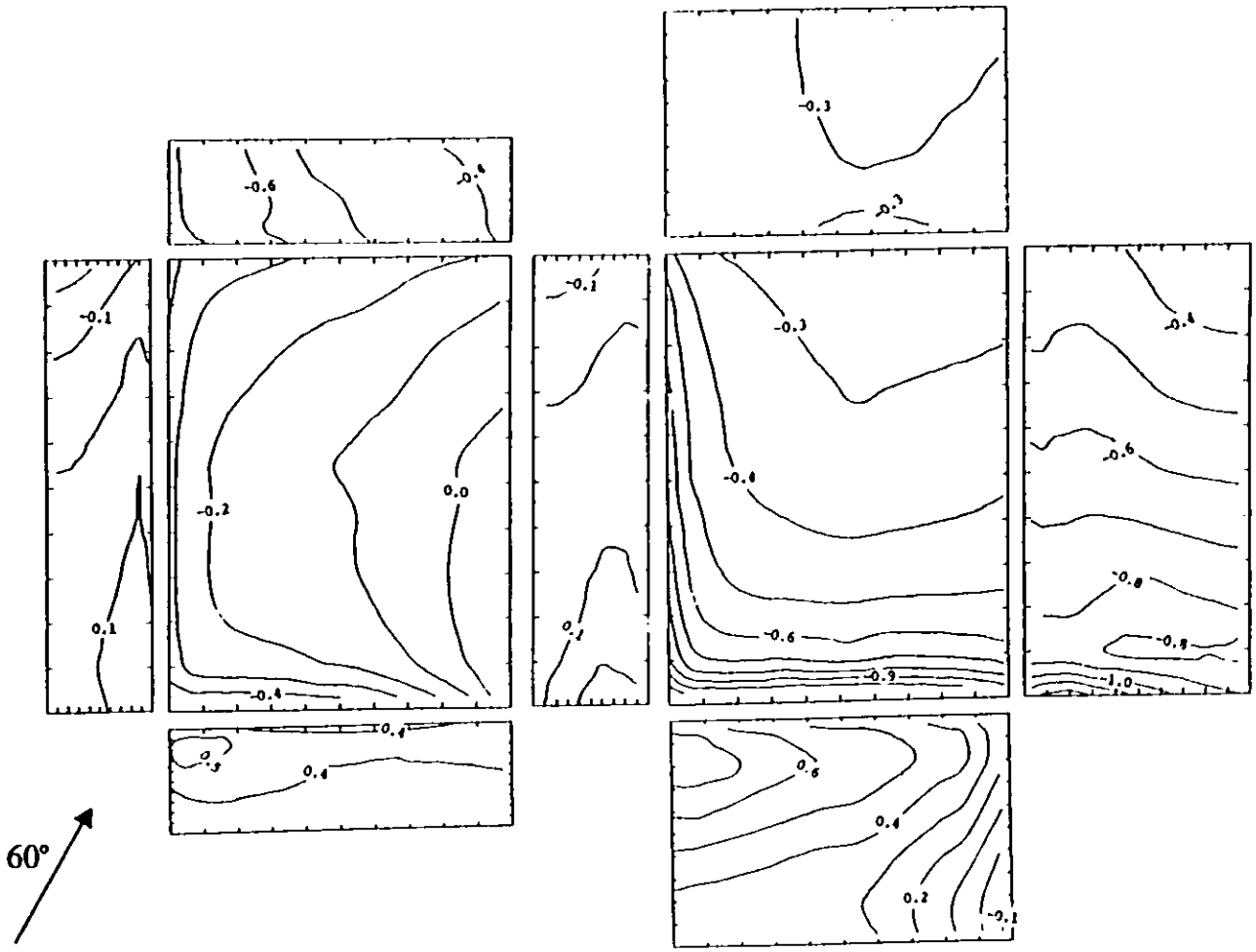

Figure 7.6 Contours of pressure coefficients on the envelope of the stepped-roof building (60° azimuth).

close to the roof step. It also shows that the highest positive pressures on the front wall and the step wall are no longer in the middle but moved upstream near the windward corners. The negative pressures on the back wall show a significant gradient due to the obliqueness of the wind whereas the negative pressure on the downwind side wall is relatively uniform. Figure 7.7 shows the pressure coefficient distribution along the centreline and the edgeline of the roof. Regarding the centreline, the general agreement is good with some underestimation of negative pressures by the numerical simulation mainly in the low roof region. As far as the edgeline is concerned, the pressures are not predicted properly. In particular, the suctions on the lower roof are significantly underestimated by the numerical simulation. Likewise, on the higher roof, the computed data show a smooth change while the experimental data show a high gradient. This suggests that the k-ε model and the two-dimensional boundary conditions may not be representative for this high vorticity region. Rodi (1980) has also stated that the k-ε model needs substantial "massage" to model properly recirculating flow regions. The numerical false diffusion due to the skewness of the air flow to the grid lines might also be a reason for this discrepancy (Patankar, 1980). It should be noted that a systematic grid refinement investigation carried out for a rectangular building model, as will be discussed in Chapter 8, has shown no improvement of the computed pressures by a grid arrangement more refined than that used in the present work.

Most of the previous studies of computational wind engineering refer only to normal wind direction since this represents the simplest flow conditions taking the

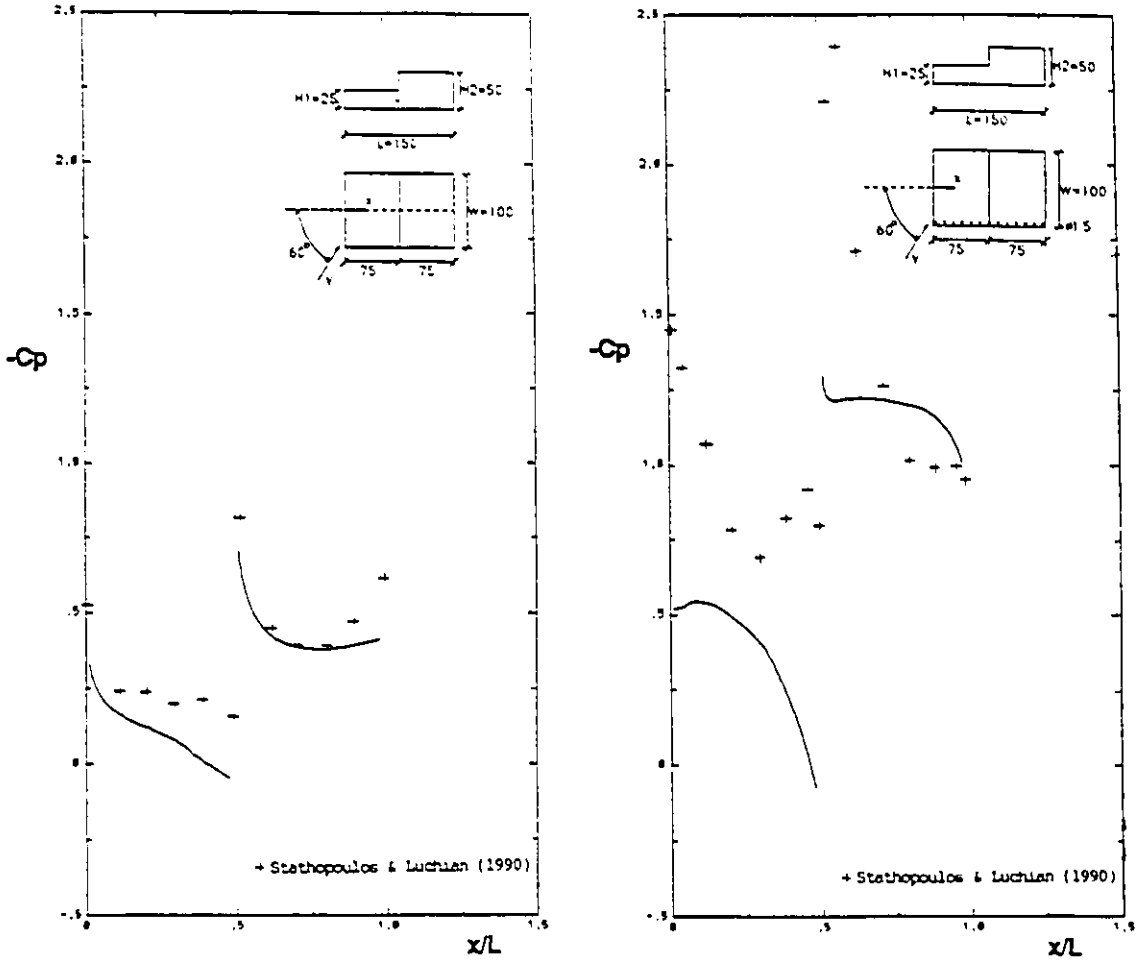

Figure 7.7 Pressure coefficients on the roofs of the stepped-roof building (60° azimuth).

advantage of symmetry and, generally, the most critical overall load effects. In the present study, the effect of different wind directions on the numerical simulation of wind conditions around a stepped roof building has been examined. In addition to the results for 60° azimuth presented in Figs. 7.6 and 7.7, the computed wind pressure at 6 typical positions on the roof surfaces of a stepped roof building has been presented in Figs. 7.8 to 7.13 for different wind directions and compared with the experimental data obtained in wind tunnel tests by Stathopoulos and Luchian (1990). The distance from the first grid line to roof surface (d_p) is 1 mm for this series of computations.

The comparison for a corner point (point 1) on the lower roof is shown in Fig. 7.8. This figure shows that the high suction at this corner point is generally underestimated especially for the critical attacking angles which made this point locate in the windward edge area. The measured suctions at the edge locations (point 2 and point 5) on the lower roof were also underestimated by the current computation but less severely as shown in Figs. 7.9 and 7.10. Actually, the general agreement between the numerical results and the experimental data is reasonable for most of the wind directions.

The wind pressure at three typical positions on the higher roof surface was presented in Fig. 7.11 to Fig. 7.13 in the same format with Fig. 7.8 to Fig. 7.10. Figure 7.11 shows wind pressure under various wind directions for a corner point (point 3) on the taller roof. The suction at this point is well predicted when the point is at a leeward position. However, large discrepancies are found when the point becomes windward

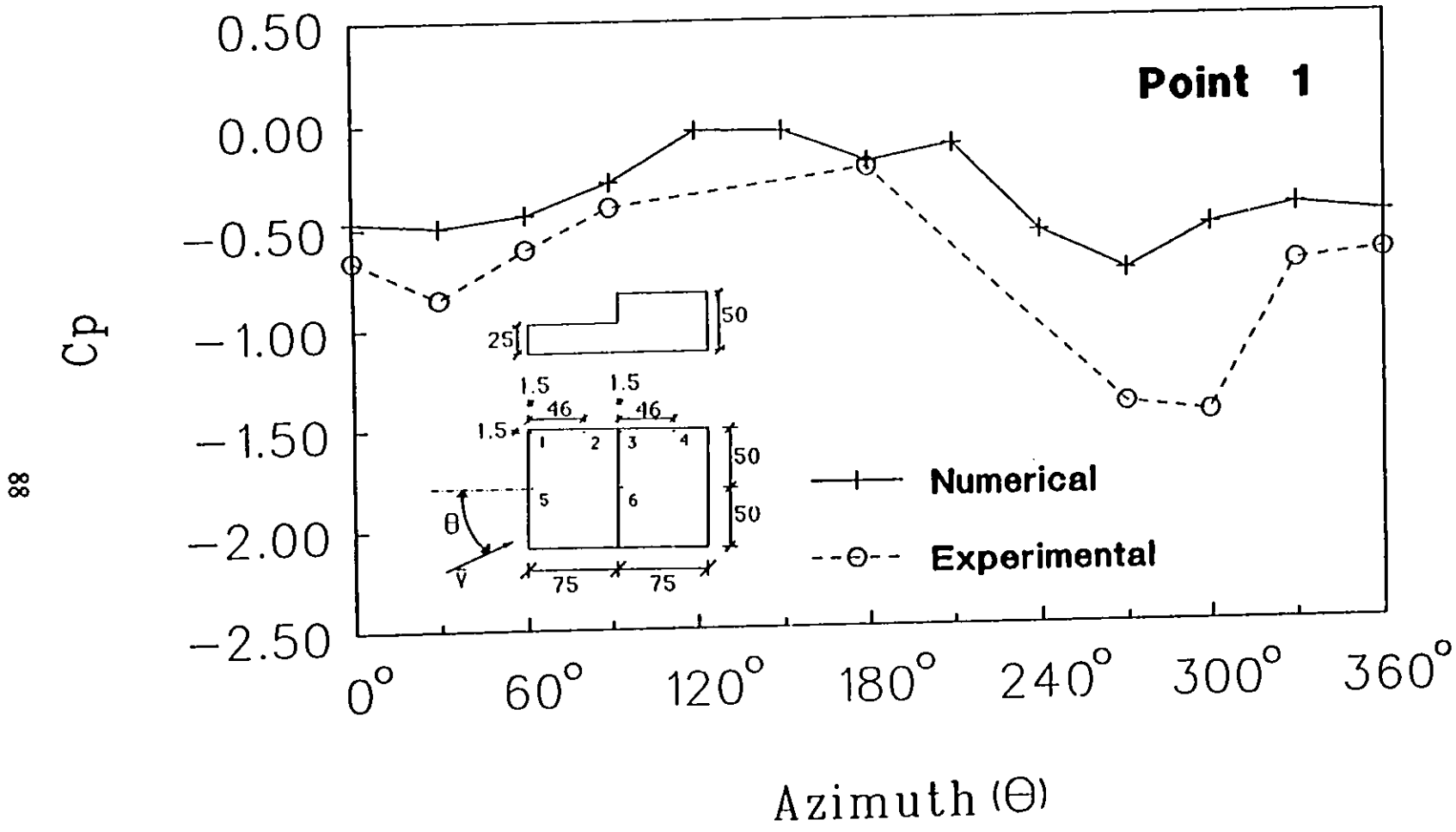

Figure 7.8 Pressure coefficients under various wind directions (corner point, lower roof).

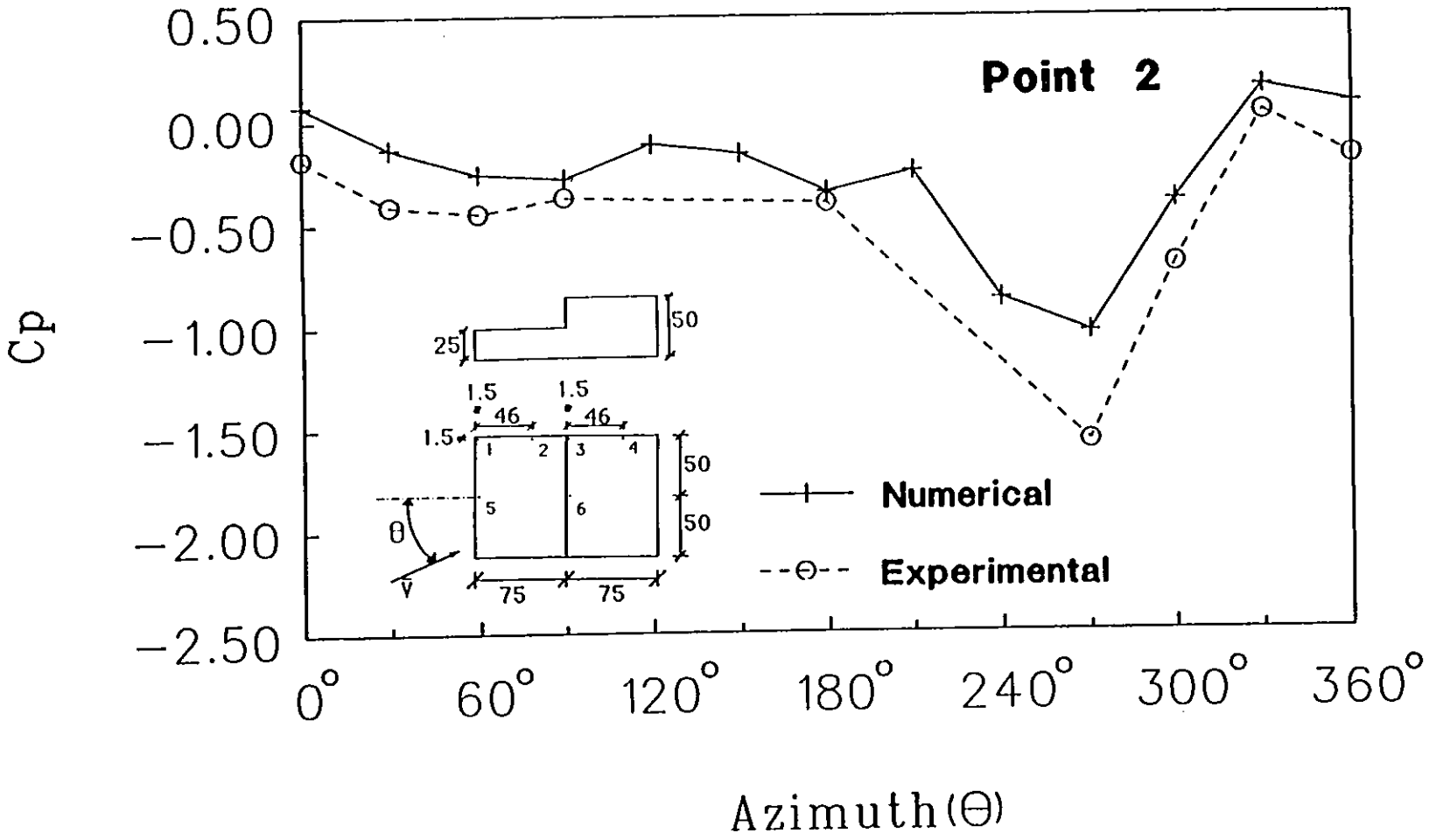

Figure 7.9 Pressure coefficients under various wind directions (edge point, lower roof).

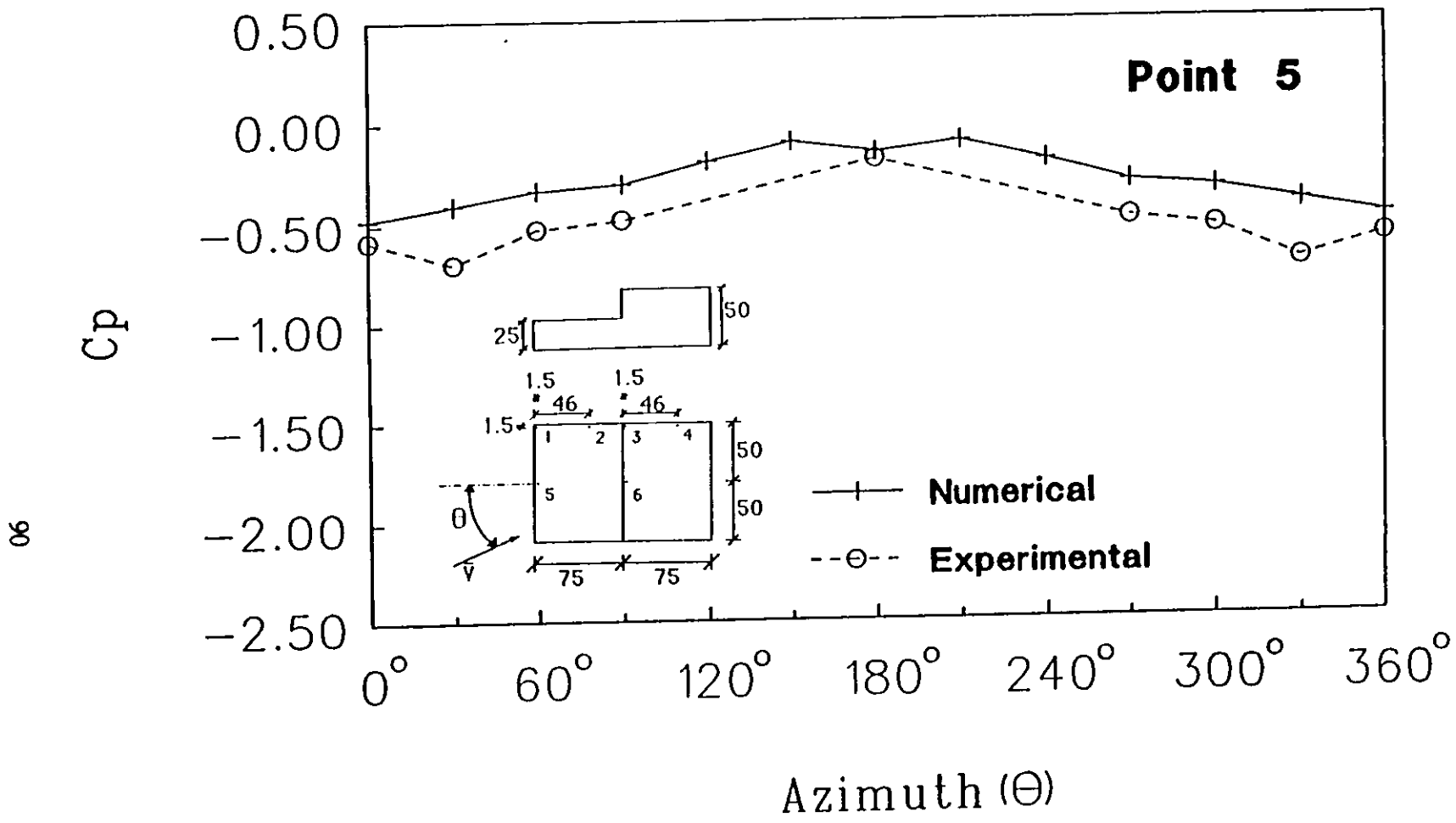

Figure 7.10 Pressure coefficients under various wind directions (edge point, lower roof).

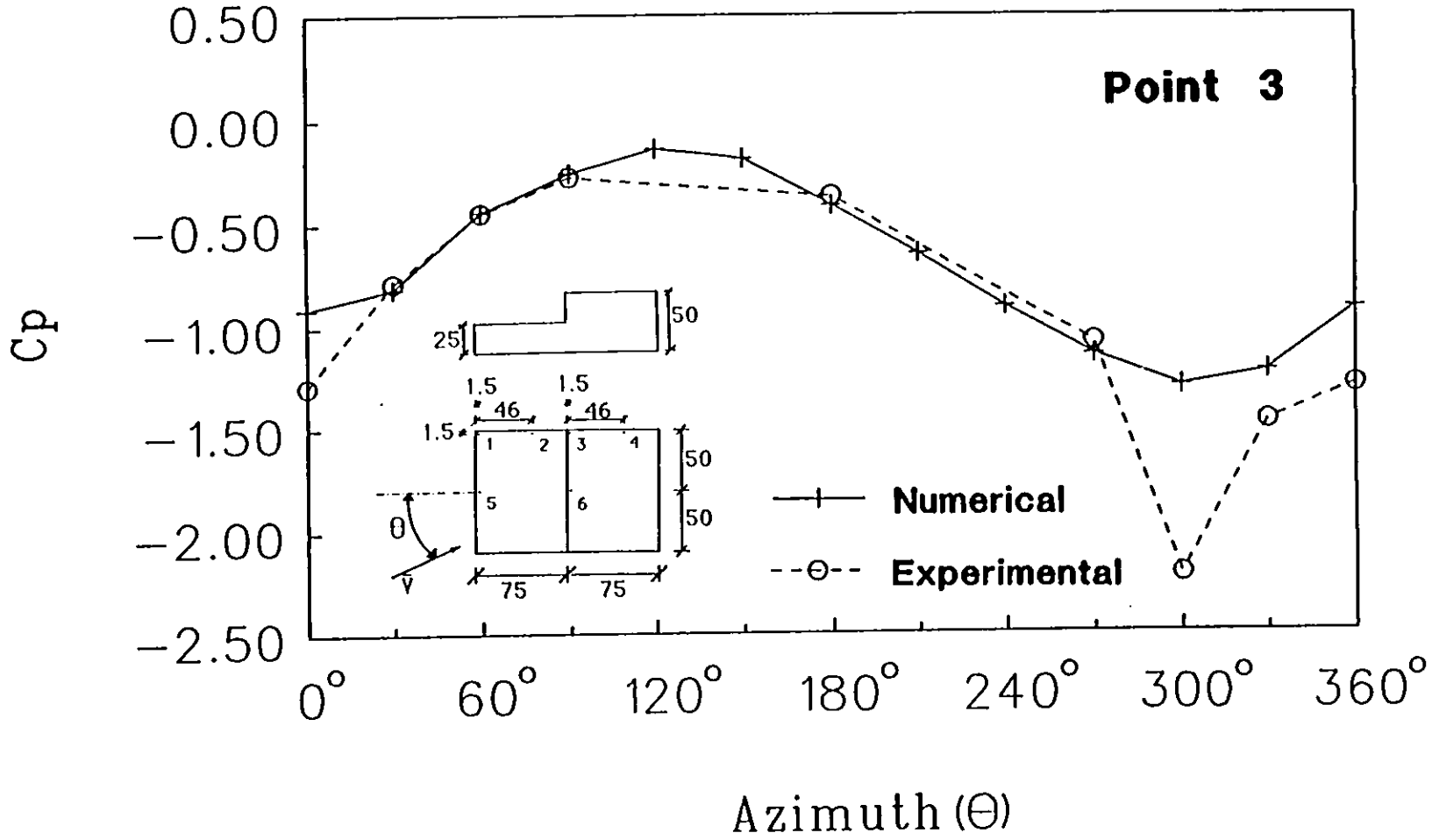

Figure 7.11 Pressure coefficients under various wind directions (corner point, taller roof).

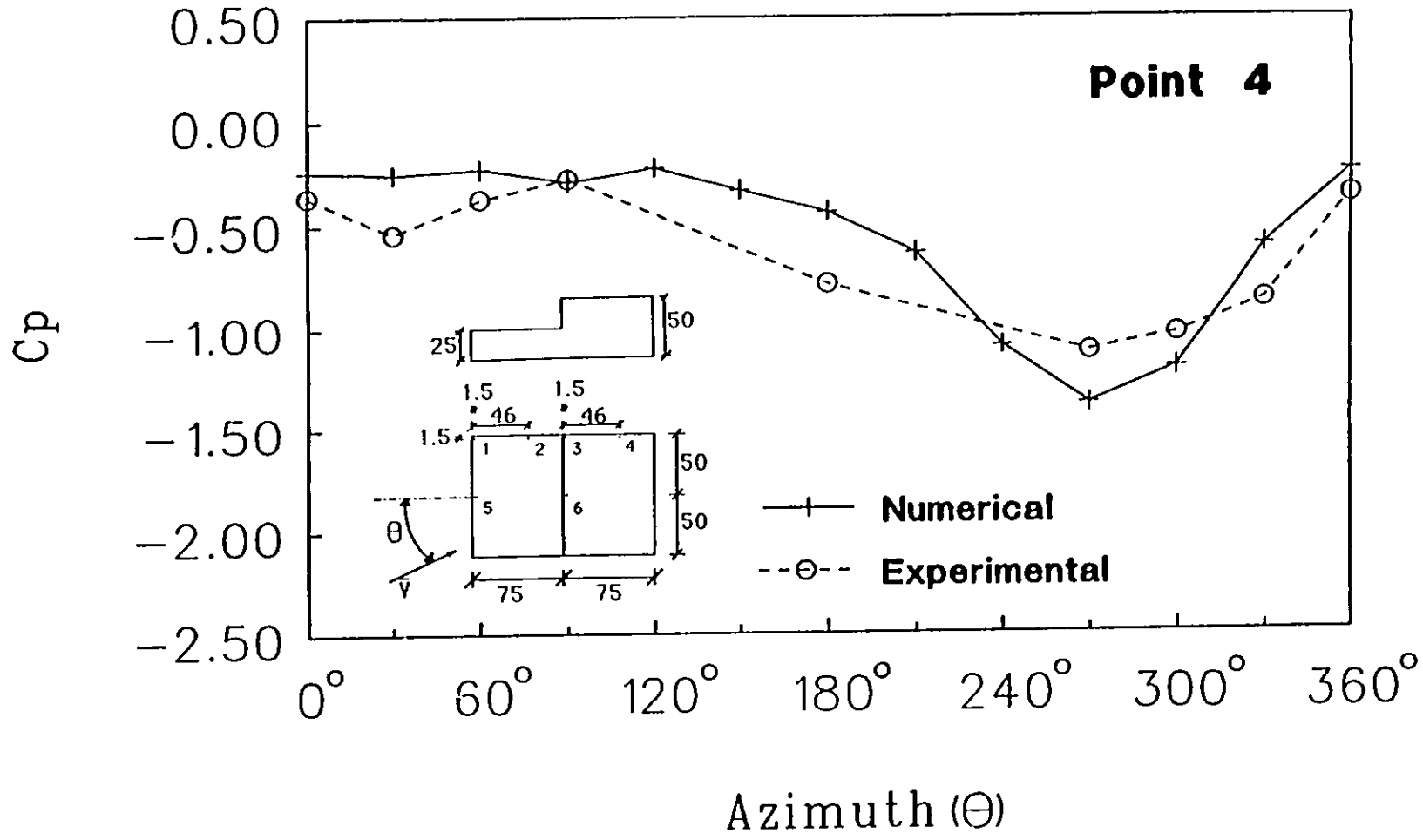

Figure 7.12 Pressure coefficients under various wind directions (edge point, taller roof).

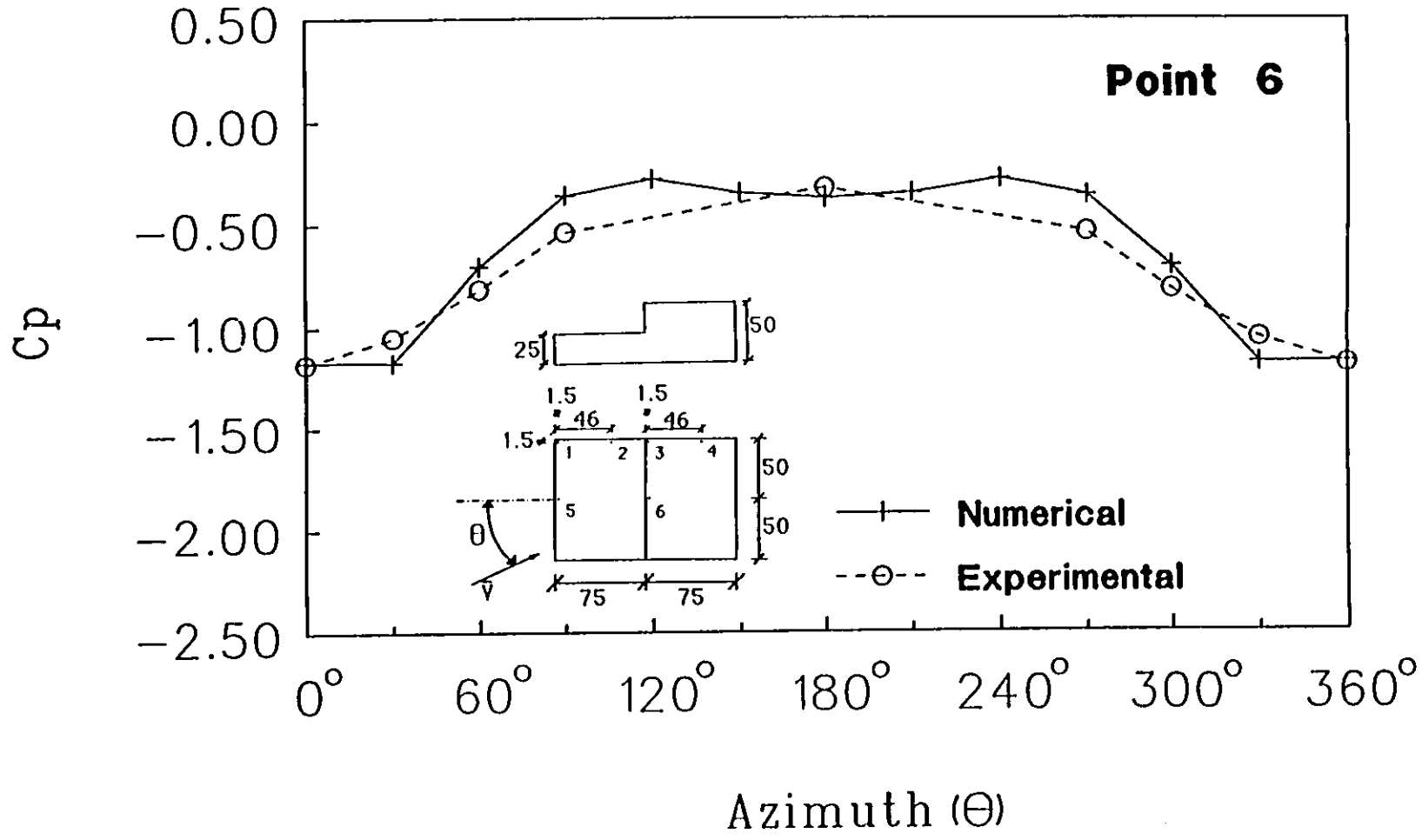

Figure 7.13 Pressure coefficients under various wind directions (edge point, taller roof).

especially for the critical oblique wind directions. The suctions on the two edge locations (point 4 and point 6) were presented in Fig. 7.12 and Fig. 7.13 and compared reasonably well with the experimental data by Stathopoulos and Luchian (1990). This implies that the distance from the first grid line to roof surface (d_p = 1 mm) used in this study is adequate for edge points particularly for the positions near the high front of the L-shaped building.

7.3.2 Plan-view L-shaped building

Computation for a normal wind direction was also attempted for the plan view L-shaped building presented in Fig. 7.1. Since there is no experimental data available for this building configuration, only the numerical results are presented in this section. Figure 7.14 shows the velocity vector field at a horizontal plane taken at half building height. In order to see the deviation of wind flow pattern around the plan view L-shaped building from that around a rectangular building, the wind velocity vector field for a rectangular building of equal height has also been plotted and presented in Figure 7.14. For both buildings the wind flows sharply away from the front face near the windward corners at high speed. However, the expected reverse flow behind the windward corners near side walls was not predicted by the current simulation. The wind flow field around the plan view L-shaped building is very similar to that for the rectangular building in the upwind region as well as the region far from the building. However, the flow patterns are totally different in the circulation region behind the buildings. For the plan view L-shaped

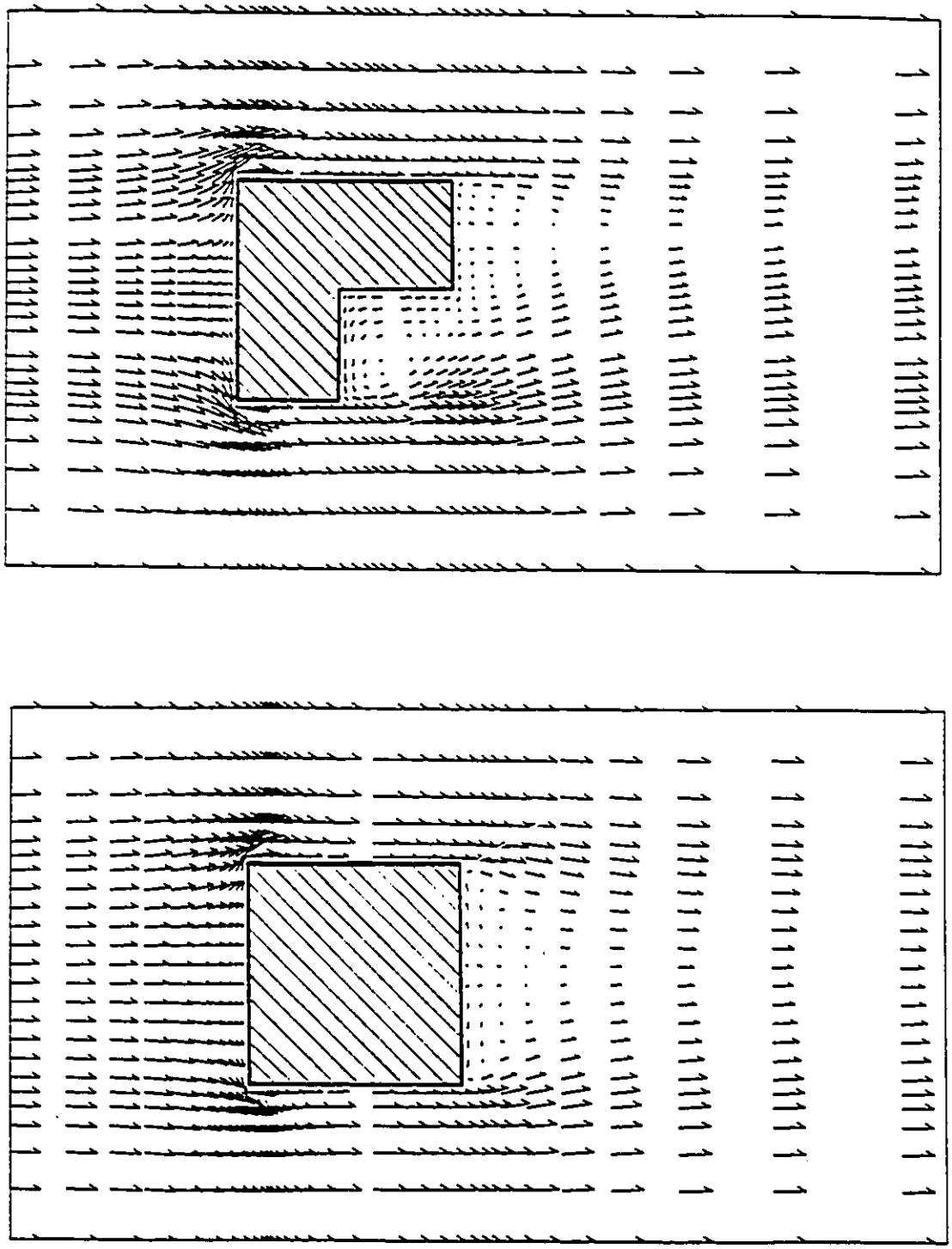

Figure 7.14 Mean flow velocity field around a plan view L-shaped building and a rectangular building of the same height (0° azimuth).

building, there is a large vortex behind the upwind back wall, while two smaller and relatively symmetrical vortices appear behind the downwind back wall. For the rectangular building case, however, only two symmetrical vortices appear in the wake region. Naturally the flow pattern for the L-shaped building is not symmetrical while that for the rectangular building is symmetrical in the whole flow field.

The pressure coefficients along the walls of this plan view L-shaped building are presented in Fig. 7.15 which clearly shows that high suctions exist in the region near the windward edges on side walls (A and F). The suctions along these side walls show similarity with the values on side wall (A) somewhat higher. The suctions on the upwind back wall (B) are generally higher than those on the downwind back wall (D), while the average suction on side wall (C) is similar to that on the upwind back wall (B) since these two walls are the solid boundaries of the same vortex (Fig. 7.14). A rather symmetrical pressure distribution still exists on front wall (E).

The suctions on the roof of this plan view L-shaped building are shown in Fig. 7.16. The highest suctions are found near the windward edge where the flow separates. Suctions along the narrow roof section (G) have magnitudes slightly higher than those along the long roof section (H) near the leeward edge. These suctions are also very similar to those on a rectangular building roof with same height.

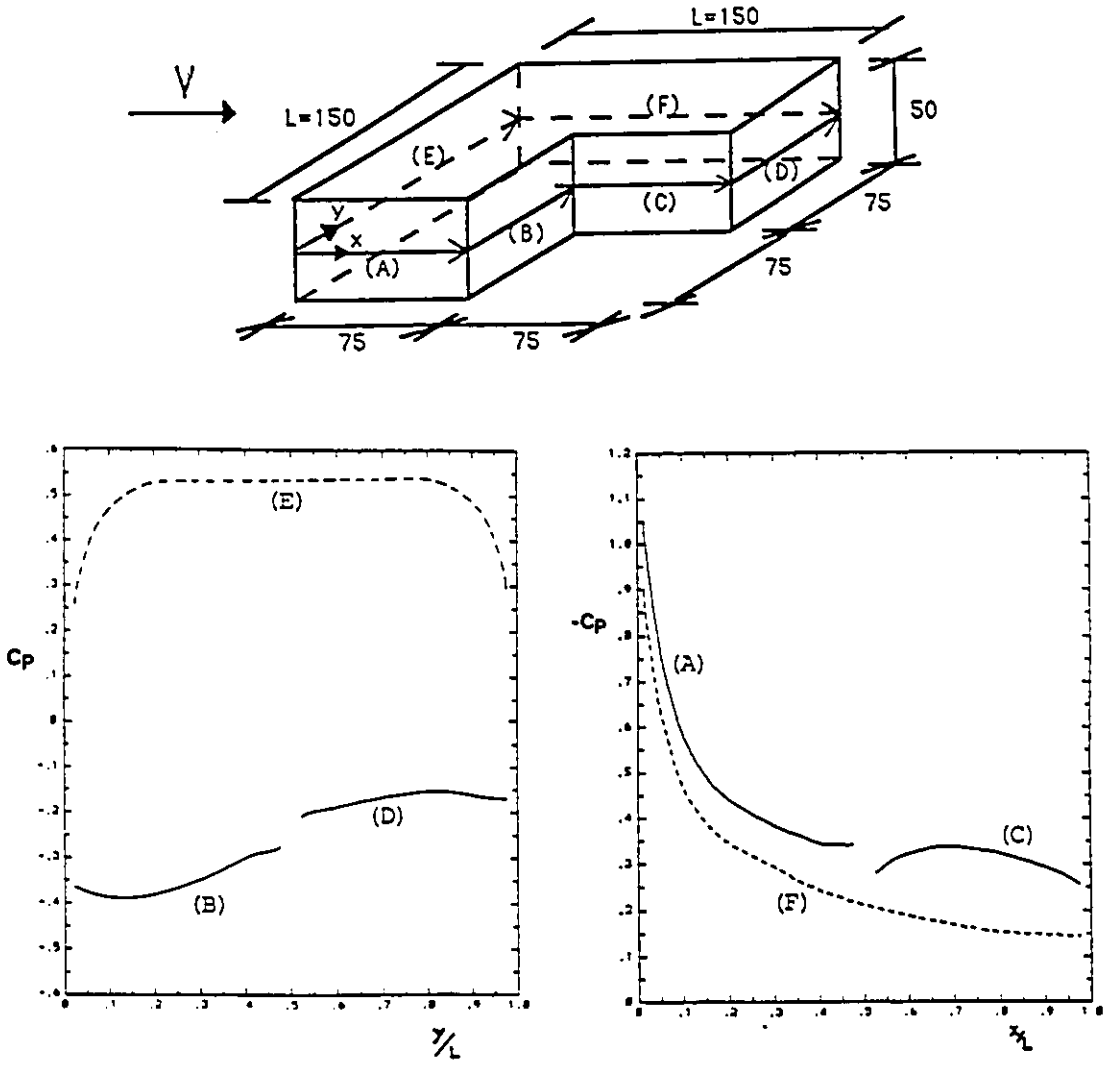

Figure 7.15 Pressure coefficients on the walls of the plan view L-shaped building.

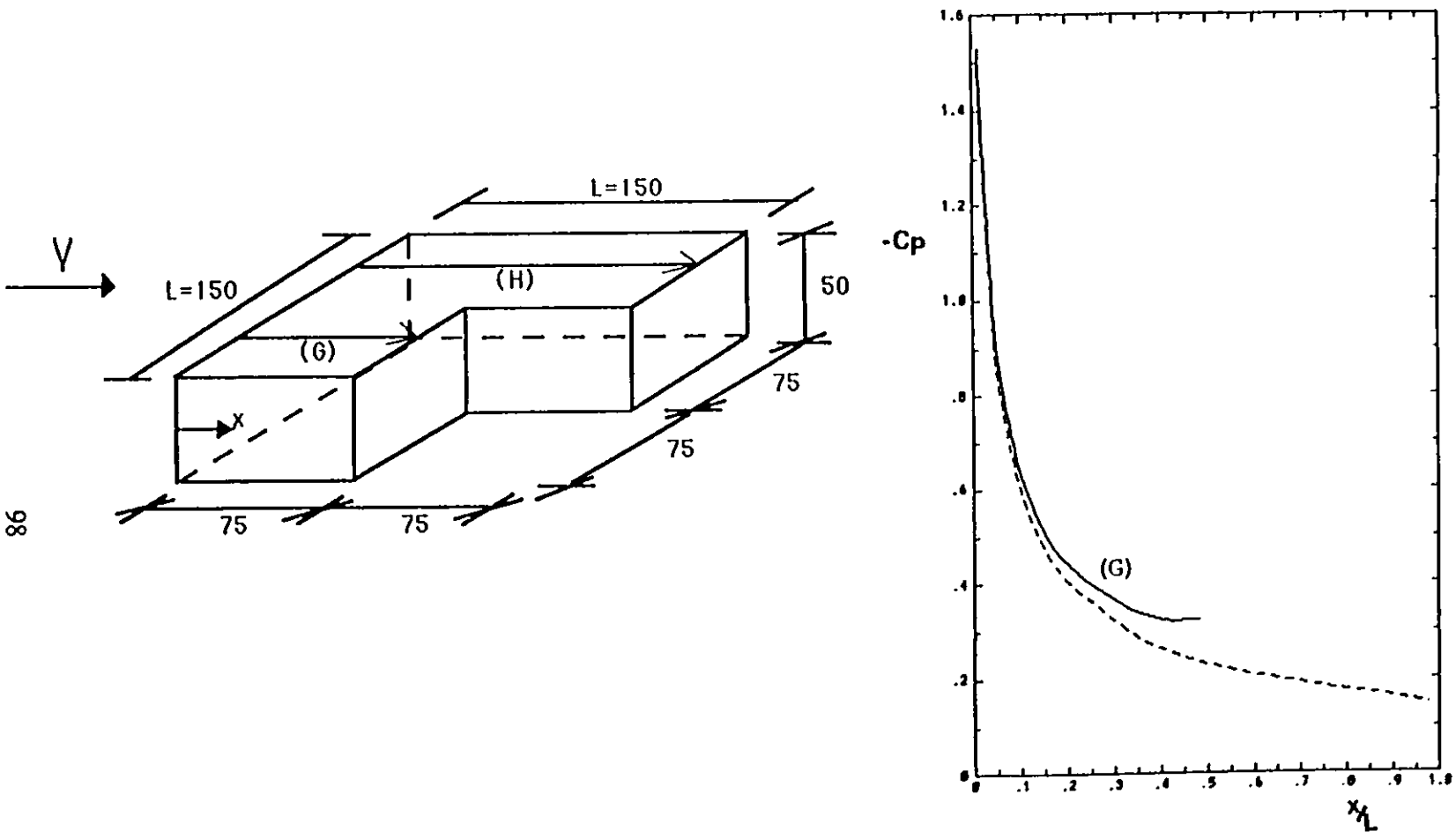

Figure 7.16 Pressure coefficients on the roof of the plan view L-shaped building.

7.3.3 Z-shaped building

The computation of wind conditions around a plan-view Z-shaped building has also been carried out with the code designed in the present study. The governing equations and the boundary conditions used are the same as those explained in section 7.2. Again, the wind blows normal to the building. The building geometry is defined by specifying H1=H2=50 mm, L1=L2=W1=W2=W3=75 mm (Fig. 3.2 and Fig. 7.17).

The computed mean flow velocity vector field taken in the horizontal plane at half building height around this Z-shaped building has been presented in Fig. 7.18. Due to the similarity of the building geometry with the plane view L-shaped building, the wind flow field around the Z-shaped building is very similar to that around the L-shaped building in the area near the front wall, beside the right-hand side wall and behind the first lee wall. High velocities have been detected near all the three windward corners. However, no reverse flows have been found beside the side walls near these windward corners. This is due to the standard k-ε turbulence model adopted in the present study which cannot represent the complex flow properties in these areas of high vorticity and under adverse pressure gradient. A reverse flow is found in the area far from the windward corner beside the first left-hand (upwind) side wall. Apparently, this reverse flow is caused by the second front wall which blocks the mean flow from going farther forward. A large vortex found behind the first lee-wall as that for the plane view L-shaped building. Two slightly asymmetrical vortices appear behind the second lee wall.

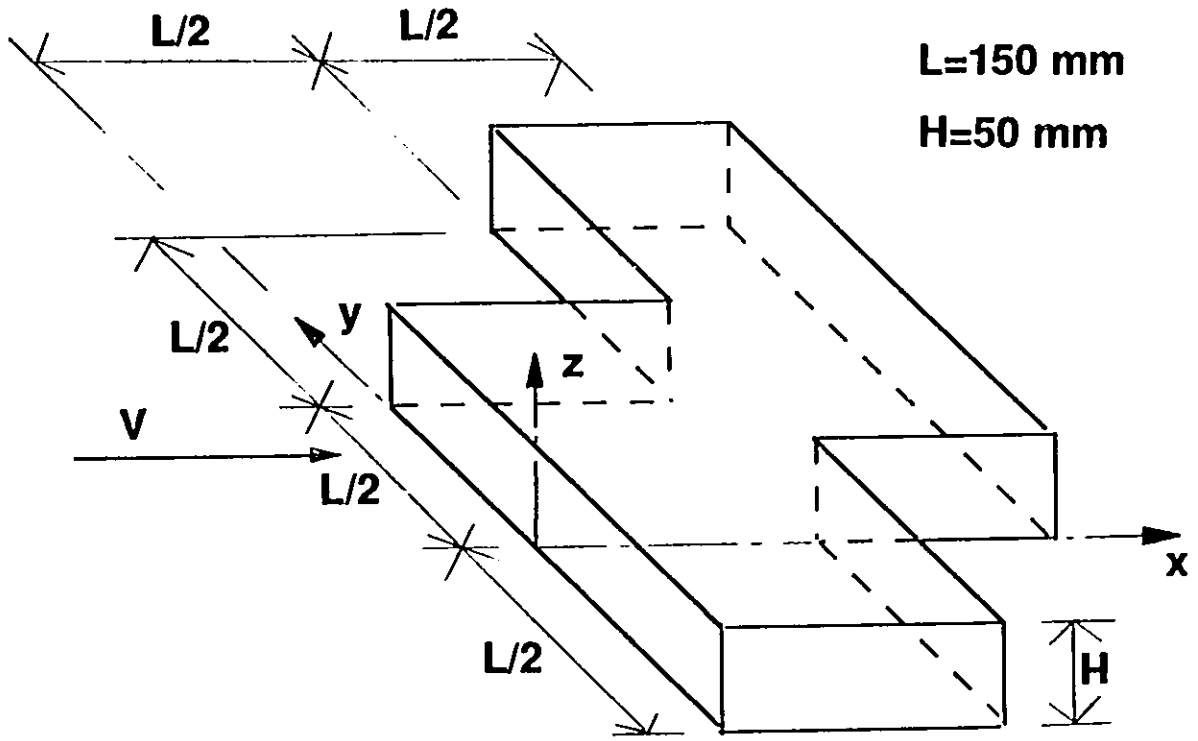

Figure 7.17 Dimension of the Z-shaped building considered.

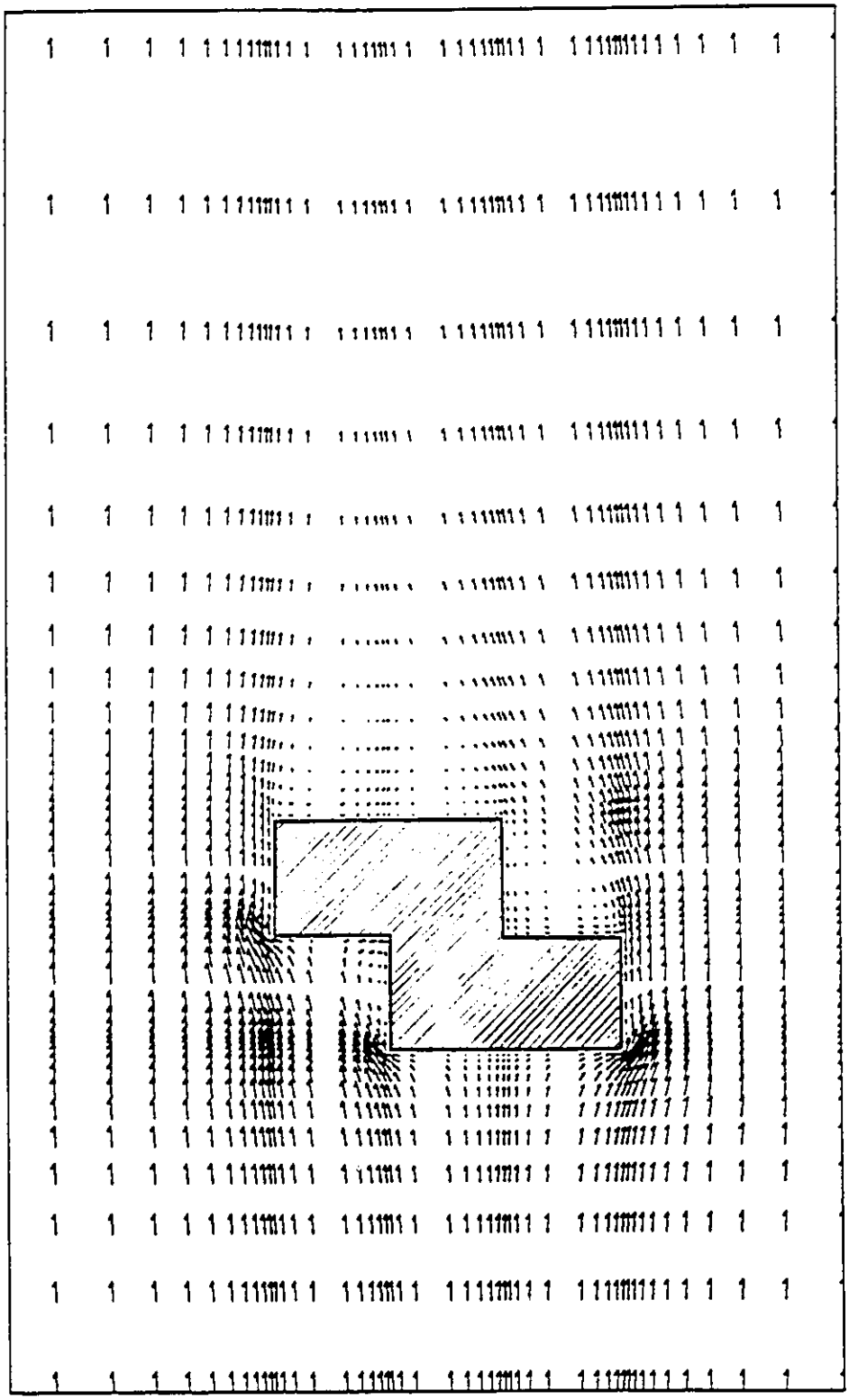

Figure 7.18 Mean flow velocity field around a Z-shaped building at 0.5H.

The wind pressure coefficients on the surface of the Z-shaped building have also been computed. Results on the front walls are presented in Fig. 7.19 along two vertical lines on the first (upwind) front wall in the middle of W1 and W2, and the vertical line on the second front wall in the centre of W3 (see Fig. 3.2 for recollection of W1, W2 and W3). As can be clearly seen, positive pressure coefficients have been found on the front walls with the pressure coefficients on the first front wall generally much higher than those on the second front wall.

The numerically predicted suctions on the roof of the Z-shaped building are shown in Fig. 7.20. Similar to Fig. 7.19, the results are presented along the central lines (B, A and C) of W1, W2 and W3 respectively. As shown by the figure, the highest suctions appear in the areas near the windward edges. The suctions along the first narrow roof (B) are slightly higher than those along the centreline of the long roof (A). These results are also similar to those on the roof of the plan view L-shaped building, whereas the suctions on the second narrow roof (C) which show a similar curve as (B) are slightly lower than those on the long roof.

The computed pressure coefficients on the lee-walls along three vertical lines have been shown in Fig. 7.21. Again, the results are presented along the lines (C, A and B) in the middle of W1, W2 and W3. It is apparent that only negative pressures have been found on the lee-walls. The pressures on the first back wall (C) are generally much lower than those on the second back wall (A and B). This is compared with the results on the

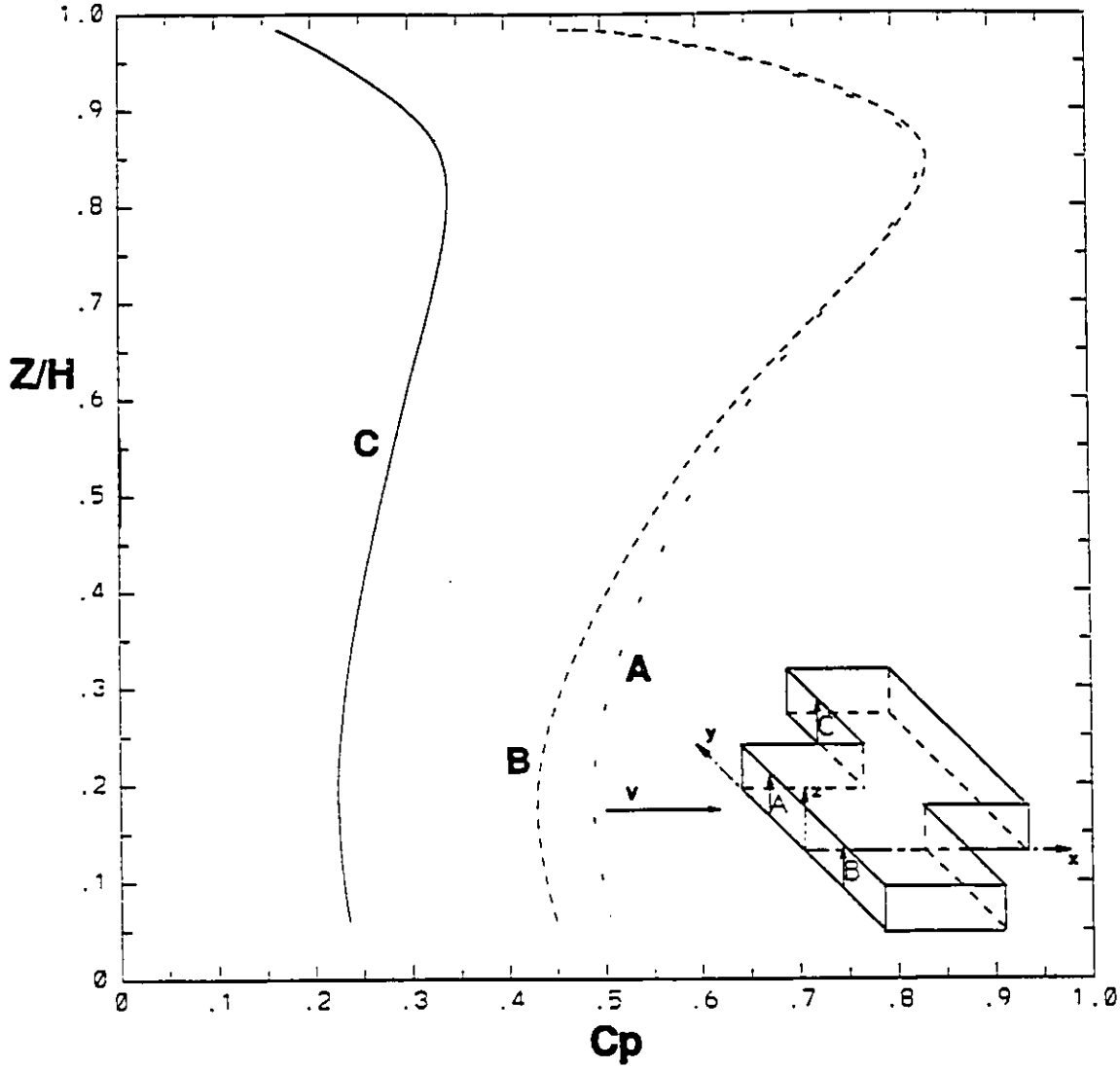

Figure 7.19 Pressure coefficients on the fronts of the Z-shaped building.

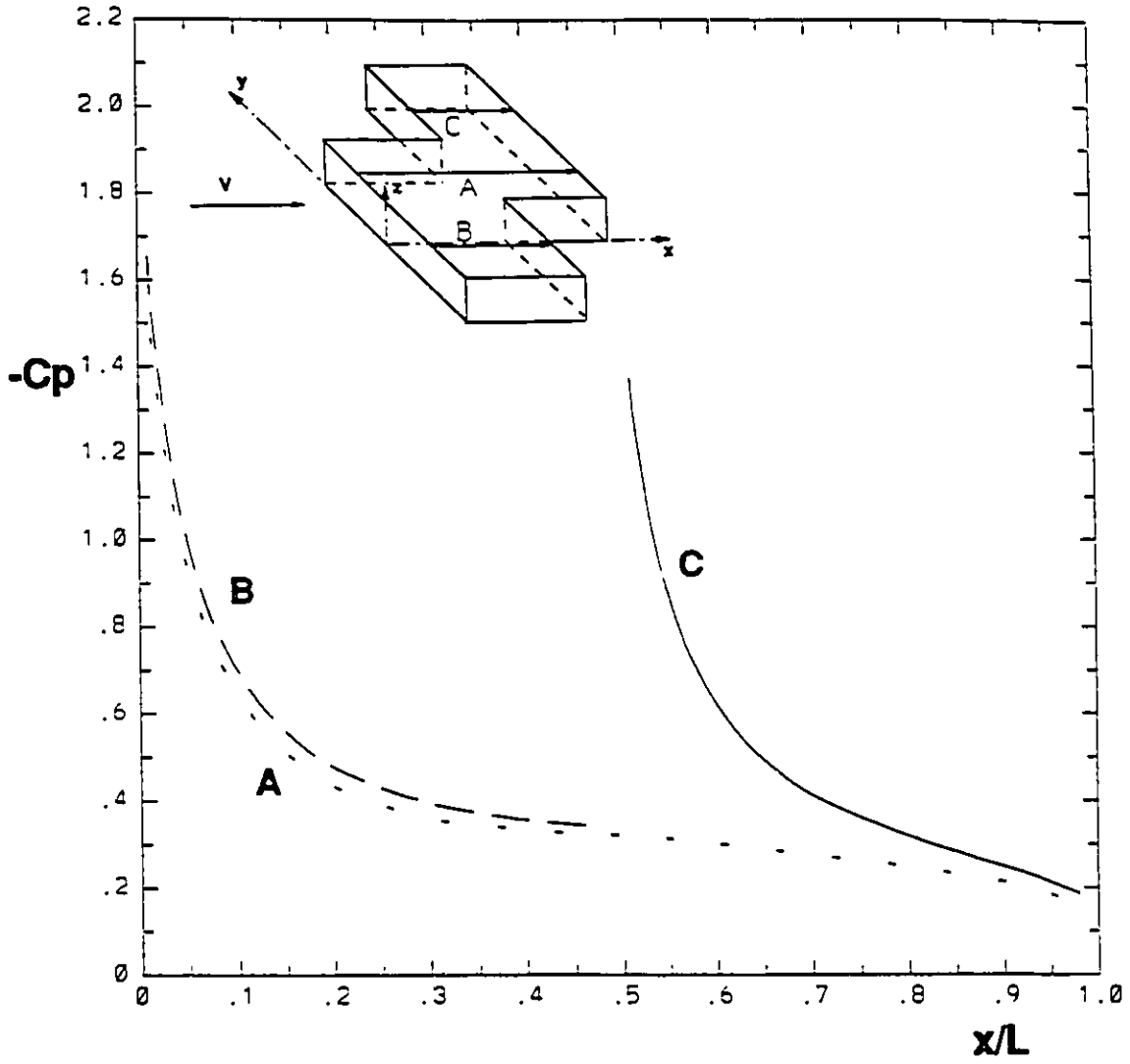

Figure 7.20 Pressure coefficients on the roof of the Z-shaped building.

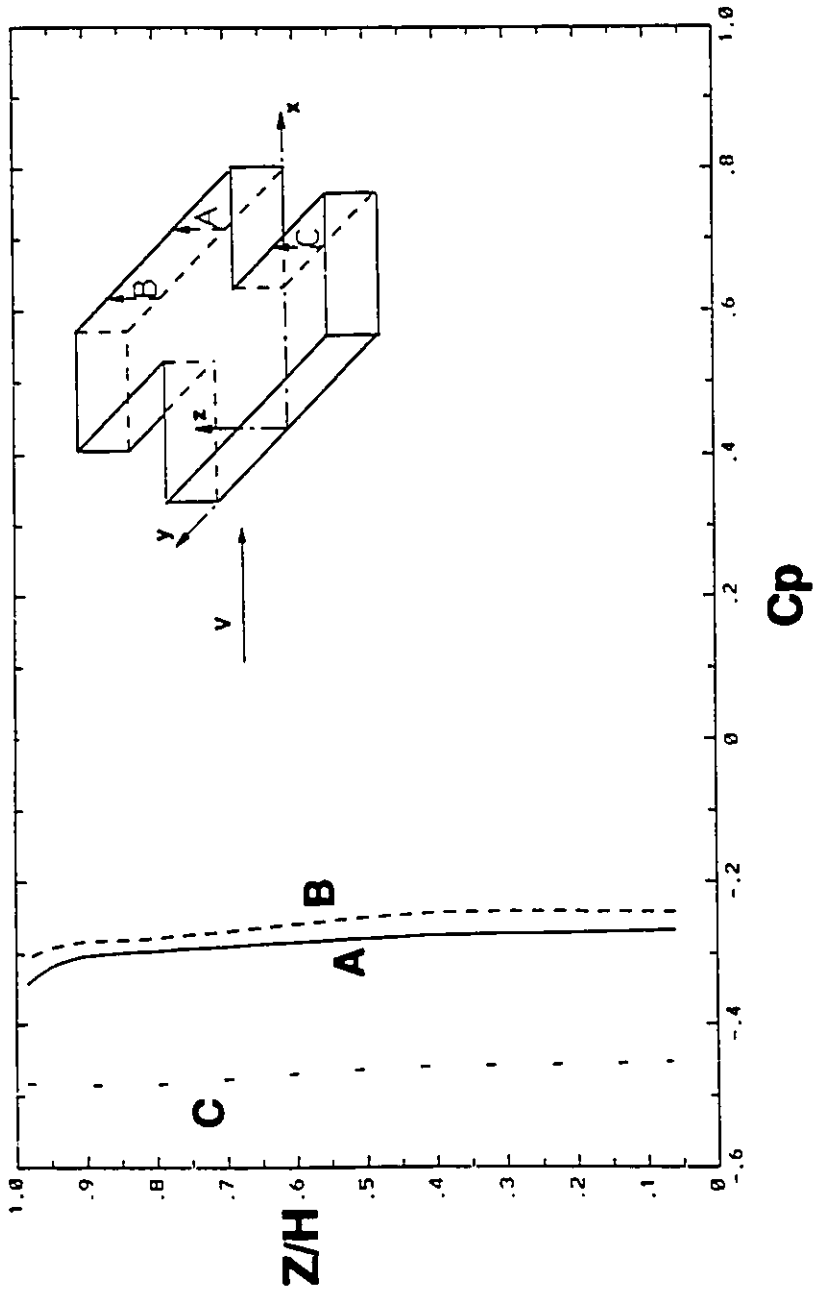

Figure 7.21 Pressure coefficients on the lee-walls of the Z-shaped building.

front walls which show much higher positive pressures on the first front wall than those on the second front wall. Consequently, the front block of the Z-shaped building suffers a much higher drag force than the second (downwind) block.

The numerically predicted wind pressures on the side walls are shown in Fig. 7.22 along the lines at half building height. High suctions on side walls are only found in the area near the windward corners. In particular, the highest suction on the first right-hand side wall (A) is similar to that on the second left-hand side wall (D) so that the Cp-curves on these two side walls are quite similar. The suctions on the first left-hand side wall (B), however, are much lower although the shape of the Cp-curve is similar to those on the other two side walls. For the side wall without a windward corner, i.e. the second right-hand side wall (C), a very uniform distribution of pressure coefficients has been found.

7.4 Conclusions

In general, numerical results from the present approach appear to provide reasonably good prediction of pressures on stepped-roof buildings with the exception of high vorticity zones and edge areas for oblique wind directions for which cases the k-ε model is inadequate to represent the turbulence conditions. Therefore, for oblique wind cases, this methodology can be used with reservations; in particular, the computed suctions on roofs may be underestimated near the windward edges. In addition, the control-volume method may have numerical problems associated with momentum fluxes

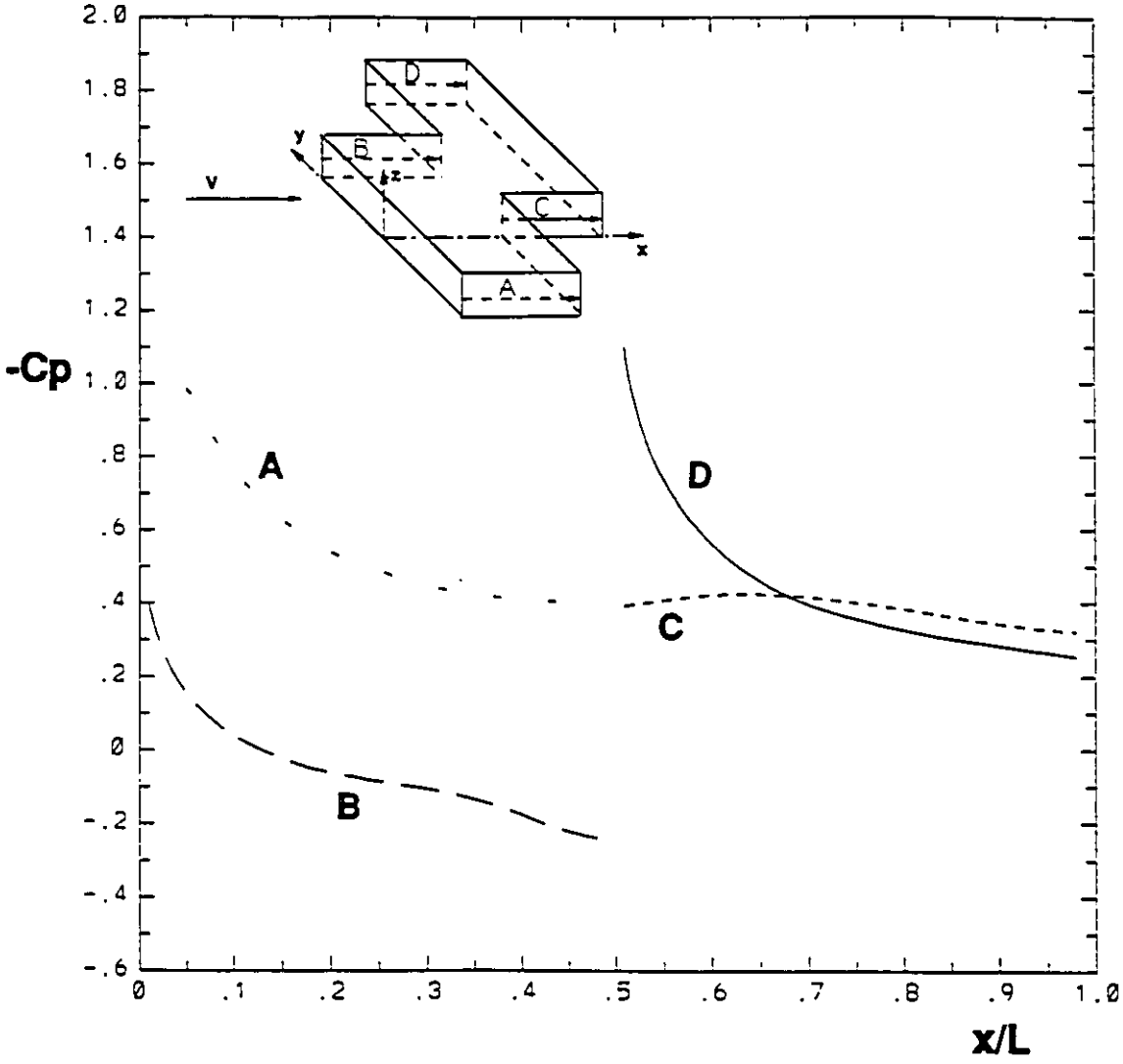

Figure 7.22 Pressure coefficients on the side walls of the Z-shaped building.

that are not perpendicular to the control-volume faces, as explained by Patankar (1980). Many researchers have also attributed the error to the coarse grid arrangement and the k-ε model adopted in the computation (Selvam, 1992b and Murakami, 1990). In order to see more clearly the effect of fine grids on the numerical results, a systematic study of wind pressures on the flat roof of rectangular buildings with different grid arrangements has been attempted in the present study and will be presented and discussed in Chapter 8.

The numerical prediction of the wind conditions around plan-view L-shaped buildings and Z-shaped buildings should also be confirmed by wind tunnel tests. However, the numerical results presented in this chapter provide useful information about the wind effects on buildings of various shapes.

Chapter 8

NUMERICAL EVALUATION OF WIND PRESSURES ON FLAT ROOFS WITH THE k-ε MODEL METHOD

8.1 Introduction

The air flow around a rectangular building model placed in the surface boundary layer is complex. It is defined by stagnation in front of the model, separation at the windward corner and a recirculation region behind the model as shown in Fig. 8.1, after Murakami (1990). The boundary layer wind flow is usually described by a power-law profile for its mean velocities. The transient wind velocity, however, is highly time-dependent due to the turbulence of the airflow.

The numerical prediction of wind pressures on the flat roof of rectangular buildings is very challenging because of the complex turbulent flow regime conditions resulting from the wind flow, particularly for oblique wind directions (Chapter 7). However, most of the previous studies have attributed the poor prediction of wind pressure on flat roofs to the coarse grid arrangements (Selvam, 1992a and Murakami, 1990).

This chapter presents the current study on the numerical evaluation of wind-induced suctions (negative pressures) on flat roofs for both normal and oblique wind

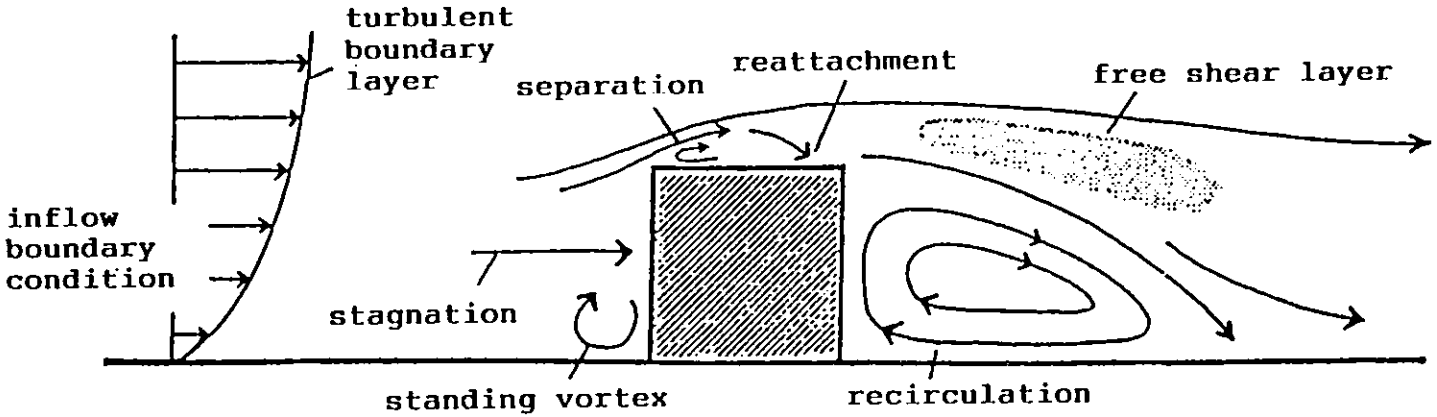

Figure 8.1 Turbulent air flow field around a cube, after Murakami (1990).

directions. The effect of distance between the first grid line and the roof surface on the computational results has been investigated. A low and a taller building were considered with the suctions evaluated on both centrelines and edgelines. Detailed experimental measurements of the suctions near the windward roof edges and corners were also carried out in the boundary layer wind tunnel of the Centre for Building Studies, Concordia University, in order to make thorough comparisons with the respective numerical values. The tap locations on the roof of this building model are shown in Fig. 8.2.

8.2 Methodology

In order to examine the effect of the distance from the first grid line above roof to the roof surface (d_p in Fig. 3.1) on the numerical pressure on roof surface, a low and a taller building are considered with the suctions taken on both centreline and edgeline. Because of the staggered grid system used, the numerical pressures on flat roofs are not evaluated on roof surface, but on the first grid line above the roof as shown in Fig. 3.1. Some researchers (Murakami, 1990 and Selvam and Paterson, 1991) linearly extrapolate the pressure on the first and second grid lines to the roof surface. Others (Paterson and Apelt, 1986 and 1990 and Baskaran and Stathopoulos, 1989) apply the values for first grid line to the roof surface. Regardless of the procedure used, the distance between this first grid line and the roof surface (denoted as d_p) appears to be a very important parameter for the numerical evaluation of roof pressures. The present study has adopted three different d_p's, namely, 0.7 mm, 1.5 mm and 3.0 mm to examine the effect of this

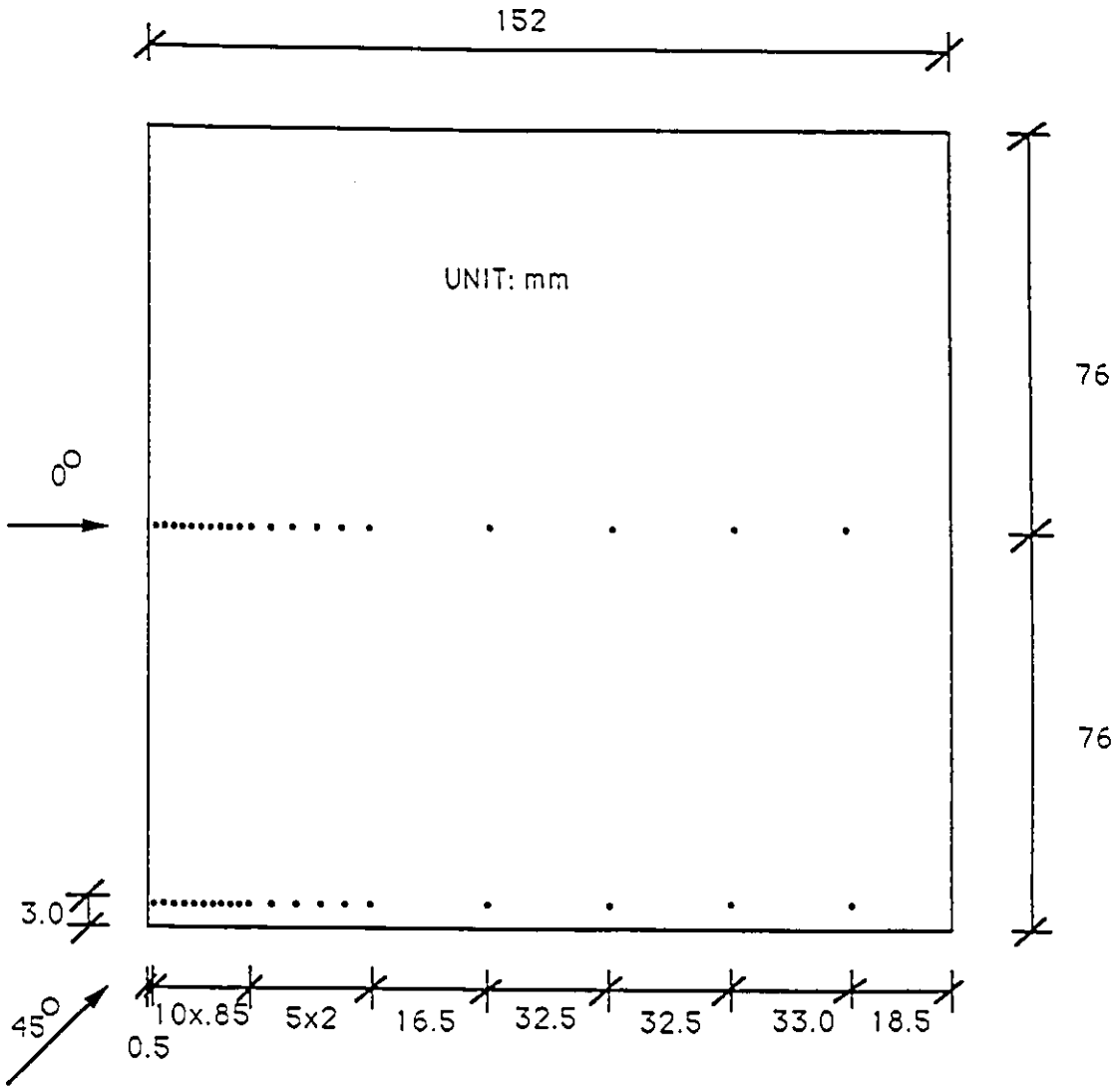

Figure 8.2 Tap locations on the roof of the wind tunnel building model.

distance. The dimensionless distance expressed in equation (5.17) in which $C_\mu^{1/4}k^{1/2}$ is the friction velocity u^* and ν is the fluid viscosity is more important. In the present calculation, this dimensionless distance is around 5 for d_p = 0.7 mm, 11 for d_p =1.5 mm and 25 for d_p = 3.0 mm.

The governing equations used are the steady state Reynolds-averaged Navier-Stokes equations and the standard k-ε turbulence model, i.e. equations (4.1), (4.2), (4.3), (4.4) and (4.6). These equations are first integrated over appropriate control volumes on the staggered grid system (see Chapter 4 and Fig. 3.1, Fig. 4.1 and Fig. 4.2), and the discretized equations obtained are solved by the well known SIMPLE method (see Chapter 4 and also Patankar, 1980). Adequate boundary conditions outlined in Chapter 5 are also used in the calculation.

Several computational grid arrangements of various densities have been tested and a sensitivity analysis has been carried out with d_p fixed at 0.7 mm. The same dimension of the computational domain has been maintained in all these computations. The results presented in Fig. 8.3 for the case of the taller building model show that when grid arrangement is reasonably dense, the effect on wind pressures on the roof surface is very limited, whereas a coarse grid arrangement, say 22 x 21 x 16, naturally causing severe non-uniformity in the mesh, apparently affects the numerical results. Based on the results of this analysis, a computational grid arrangement of 46 x 38 x 34 has been used for the taller building model whereas a smaller grid 44 x 34 x 26 has been selected for the low

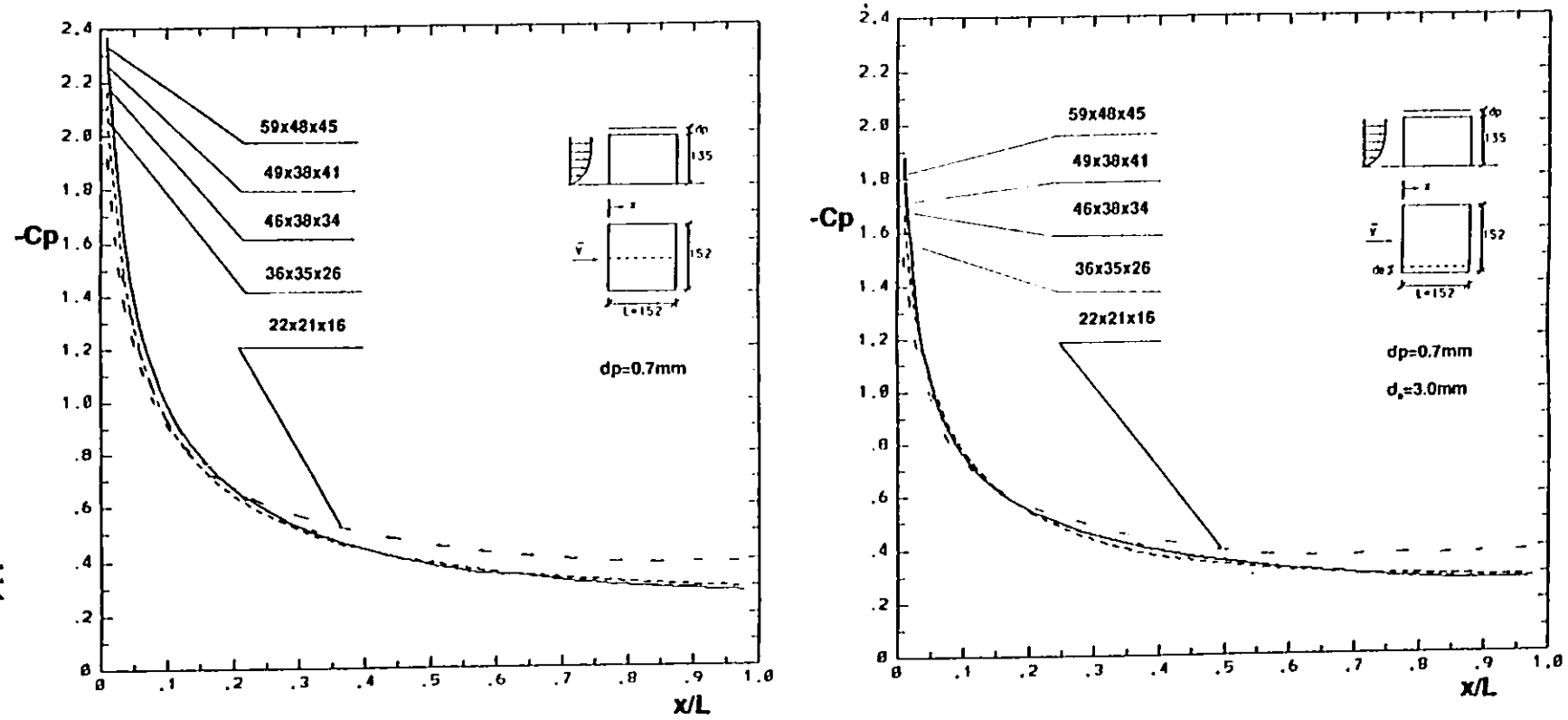

Figure 8.3 Effect of grid density on the numerical pressure on roof.

building model.

8.3 Test of Convergence

To check the convergence of the computations with the current code, numerical simulation of wind flow conditions around the low rectangular building has been carried out until the residues of all the equations reach the round-off limit of machine accuracy. The convergence of the computation is evaluated by relative residues of all the equations (momentum, continuity, k- and ε- equations, see Chapter 4). The relative residues of all six equations for the computation have been presented in Fig. 8.4. Results show that although there are some fluctuations, the relative residues of all six equations decrease consistently, and will all be below 10^{-6} after about 600 iterations. However, for engineering applications, a value of relative residue of 0.02 would be sufficient as already discussed in Chapter 4.

8.4 Results and Discussion

Previous studies on the computational evaluation of wind pressures on roofs have reported results mainly along the central axis of the roof and usually, for normal wind direction only. Such numerical suctions on the roof have been plotted along with the available experimental data (discrete symbols) for both lower buildings ($H/L < 0.4$) and taller buildings ($H/L > 0.85$) in Fig. 8.5. For low-rise buildings, considering the

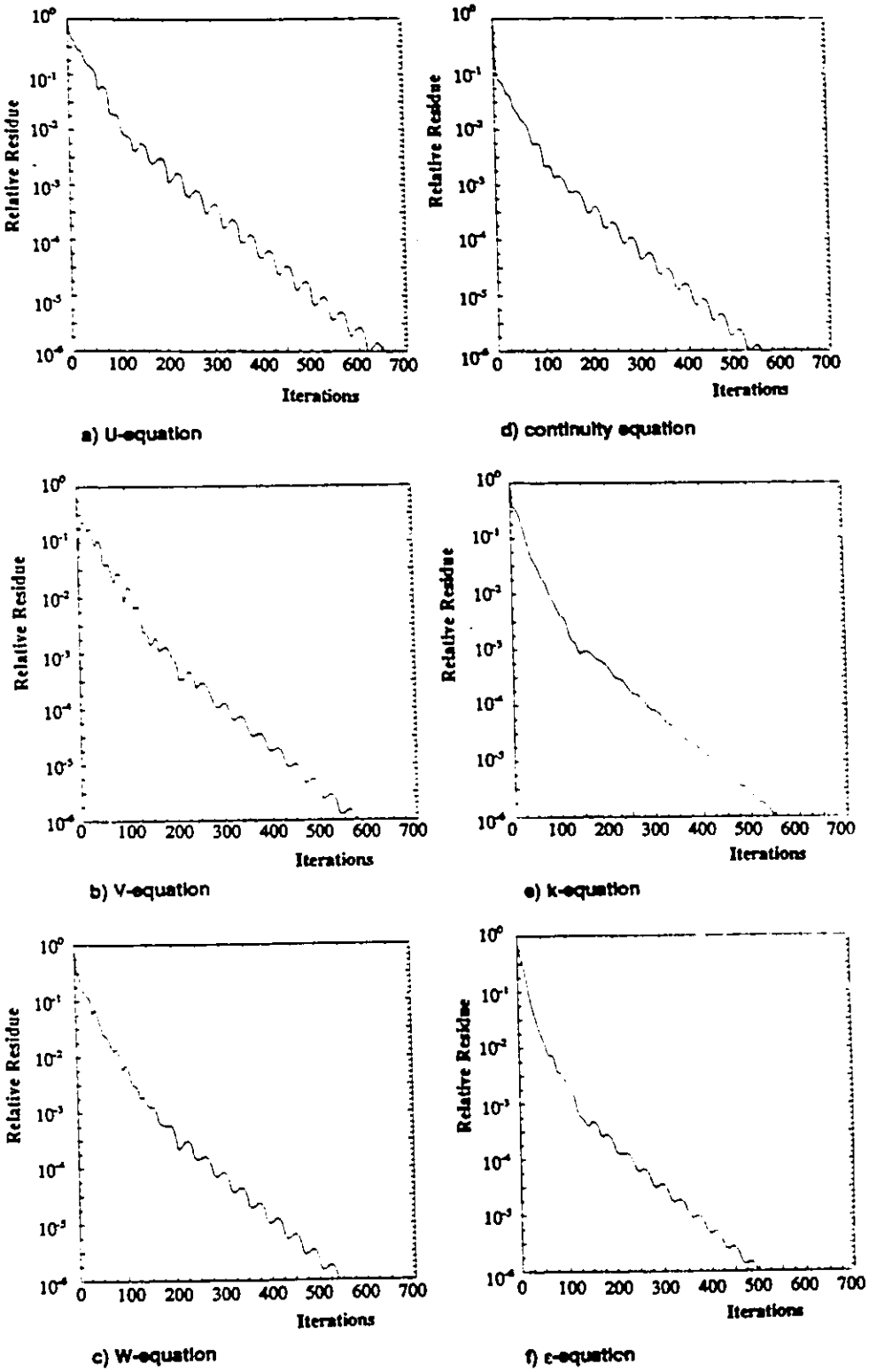

Figure 8.4 Relative residues of all six equations

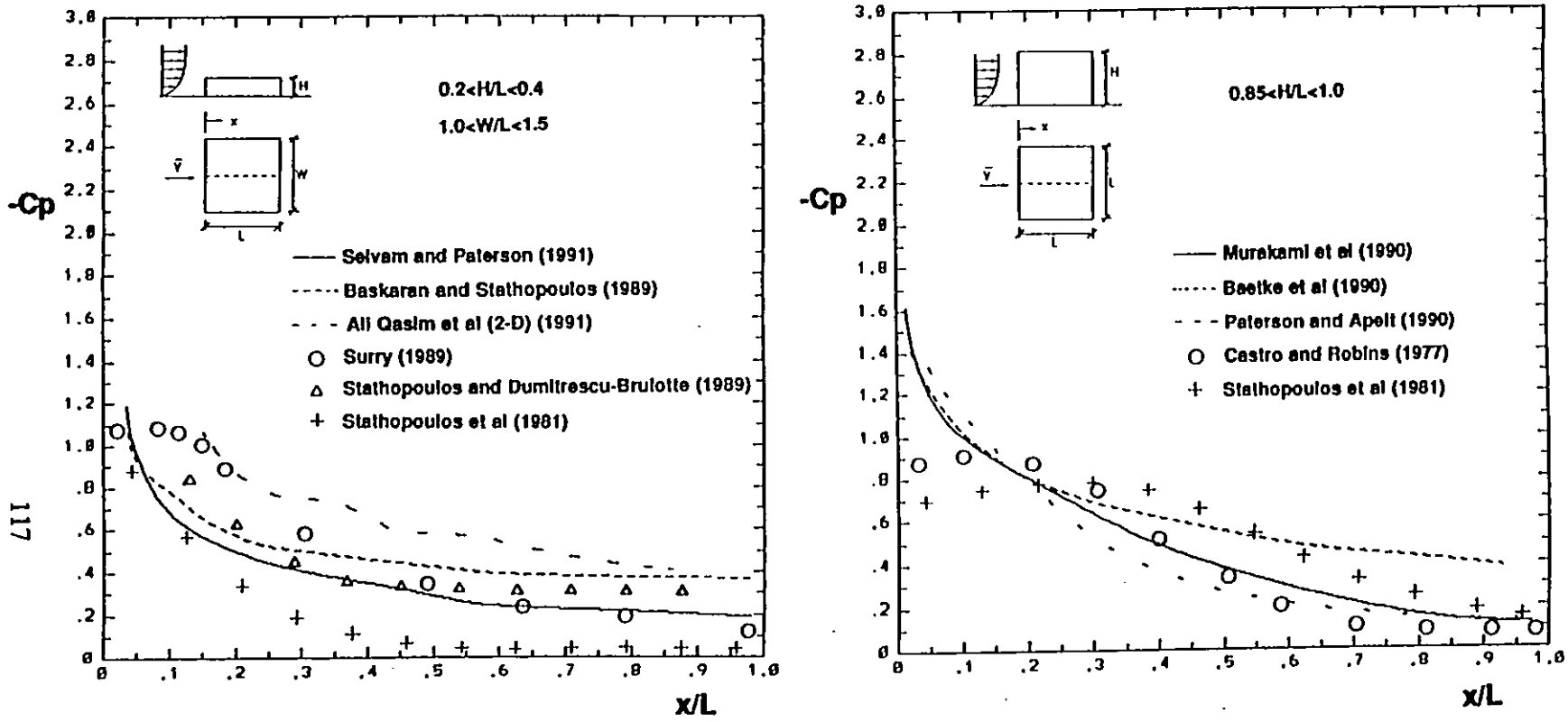

Figure 8.5 Previous predictions of wind pressure coefficients on the centreline of flat roofs (0^o azimuth).

differences in the geometries and the exposure characteristics of the various cases, the agreement between the computed and experimental data is fairly good with the exception of a 2-D simulation that gives an overall overestimation of the suctions. For taller buildings, the numerical results agree reasonably well with the experimental data except in the windward edge region where the numerically predicted negative pressures show an apparent overestimation of the experimental pressure data. In fact, the curvatures of experimental and computational curves have opposite signs in this region regardless of the different sources of experimental data. It should be noticed that the distance from the first grid line to roof surface used in these computations is 5 mm or larger (Baetke, Werner and Wengle, 1990 and Paterson and Apelt, 1990).

Numerically evaluated pressures along the edgeline of a flat roof have seldom appeared in the literature. In the present study, roof pressures have been computed at a distance d_e = 3 mm from the roof edge for both lower and taller building models. Data have also been obtained at the same location from wind tunnel measurements recently carried out in the Building Aerodynamics Laboratory of the Centre for Building Studies, Concordia University. The tap locations on the flat roof are shown in Fig. 8.2. The computed results are compared with these measured data in Fig. 8.6 for normal wind direction. It should be noted that the first grid line above the roof has been placed at a distance d_p = 5 mm from the roof surface and the computed pressures on the roof have been found by linear extrapolation. Experimental data from a previous study by Stathopoulos, Surry and Davenport (1981) have also been included in the comparison

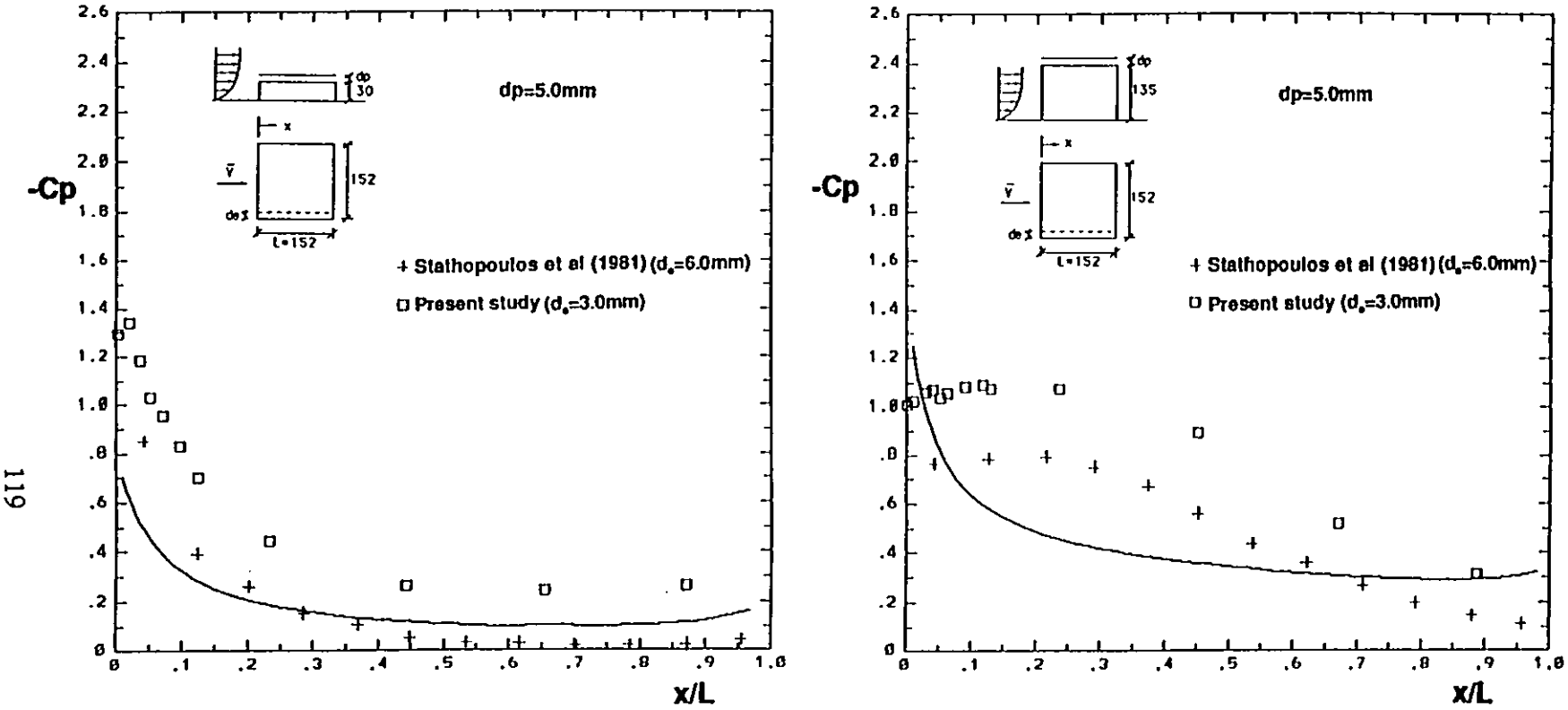

Figure 8.6 Pressure coefficients on the edgeline of flat roofs (0° azimuth).

although these data have been measured at a distance d_e = 6 mm from the edge. Computational results have been denoted by a continuous line whereas experimental data have been indicated by discrete symbols throughout this chapter.

The comparison between computed and measured data shown in Fig. 8.6 clearly indicates that in the case of low building model, the computed results underestimate the measured values significantly near the windward edge where the highest suctions occur. For the higher building model for which the distance d_p = 5 mm is relatively smaller in terms of building height, the computed data are near the measured values at the windward edge but they drop sharply causing underestimation of suctions farther downstream.

In the light of the above comparisons and previous findings (see Fig. 8.5) as well, it was decided to investigate more thoroughly the effect of distance between the first computational grid line and the roof surface on the computed pressure coefficients. Although different wind directions from 0^o to 180^o have been examined, only the typical results for 0^o and 45^o are presented in this chapter along with the limited experimental data available for comparison. The simulation of oblique wind cases is achieved by rotating the flow field rather than the building itself to avoid the difficulty in re-arranging the grid nodes.

Figure 8.7 shows the results of this investigation for both centreline and edgeline (d_e = 3 mm) on the roof of the low building model by using three distances - d_p's -

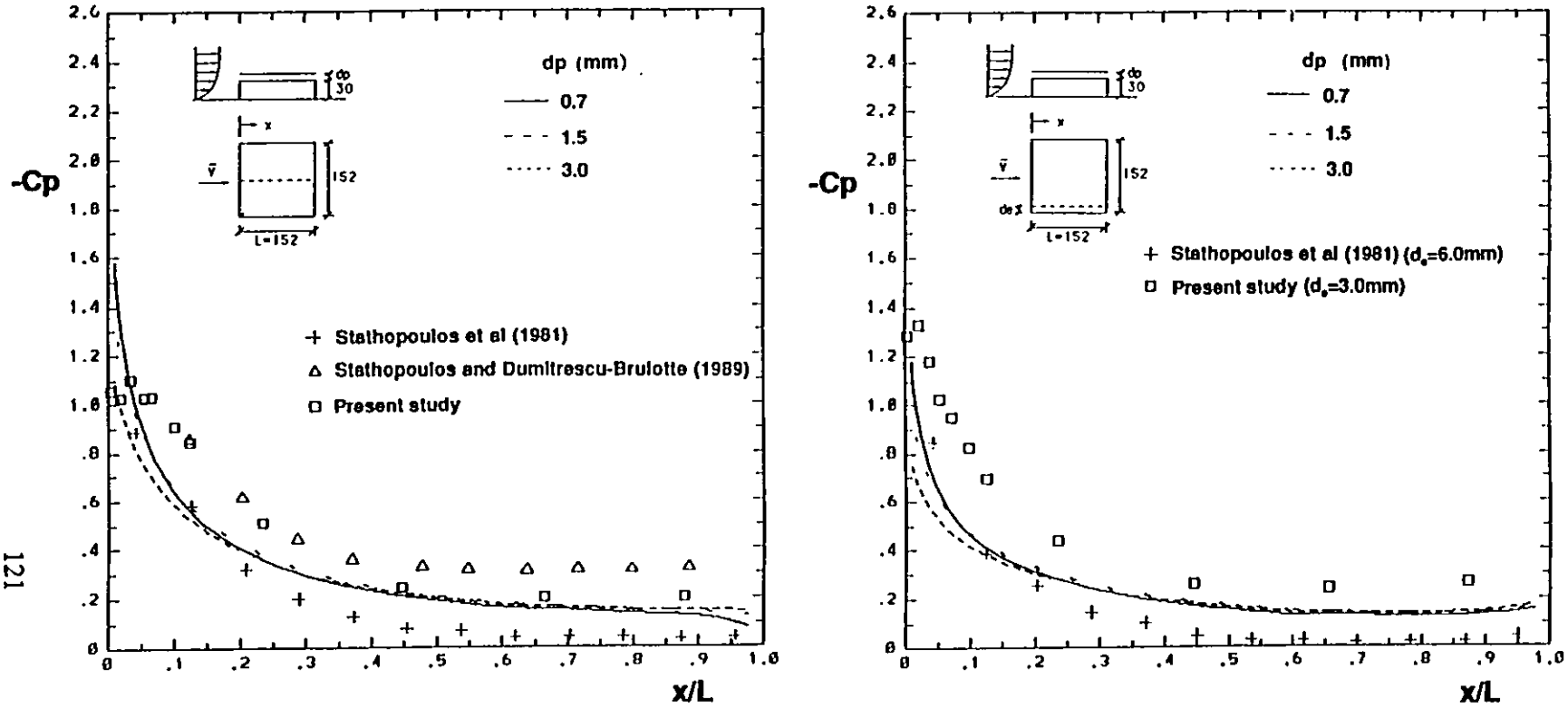

Figure 8.7 Pressure coefficients on roof (low building, 0° azimuth).

between the first grid line and the roof surface, namely 0.7 mm, 1.5 mm and 3.0 mm. For such small values of d_p, differences between the results computed with linear extrapolation to the roof surface and those computed without extrapolation are very small. Therefore, the pressure coefficients presented hereafter are those found on the first grid line without extrapolation. Experimentally determined pressure coefficients have also been included in the graphs for comparison purposes. However, it should be noted that only those referred to as "present study" correspond to the exact geometrical configuration and terrain exposure assumed in the computation.

Two matters are worthy of consideration in these comparisons. First the similarity of the three computational data sets for both centreline and edgeline of the low roof except near the windward edge - in a zone equal to about 10% of the width of the model - where significant discrepancies occur. In particular, the lower the distance (d_p), the higher the computed suction coefficients, whereas for the same d_p the suctions computed on the edgeline were lower than the corresponding values computed on the centreline. The other point to be made here is the general similarity between the computed and measured data although the computed values seem to underestimate the experimental results except near the centre of windward edge for which the opposite trend is observed.

Such investigations for the taller building were also attempted and the results have been shown in Fig. 8.8, in the same format with Fig. 8.7. These results have been compared with available experimental data including those obtained in the present study

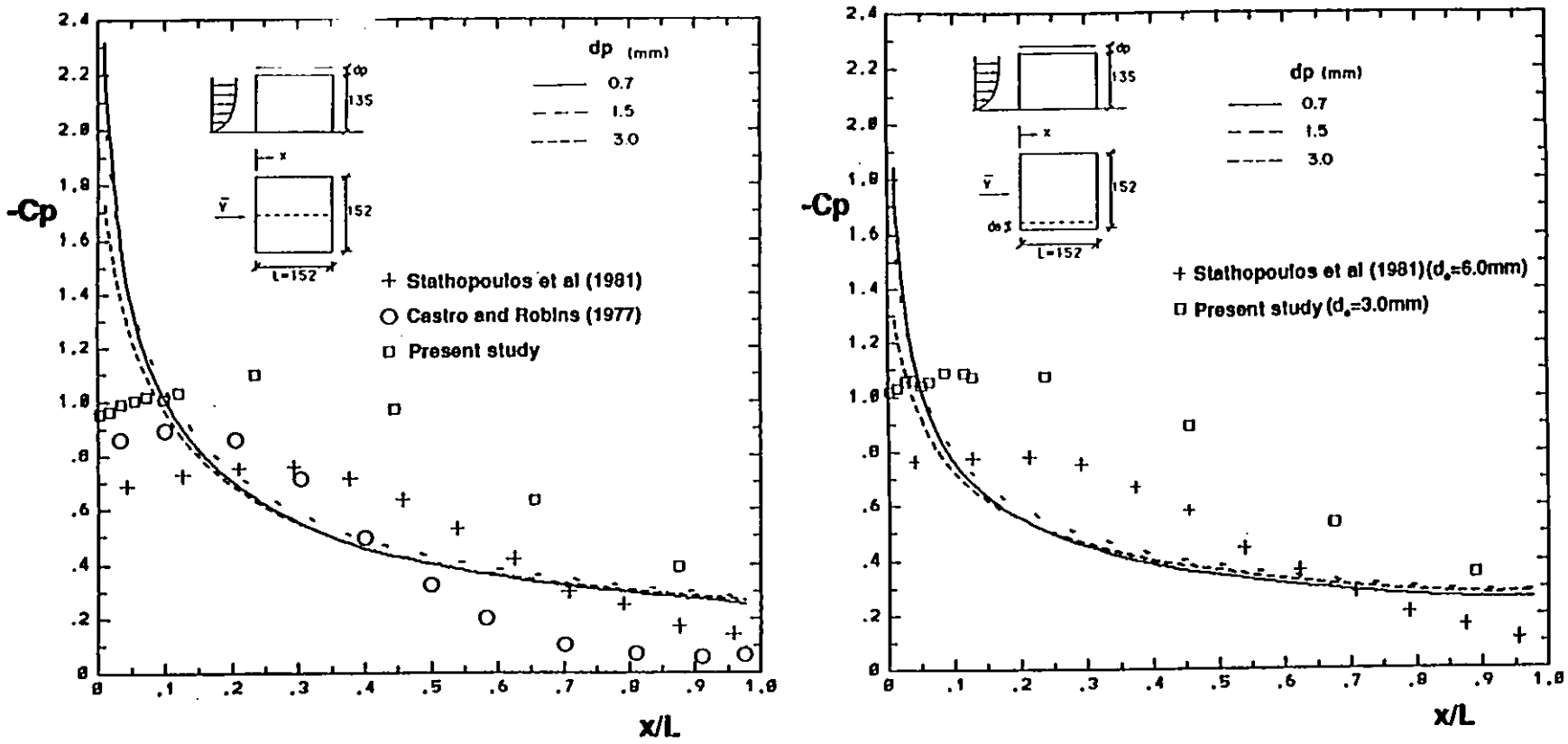

Figure 8.8 Pressure coefficients on roof (tall building, 0° azimuth).

with taps placed as close as 0.5 mm to the windward edge - see Fig. 8.2 for tap locations. The figure enhances the fact that for a taller building, the curve of the numerical pressure coefficients follow a pattern which is different from the curve the experimental data follow. The comparison also shows that the computed results generally underestimate the experimental data with the exception of a small region near the windward edge where the suctions on the roof are apparently overestimated. It should be noted that the proximity of the first grid line to the roof surface does not improve the computed data in this windward edge region. In fact, the smallest d_p causes the maximum overestimation of suctions. This is attributed to the limitations of the k-ε model which fails to predict the reverse flow over the roof (Selvam and Paterson, 1991 and Murakami, Mochida and Hayashi, 1990) by overestimating the k values and, consequently, the skin friction values (Rodi and Scheuerer,1986). Furthermore, the boundary conditions used are deduced from a 2-D fully developed turbulent flow over a large plane and these are not fully applicable even to the region far from the windward edges. The application of these coarse boundary conditions in the windward edge region cannot provide accurate predictions.

The influence of the magnitude of the distance d_p on the numerical roof suctions has been examined in detail at four typical positions on roof surface. Results of this investigation are presented in Fig. 8.9 for both low building and taller building configurations. Numerically evaluated wind pressure coefficients are almost d_p-independent at positions far enough from the windward edge (point 2 and 4). However, at positions close to the windward edge (point 1 and 3), suction coefficients increase

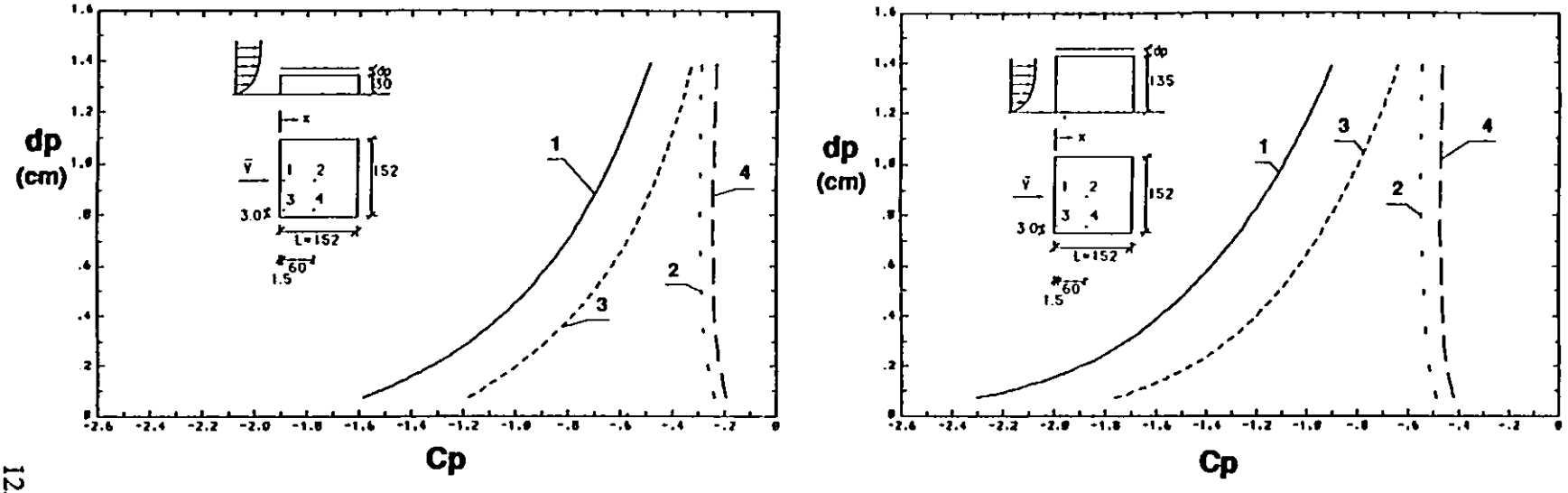

Figure 8.9 Pressure variation due to different d_p (0° azimuth).

dramatically with decreasing d_p, particularly for the taller building. The positions examined represent two distinct regions, namely the low pressure gradient zone far from the windward edge - say x is larger than 10% of building width - in which the numerical pressures are almost d_p-independent; and the high pressure gradient region next to the windward edge which shows the drastic influence of the d_p on the computed results.

Pressure coefficients at these four positions for the oblique wind condition (45^o) have also been examined and are presented in Fig. 8.10 in the same format with Fig. 8.9. Under this wind direction, position 4 is no longer an inside roof point. Therefore, pressure coefficients at this position are also d_p-dependent similar to those computed at position 1. However, the pressure gradients at these positions (1 and 4) are relatively smaller than that at position 3 (corner point). For the position far from both windward edges (point 2), the pressure coefficients are still almost d_p-independent.

For oblique wind directions, the flow conditions above the roof are more complex with conical vortices developing along the roof edges. Pressure coefficients for 45^o oblique wind direction have been computed for three different d_p's on the roof of a low building. Results are presented for both the centreline and the edgeline of the roof in Fig. 8.11 and compared with the previously and currently obtained experimental data. The similarity of the three computational data sets for the centreline is apparent except near the windward edge where discrepancies occur; in particular, the smaller the d_p the higher the computational suctions. Discrepancies, however, exist among these three computed

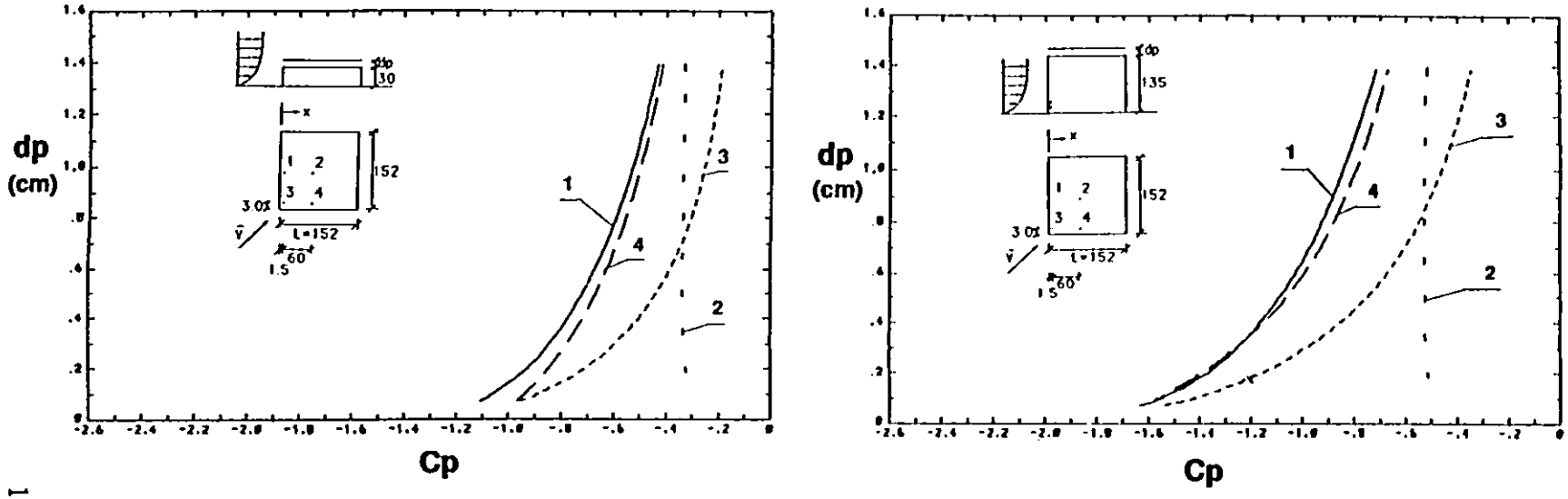

Figure 8.10 Pressure variation due to different d_p (45° azimuth).

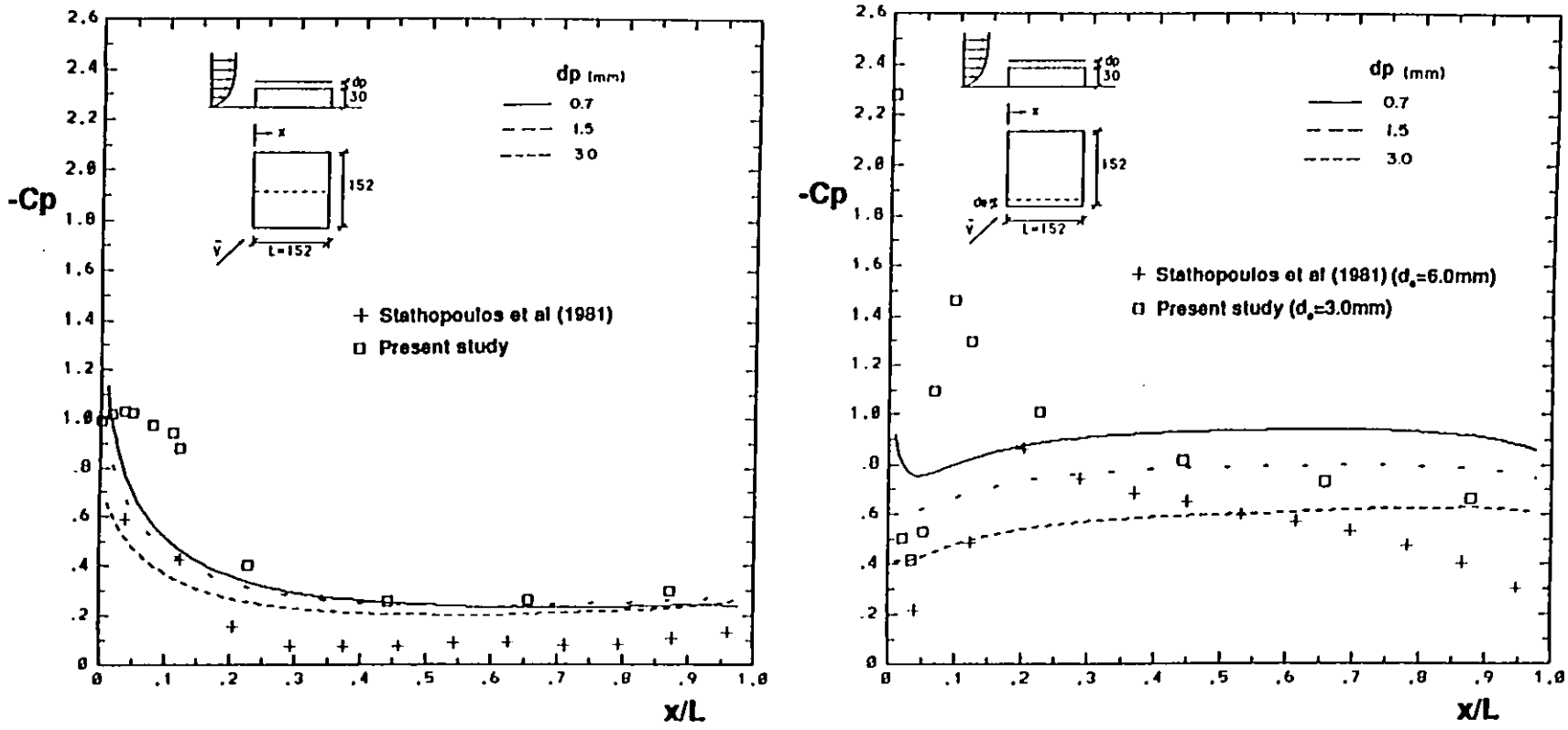

Figure 8.11 Pressure coefficients on roof (low building, 45° azimuth).

data sets for the edgeline with the smallest d_p providing the highest suctions. The agreement between computed and experimental data for centreline is generally good except in the windward edge region where the computed values underestimate the measured data. However, the prediction of pressure coefficients along the edgeline is far from satisfactory. In particular, regardless of the magnitude of d_p, the computed results show a smooth change of suction coefficients while the experimental data follow a different pattern. This discrepancy is possibly caused by the k-ε model which is not representative for this high vorticity region. The numerical false diffusion due to the skewness of the main flow to the grid lines described by Patankar (1980) may be another reason for this discrepancy.

Figure 8.12 shows comparisons for the case of a taller building. The data show similar trends with those discussed in Fig. 8.11. In particular, the numerically evaluated suctions along the centreline agree fairly well with the experimental data only for x/L greater than about 0.2, contrary to the region near the windward edge where the high suctions are clearly underestimated by the computational approach. Regarding the windward edge region of the roof, the present methodology does not provide appropriate values of pressure coefficients. Numerically-evaluated data either underestimate or overestimate the experimental results more significantly than in the case of lower building. Numerical false diffusion and the inability of the k-ε model to describe the flow conditions near the windward roof edges and corners are the main attributes for this discrepancy. However, numerically-evaluated pressures on the other regions of the roof

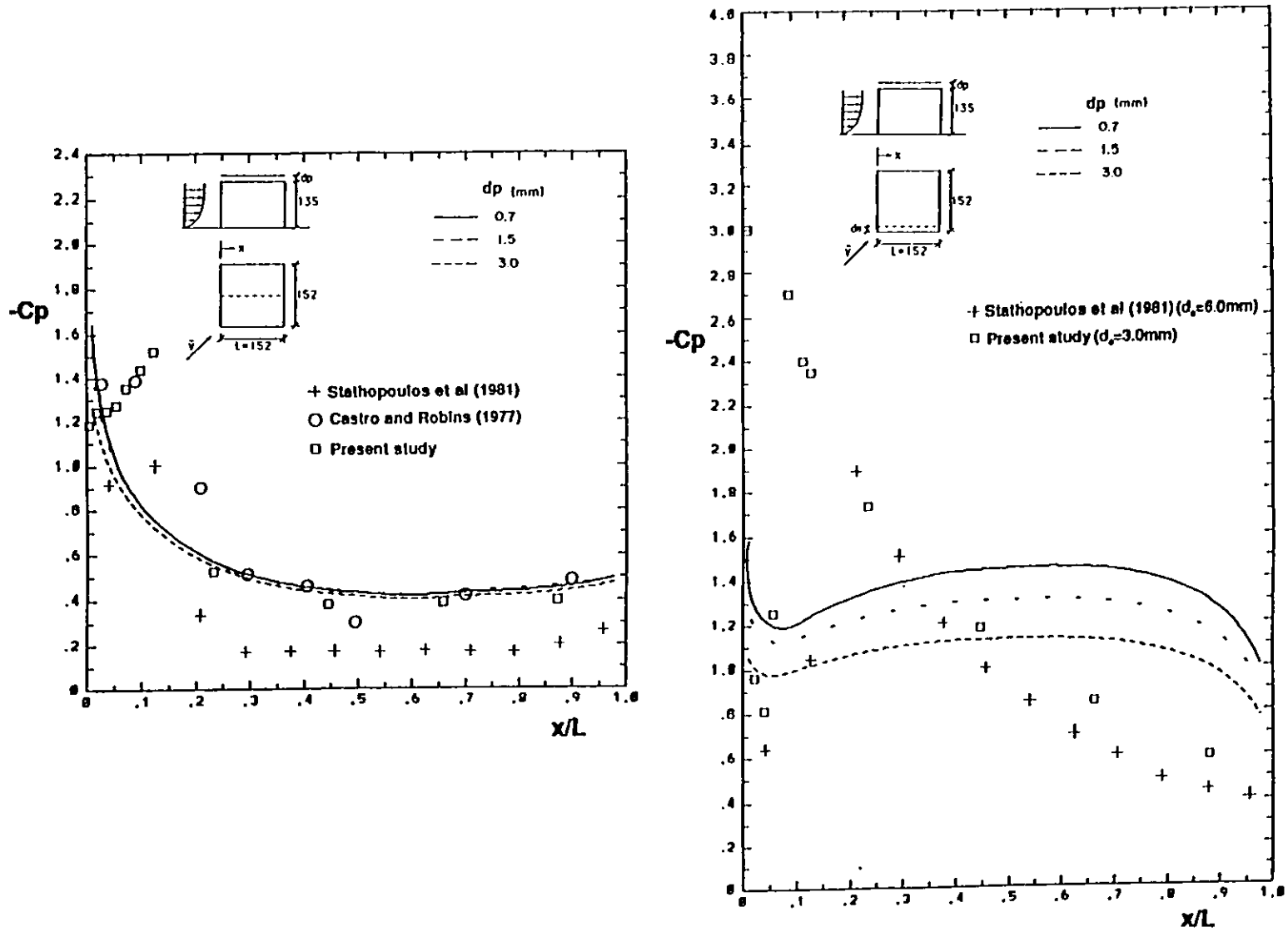

Figure 8.12 Pressure coefficients on roof (tall building, 45° azimuth).

agree well with the experimental data, particularly for small d_p values.

8.5 Conclusions

The wind flow over the roof of a rectangular building is very complex since it involves high turbulence, severe and adverse pressure gradients, and flow separation and reattachment. This makes the numerical modelling and evaluation of wind-induced pressures on roofs very difficult.

In general, the commonly used Reynolds averaged Navier-Stokes equations with the k-ε model for closure can predict the wind pressures on the centreline of the flat roof of a low aspect ratio building for normal wind conditions when adequate d_p is used. For a taller building, the k-ε model can only be used with major reservations; in particular, the suctions very close to the windward edge on the flat roof of a tall building will be overestimated while suctions just downwind will be underestimated. This is possibly due to the limitation of the standard k-ε model which overpredicts the skin friction and has the tendency of keeping the calculated flow attached on the roof in the areas where the experiments indicate separation (see Rodi and Scheuerer,1986). It should also be noted that the boundary conditions, e.g. the wall functions used for this region, are only valid for the turbulent flow near a large plane under zero pressure gradient (see Chapter 5, Chapter 9 and also Rodi and Scheuerer, 1986). Such boundary conditions are approximately accurate in the region far from the windward edge and too coarse to

provide good predictions elsewhere. The deviation of numerical pressure from the experimental data at the roof edge regions is more apparent under oblique wind direction especially for the taller building model. This may be attributed to the high vorticity in this separation region which is not well represented by the standard k-ε model. The numerical false diffusion caused by the skewness of wind velocity to grid lines described by Patankar (1980) is possibly another reason for this discrepancy. Better prediction may be achieved by a more detailed mathematical model such as two-layer model (see Chapter 9) or large eddy simulation (LES) (Murakami, 1990). More accurate 3-D boundary conditions for the roof corner and the windward roof edge regions are also needed. The partial success of the k-ε model in predicting wind pressures on the roof of a low rise rectangular building is also shown in the case of a low-rise stepped-roof building as presented in the previous chapter.

In the present study, the computations of wind pressures on flat roofs have been made for three different distances (d_p) of the first grid line to the roof surface, namely, 0.7 mm, 1.5 mm and 3.0 mm. The pressure coefficient variation versus d_p has also been investigated at four typical roof locations. It has been shown that the roof surface can be divided into two subregions, i.e. the high pressure gradient region where the computed pressure is highly dependent on the distance d_p and the low pressure gradient region in which the computed pressure is nearly d_p-independent for d_p less than 10% of the building width. Under normal wind conditions, the high pressure gradient region is small (approximately 10% of the roof surface) whereas the high pressure gradient region for

oblique wind conditions is larger - around 20% of the roof surface. The influence of d_p on the predicted pressure near the windward edge is dramatic especially for the oblique wind cases whereas the pressure outside the separation region is not apparently affected. The comparisons with experimental data have indicated that the computed results in the d_p-dependent region always show larger differences, whereas grid refinement can give improved results only for the low building model.

Chapter 9

A COMPUTER SIMULATION OF 3D WIND FLOW AROUND A BUILDING WITH TWO-LAYER METHODS

9.1 General Background

In this chapter, the two-layer methods combining the k-ε model in external fully turbulent flow region with either the one-equation model or the low Reynolds number modified k-ε model in the near wall area have been tested in computing the wind conditions around a cubic building. Results were compared with those from the k-ε model computation as well as from the experiments. Comparison shows that neither the k-ε model approach nor the two-layer method based on the modified k-ε model can represent the flow separation above roof surface and near the side walls. The one-equation model based two-layer approach, however, is effective in predicting the separation. The numerical prediction of the wind-induced pressure on building surfaces, especially on roof and side walls, is also improved as compared with the other two methods.

As stated in the previous chapters, the LES can only be applied to the unsteady-state large scale motion of turbulent flow and needs finer grid arrangement, it takes much more computational time than the k-ε model method which can be applied to the steady-state mean flow. Therefore, the k-ε model method is very attractive to wind engineers

since it needs much less computational power than the LES method. However, when applied to the wind flow around a rectangular building, the k-ε model method cannot correctly predict the reverse flow after separation on the roof surface and the side walls (see Chapters 7 and 8 and also Figure 9.1). This flow separation, well known by experiments (Hosker, 1985), can be predicted numerically as shown by Murakami (1990), who applied the LES method at a much higher computational cost. Therefore, the objective of this study was to find a model which can predict the separation properties as accurately as LES while keeping the simplicity of the k-ε model approach.

The previous studies (Murakami, Mochida and Hayashi, 1990, Chen and Patel, 1987 and Stathopoulos and Zhou, 1992) have shown that the well-known k-ε model can predict very well the general wind conditions around buildings except those in the separation regions above roof surface and near side walls. To keep the advantages of k-ε model for external flow properties, and to avoid its shortcomings for the near wall regions, a two-layer method to simulate the wind conditions around a cubic building was adopted by Zhou and Stathopoulos (1995). In this two-layer approach, the computational region was divided into two layers, namely inner region and external region, as shown in Fig. 9.2. The wind flow in all external regions is computed with the standard k-ε model, whereas the flow near building surfaces (inner regions) is simulated with a near wall model. Two near wall models have been chosen in the current study: first, the one-equation model proposed by Norris and Reynolds (1975) which was also adopted by Rodi and Scheuerer (1986) in investigating the effects of adverse pressure gradient on shear

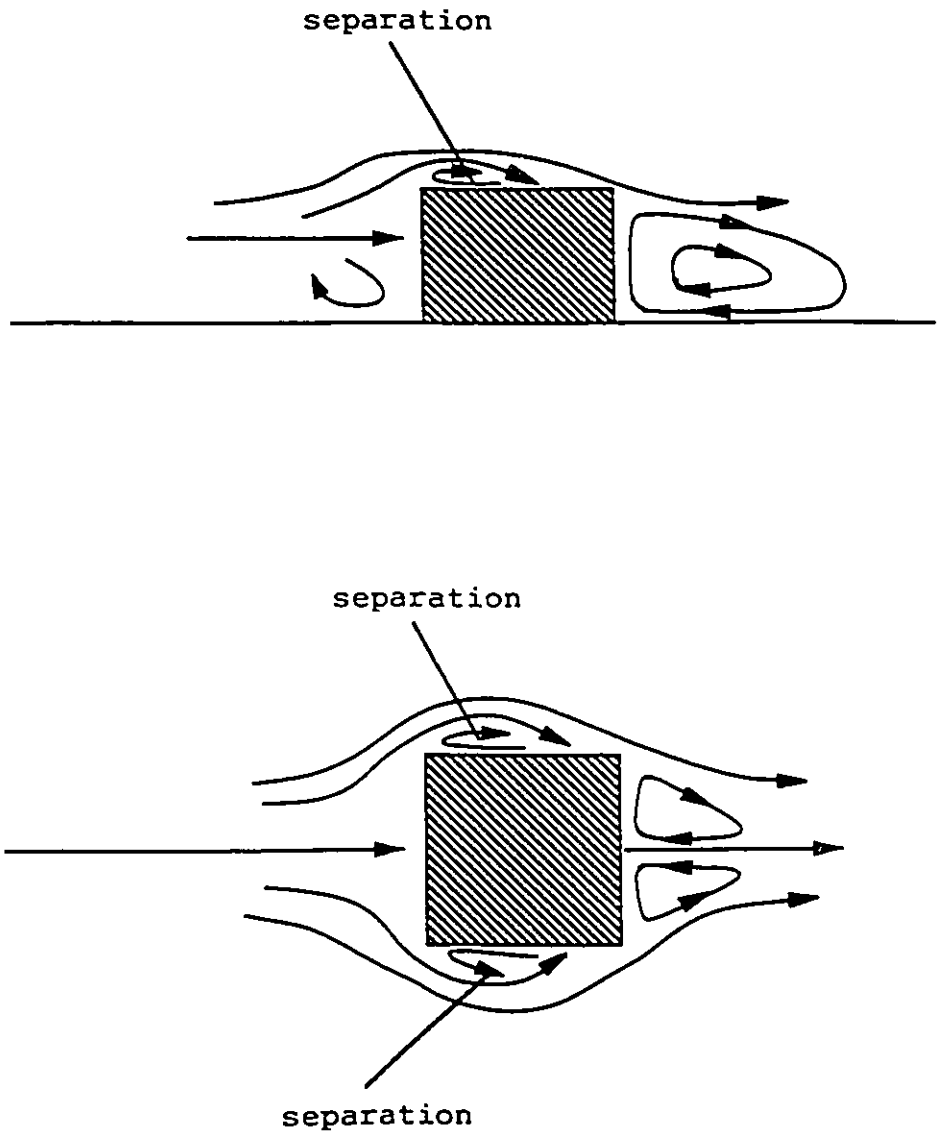

Figure 9.1 Mean flow field around a rectangular building.

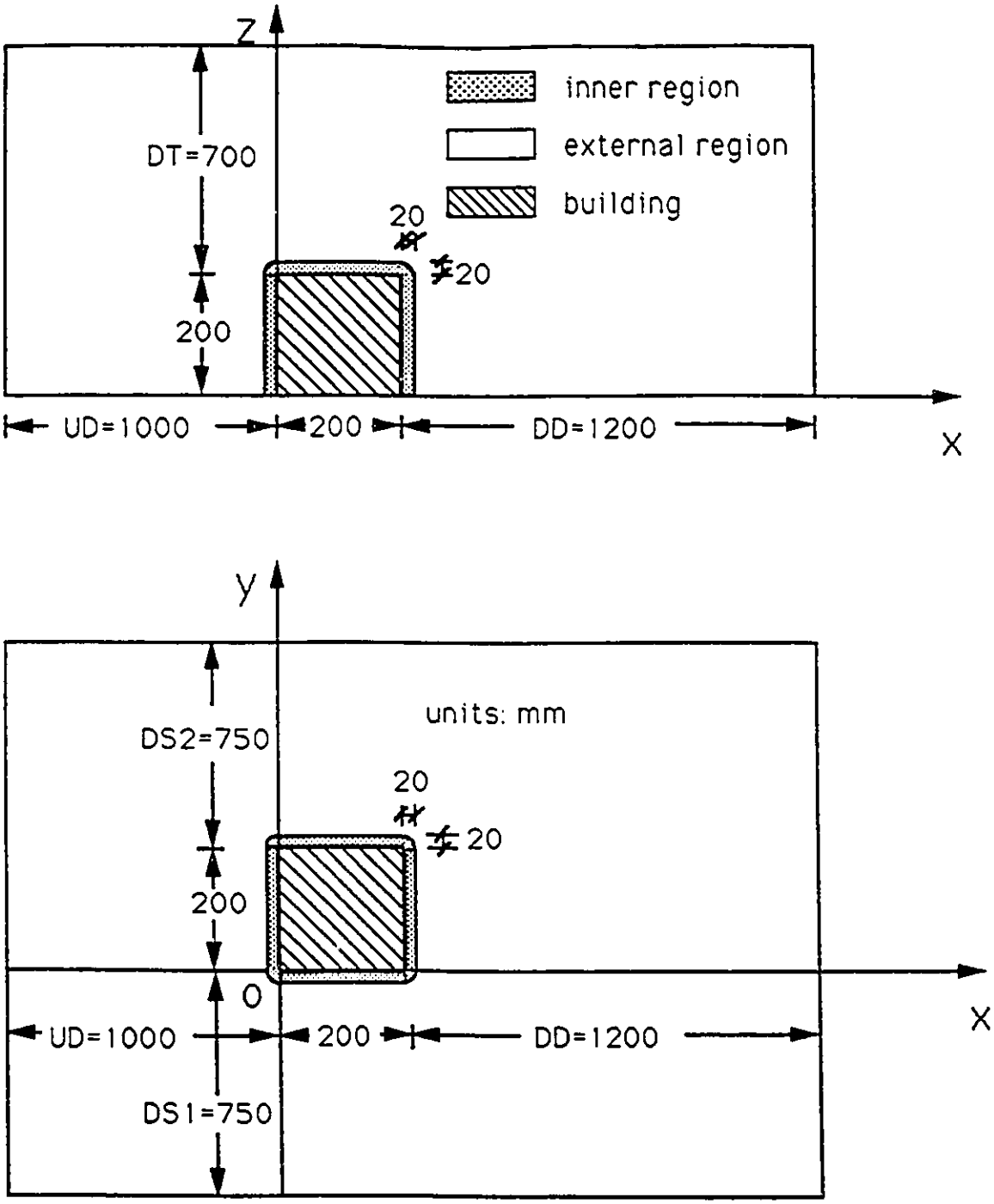

Figure 9.2 Computational domain for the two-layer method.

layers; and second, the two-equation modified k-ε model for low Reynolds number turbulent flow proposed by Lam and Bremhorst (1981). In this paper, the two-layer method adopting Norris and Reynolds' one-equation model in inner region is called **N-R** two-layer method while the one using Lam and Bremhorst's modified k-ε model in the inner layer is called **L-B** two-layer method.

A two-layer method has also been adopted by Chen and Patel (1987) to simulate the turbulent fluid flow around an elliptic body by using the one-equation model proposed by Wolfshtein (1969) in the inner flow region close to the solid walls and the k-ε model for the external flow region far from the solid walls. When compared with experimental results, this two-layer method provided apparent improvements compared with the usual k-ε model method in separation regions (Chen and Patel, 1987), whereas such improvement in other regions was not apparent. This approach was also adopted by Franke and Rodi (1991) in numerically simulating two-dimensional periodic shedding motion around a rectangular cylinder with Norris and Reynolds' one-equation model as the near wall model. A slight improvement in predicting the mean flow properties behind the structure was achieved by the two-layer method as compared with the k-ε model approach.

In the present paper, in applying both the L-B and the N-R two-layer approaches, the computations were made for both normal (0° azimuth) and oblique (45° azimuth) wind conditions. The oncoming wind follows the power-law velocity profile in a turbulent

boundary layer. In order to save computational time, the two-layer methods are only applied to the building surfaces. For the flow near the ground, the usual wall function method, which needs fewer grid nodes, is used (Chen and Patel, 1987). The computed wind pressures on building surfaces have been compared with the experimental data of Castro and Robins (1977), Stathopoulos, Surry and Davenport (1981) and Hunt (1982). Computed results with the standard k-ε model method from the present computation were also included in the comparison. Finally, the computed velocity vector fields have been compared with the experimental data of Murakami, Mochida and Hayashi (1990).

9.2 Two-Layer Mathematical Models

9.2.1 Governing equations for the external flow region

For the external flow region, the Reynolds averaged Navier-Stokes (RANS) equations together with the k-ε turbulence model - i.e. equations (4.1) to (4.4) and (4.6) presented in Chapter 4 - are solved for the mean flow properties.

9.2.2 Governing equations for the inner flow region

In the inner flow region near solid walls, both the one-equation model of Norris and Reynolds (1975) and the two-equation modified k-ε model of Lam and Bremhorst (1981) have been used in the current computation.

Norris and Reynolds' One-Equation Model: The turbulence model adopted in N-R two-layer method in the near wall region is the one-equation model by Norris and Reynolds (1975). This model was also adopted by Rodi and Scheuerer (1986) in evaluating the effects of adverse pressure gradient in shear layer flow. According to Norris and Reynolds (1975), the dissipation of turbulence kinetic energy (ε) in equation (4.3) is scaled as $\nu k/L^2$ at low Reynolds numbers while the length scale L is proportional to the distance from the solid wall (denoted as d) so that the dissipation in equation (4.3) is represented by:

$$\varepsilon=\frac{k^{\frac{3}{2}}}{L}\left(1+\frac{C_\varepsilon}{k^{\frac{1}{2}}L/\nu}\right) \tag{9.1}$$

where L is a length-scale defined by the formula:

$$L=C_D\kappa d \tag{9.2}$$

The empirical constants have the values C_ε = 13.2, C_D = 6.41, κ = 0.41. By noticing k ~ d^2 near the wall, equation (9.1) becomes $\varepsilon \approx C_\varepsilon \nu k/L^2$ when d is very small, and ε approaches a constant as $d \rightarrow 0$. This is indeed the proper physical behaviour of the dissipation (Reynolds, 1976). Unlike the k-ε model in which equation (4.6) containing both k and ε is used to determine the eddy viscosity, one-equation models evaluate the eddy viscosity without ε. In the one-equation model by Norris and Reynolds (1975), the eddy viscosity is given by the following equation:

$$\nu_t=C_\mu f_\mu k^{1/2}L \tag{9.3}$$

where ε appears as the length scale L and f_μ = 1-exp(-0.0198R_d) is a damping function

in which $R_d = dk^{1/2}/\nu$ is the turbulence Reynolds number. This damping function is introduced in this equation by noticing that the turbulent transport is suppressed by the presence of the wall. As $d \rightarrow 0$, equation (9.3) gives $\nu_t \sim d^4$ as explained by Reynolds (1976).

In the inner flow region where the one-equation model is used, equations (4.1) to (4.3) will still be used for the solutions of mean velocity components (U_i) and turbulence kinetic energy (k), while equations (4.4) and (4.6) will be replaced by equations (9.1) and (9.3) respectively to determine the turbulence dissipation (ε) and eddy viscosity (ν_t).

Lam and Bremhorst's Modified k-ε Model: One of the most often used low Reynolds number modified k-ε model is that proposed by Lam and Bremhorst (1981). According to this model, equation (4.4), i.e. the ε-equation, is modified by adjusting the parameters C_1 and C_2 with functions f_1 and f_2 so that it becomes:

$$U_j\frac{\partial e}{\partial x_j}=\frac{\partial}{\partial x_j}\left[\left(\nu+\frac{\nu_t}{\sigma_e}\right)\frac{\partial e}{\partial x_j}\right]+C_1 f_1\frac{e}{k}\nu_t\left(\frac{\partial U_i}{\partial x_j}+\frac{\partial U_j}{\partial x_i}\right)\frac{\partial U_i}{\partial x_j}-C_2 f_2\frac{e^2}{k} \qquad (9.4)$$

The eddy viscosity in equation (4.6) is also adjusted, similar to Norris and Reynolds' one-equation model, with a damping function f_μ:

$$\nu_t=C_\mu f_\mu\frac{k^2}{\varepsilon} \qquad (9.5)$$

In equations (9.4) and (9.5), the functions f_1, f_2 and f_μ are as follows:

$$f_\mu = [1-\exp(-0.0165R_k)]^2\left(1+\frac{20.5}{R_t}\right) \tag{9.6}$$

$$f_1 = 1+\left(\frac{0.05}{f_\mu}\right)^3 \tag{9.7}$$

$$f_2 = 1-\exp(-R_t^2) \tag{9.8}$$

where $R_t = k^2/\nu\varepsilon$ and $R_k = k^{1/2}d/\nu$ are the turbulence Reynolds numbers.

Note that for the L-B two-layer approach, equations (4.4) and (4.6) will be replaced by equations (9.4) and (9.5) in the inner layer to determine the turbulence dissipation (ε) and eddy viscosity (ν_t).

9.3 Grid Arrangement

Since the building is a rectangular block, the rectangular grid system has been used in this study. The grid nodes for velocities (U_i) and those for pressures (P) and turbulence properties (k and ε) are arranged staggered (see Figure 3.1). Although the non-staggered grid system is a little easier to use, the staggered grid is preferred since it avoids the evaluation of the boundary condition of pressures (Patankar, 1980). In fact, the pressures near solid walls can be obtained directly without extrapolation which is needed for non-staggered grids (Peric, Kessler and Scheuerer, 1988). In this study, a computational grid arrangement of 54x48x33 points has been used for a 20 cm cubic building model under normal wind conditions. To apply the two-layer method, very dense grids have been put near building surfaces and a relatively coarse grid arrangement is

used in other regions. In particular, 8 grid lines were set in each inner layer whereas only 10 to 13 grid lines were used for the external layers with dimension varying from 70 to 120 cm as shown in Fig. 9.2 for the normal wind case. To obtain the detailed information near windward corner, and also to apply the two-layer method near the building surfaces, the distance between the first grid line and the building walls (d_p) - see Figure 3.1 - is selected as small as 0.3 mm. The corresponding dimensionless distance is:

$$Y_p^+ = \frac{u^* d_p}{\nu} \tag{9.9}$$

in which u^* is the friction velocity. Equation (9.9) shows that Y^+_p is approximately equal to 3, which is well within the linear-viscous-sublayer (see Bradshaw, 1976 and Chapter 5). The inner region, where the one-equation model is used, has a thickness d = 2 cm which corresponds to a dimensionless thickness $Y^+ = u^* d/\nu$ equal to 200, i.e. is far enough from the wall to ensure the external flow to be fully turbulent outside the linear viscous sublayer and buffer region (see Chen and Patel, 1987, Bradshaw, 1976 and Chapter 5). The airflow in the inner region ($Y^+ < 200$) can be represented by the Norris-Reynolds one-equation model very accurately, see Rodi and Scheuerer (1986). The dependence of the numerical results on the domain size and the overall grid density has been examined. Results show that the current computational domain size and grid arrangement, is adequate. Negligible effects were found when a larger domain size and/or more grids were adopted. The computational grid system used is shown in Figure 9.3.

The simulation of oblique wind cases is achieved by rotating the flow field rather

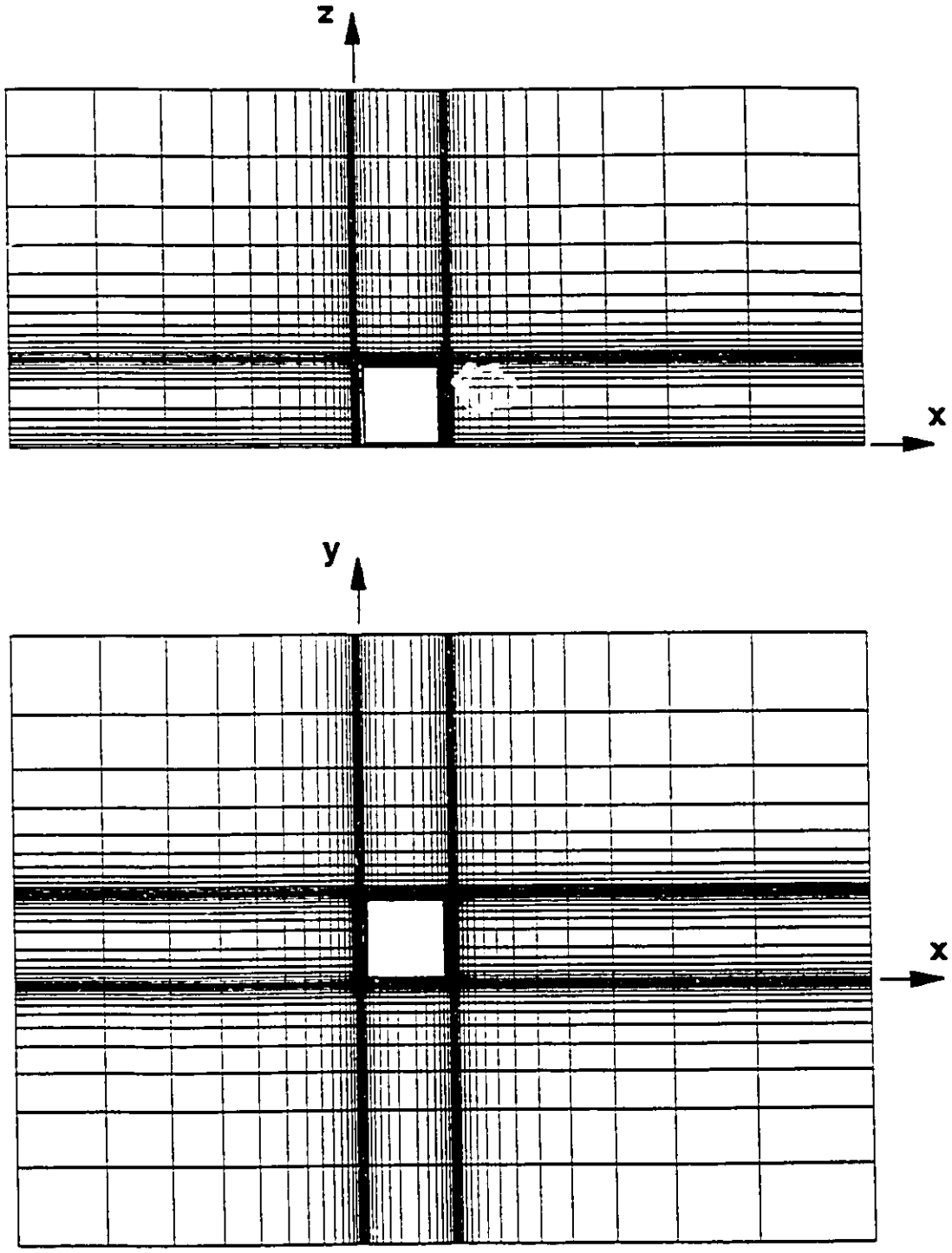

Figure 9.3 Computational grid system for the two-layer method.

than the building itself to avoid the difficulty of rearranging the grid nodes and to ensure that the solid boundary conditions for normal wind conditions can also be used for the oblique wind cases. For the current numerical solution for 45° azimuth both the region of computation and the grid system are arranged symmetrical about the diagonal of the building; in particular, UD=DS1=100 cm, DD=DS2=120 cm and DT=70 cm. The plan-view of this computational domain is shown in Figure 9.4.

9.4 Boundary Conditions

9.4.1 Free boundary conditions

The boundary conditions of velocity at free boundaries are fixed at the initial power-law velocity profile appropriate for suburban terrain conditions, i.e. $U/Ug = (Z/Zg)^{0.25}$, V=0 and W=0. The corresponding initial turbulence properties, i.e. the turbulence properties k and ε obtained through a computation of k and ε equations - equations (4.4) and (4.6) - with the known power-law velocity field, are also used as the free boundary conditions.

9.4.2 Solid boundary conditions

For the calculation of tangential velocity components on the first grid line near a solid boundary, a correction in the source term of the discretized RANS equations is

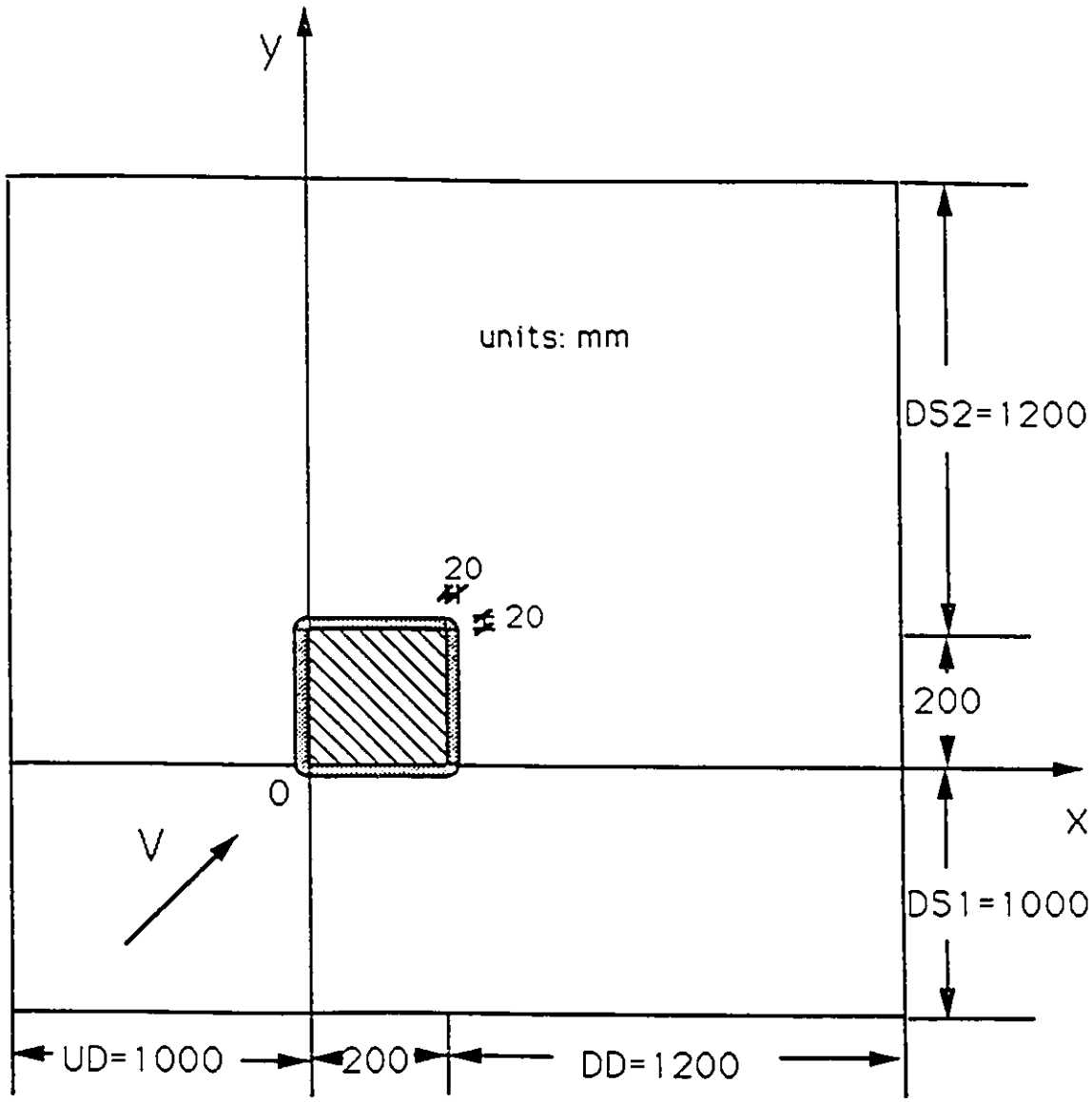

Figure 9.4 Plan-view of the computational domain for the two-layer method under oblique wind direction (45° azimuth).

needed to account for the friction effect from the boundary evaluated by the well known wall functions which are already shown in Chapter 5 [equations (5.15) and (5.16)]. The calculation of velocities farther away from the solid wall uses the finite difference form of RANS equations without correction in the source terms. Since the value of d_p used for the computation near the building surface is very small, only the linear-law, equation (5.16), is actually used in these regions. It should be noted that the no-slip boundary conditions are not adequate for these regions due to the very high gradient of flow properties requiring very dense grids.

To evaluate the turbulence kinetic energy (k) on the first grid line near building surfaces and the ground, the kinetic energy at second grid line (see Figure 3.1) near the surfaces is extrapolated to the first grid line. This extrapolation takes into account the fact that k is proportional to d^2, where, d is the distance from the solid surface to the position of interest, i.e:

$$k_p = k_q \frac{d_p^2}{d_q^2} \qquad (9.10)$$

where k_q, k_p are kinetic energy on the second grid line and first grid line at the distances d_q, d_p away from solid walls.

The turbulence energy dissipation rate (ε) at the first grid line near ground where the N-R two-layer method is not applied is evaluated by (see Stathopoulos and Baskaran, 1990):

$$\epsilon_p = \frac{2\nu k_p}{d_p^2} \qquad (9.11)$$

For building surfaces where the N-R two-layer method is used, equation (9.1) will be applied down to the solid surfaces so that the boundary conditions for ε are not necessary.

9.4.3 Solution procedure

Under a given grid arrangement and boundary conditions, the well-known SIMPLE method is adopted for the numerical solution of the two models for both the external flow and the inner flow region. For the N-R two-layer method, the Payne-Irons method has been used for the inner region to set the dissipation rate of the turbulence kinetic energy (ε) at the value given by equation (9.1). The computation can thus be carried out simultaneously in both the inner and outer flow region. The convergence of the computation is evaluated by relative residues of all the equations as explained in Chapter 4 and Chapter 8.

9.5 Results and Discussion

The wind conditions around a 20 cm cubic building model have been numerically simulated with the two-layer methods as well as with the usual k-ε model method. As previously mentioned, the power-law exponent used for the velocity profile is 0.25 which

corresponds to an upstream exposure of suburban terrain. Results are presented in this section for both normal (0^o azimuth) and oblique (45^o azimuth) wind conditions. The pressures on building surfaces are shown in terms of pressure coefficients, i.e. pressures normalized by the upstream dynamic pressure at roof height. The computed wind pressures are compared with the experimental data by Castro and Robins (1977), Stathopoulos, Surry and Davenport (1981) and Hunt (1982).

The mean velocity vector fields in the vertical cross-section through the centre of the building obtained from the two-layer methods and the k-ε model computation are presented in Fig. 9.5 and compared with the velocity vector field from the experiments by Murakami (1990). Figure 9.5 shows that the reverse flow behind the building, the reverse flow in front of the building near the ground and the high velocity near the windward corner found in experiments have been successfully predicted by the k-ε model method and both two-layer methods. However, the separation region above the roof shown in Fig. 9.5a by experiments cannot be predicted by the usual k-ε model computation as shown in Fig. 9.5b or the L-B two-layer computation as shown in Fig. 9.5c. This separation, however, has been successfully predicted by using the N-R two-layer method as shown in Fig. 9.5d. The failure of k-ε model approach in predicting the flow separation on the roof is not surprising because this model is not valid in the near wall region where the flow is not fully turbulent. The Lam and Bremhorst's modified k-ε model which was determined by reference to zero pressure gradient boundary layers seems also to be inadequate in the roof region near windward edge where pressure

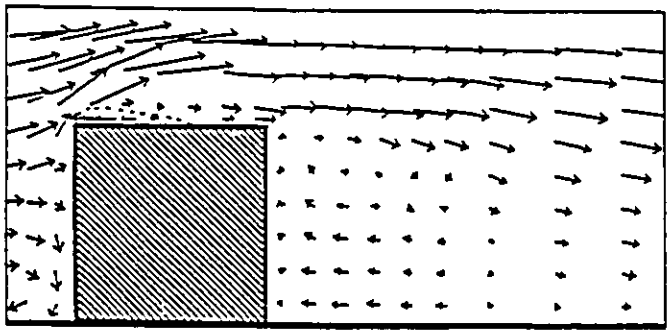

a) Experiment (Murakami, 1990)

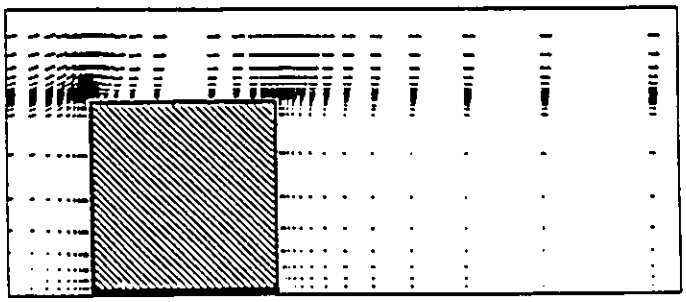

b) k-ε model computation

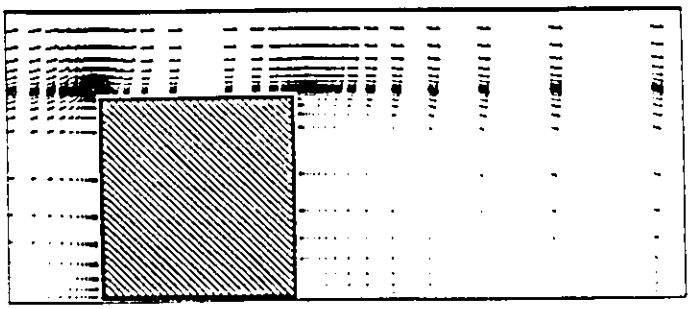

c) L-B two-layer computation

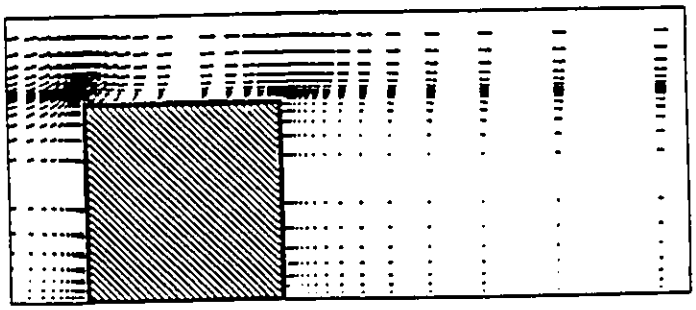

d) N-R two-layer computation

Figure 9.5 Mean velocity vector field around the building (vertical cross-section, 0° azimuth).

gradient is adverse (Rodi and Scheuerer, 1986). Therefore, the failure for the standard k-ε model and the L-B two-layer method to predict the flow separation above the roof surface is mainly due to the over-predicted mixing length scale near walls, especially near windward corners. This leads to the over-prediction of eddy viscosity in this region which in fact causes the failure of predicting the separation (see Rodi and Scheuerer, 1986).

The mean velocity vector fields obtained from the two-layer approaches and the k-ε model method on a horizontal plane at half building height are presented in Fig. 9.6. As shown in the figure, the separation regions found in the experiments by Murakami (1990) beside the side walls (Fig. 9.6a) have been successfully predicted using the N-R two-layer method (Fig. 9.6d). However, these flow separations cannot be obtained from the usual k-ε model computation or the L-B two-layer approach (Figs. 9.6b and 9.6c). The overall flow fields in other areas predicted by these methods, however, are quite similar.

The computed velocity profiles at three typical locations have been presented in Figures 9.7, 9.8 and 9.9 and compared with the experimental data by Castro and Robins (1977). The velocities presented have been normalized by the upstream velocity at reference height (Z_r = 200 cm) above the ground. All three velocity profiles are presented in the x-z vertical plane going through the centre of the building.

Figure 9.7 shows the vertical profile of the longitudinal velocity above the cube

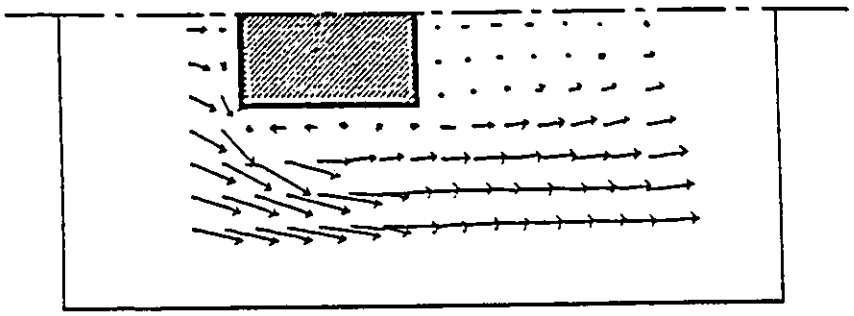

a) Experiment (Murakami, 1990)

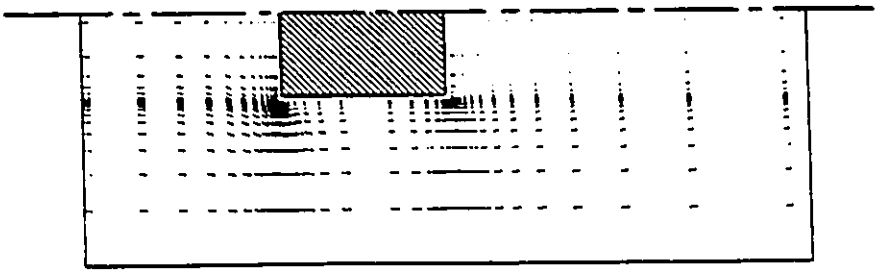

b) k-ε model computation

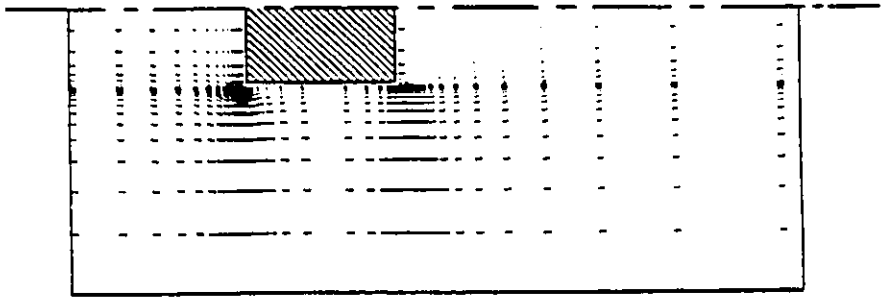

c) L-B two-layer computation

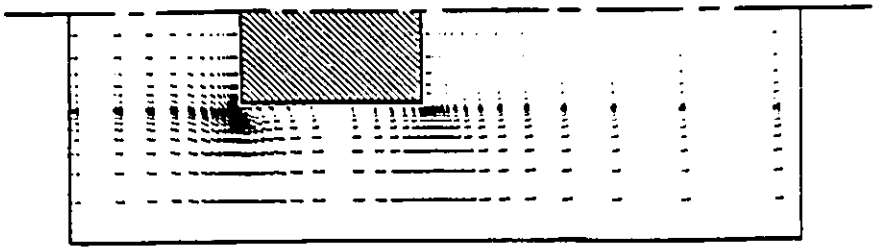

d) N-R two-layer computation

Figure 9.6 Mean velocity vector field around the building (plan-view, 0° azimuth).

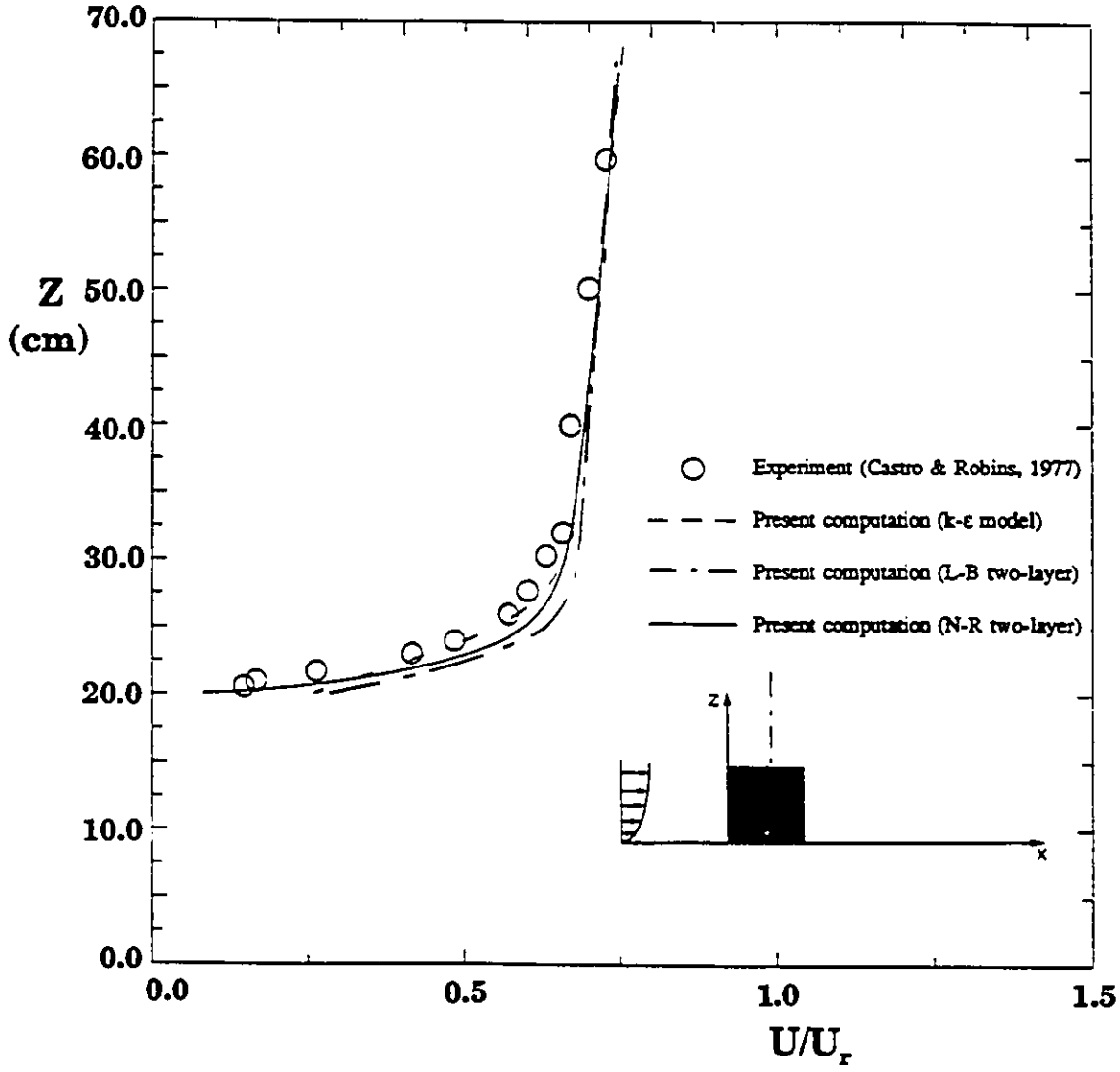

Figure 9.7 Mean velocity profile above the roof

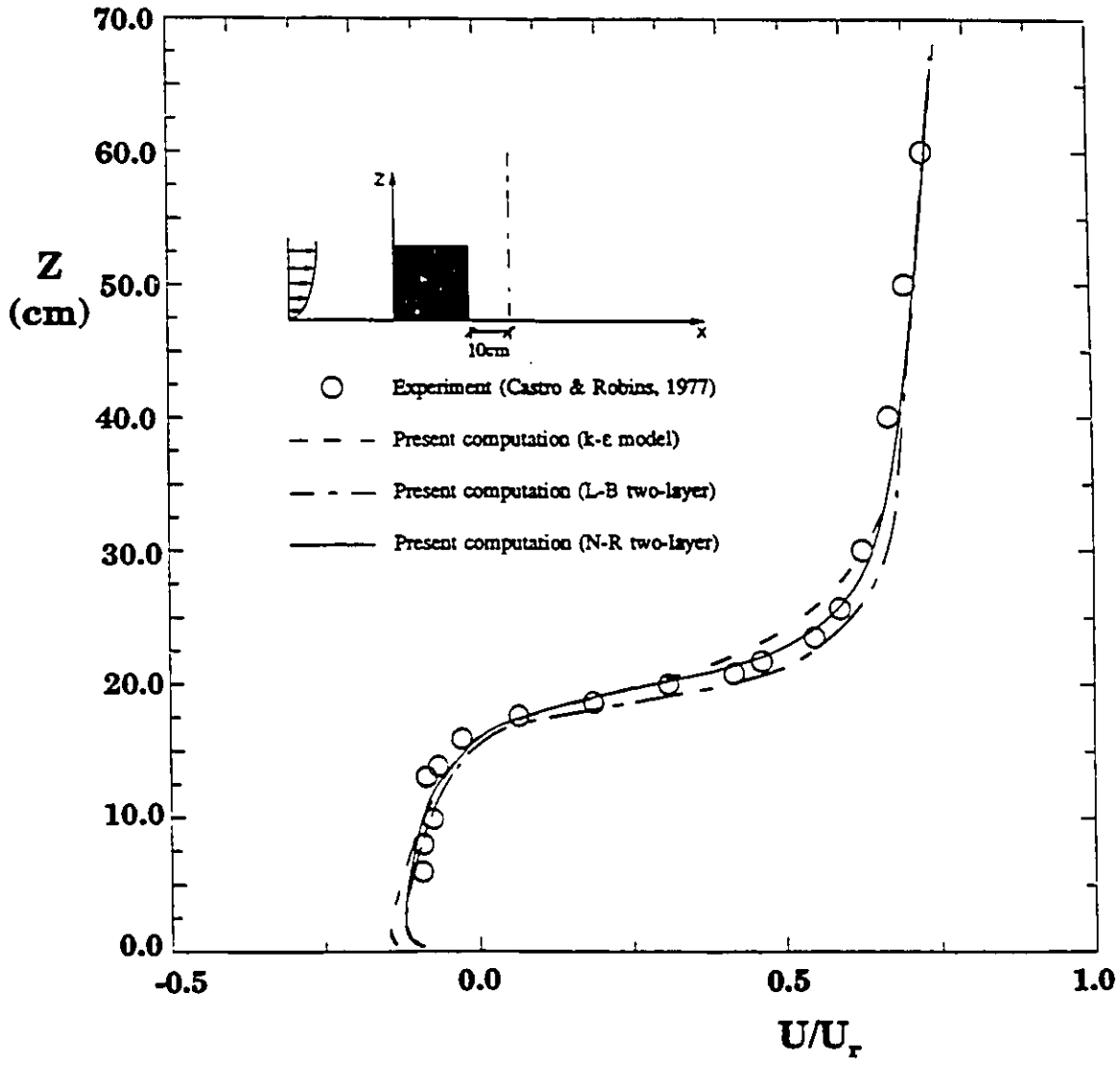

Figure 9.8 Mean velocity profile in the wake of the building (10cm)

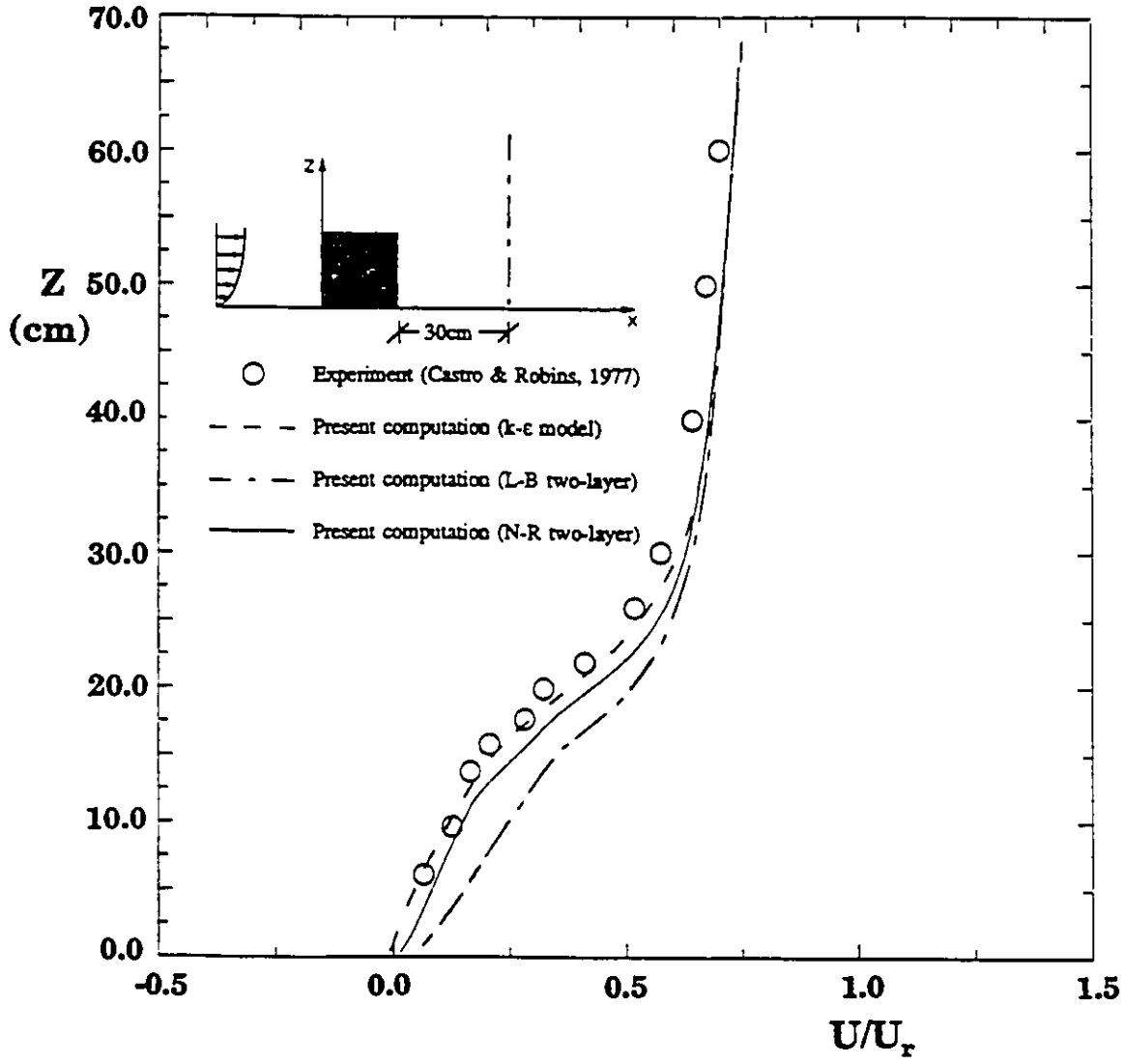

Figure 9.9 Mean velocity profile in the wake of the building (30cm)

at the centre of the building. The computed velocities from all three methods have been presented and compared with the experimental data by Castro and Robins (1977). The comparison shows good agreement between the numerical results and the experimental data, except in the area near building roof where the longitudinal velocity was somewhat overestimated by the k-ε model computation and the L-B two-layer method. Such discrepancy, however, has been apparently reduced by the N-R two-layer approach.

It is also of interest to check the velocities in the wake behind the cube. To achieve this, the velocity profiles located at x=30 cm and 50 cm (i.e. 10 cm and 30 cm behind the building) have been computed and compared with the available experimental data. The computed vertical velocity profiles 10 cm behind the cubic building are presented in Fig. 9.8 in the same format with Fig. 9.7. Results from three different numerical methods are quite similar, and the agreement between the numerical results and the experimental data is very good, especially for those from the N-R two-layer computation. Data for the velocity profiles at 30 cm behind the building are shown in Fig. 9.9. The agreement between numerical results and the experimental data is reasonably good except that the L-B two-layer method underestimates the reverse flow behind the building.

The contourlines of the computed pressure coefficients on the building surfaces have been shown in Figure 9.10. Very dense contourlines near the windward comers on front wall, side wall and roof surface indicate high pressure gradient in these regions. The

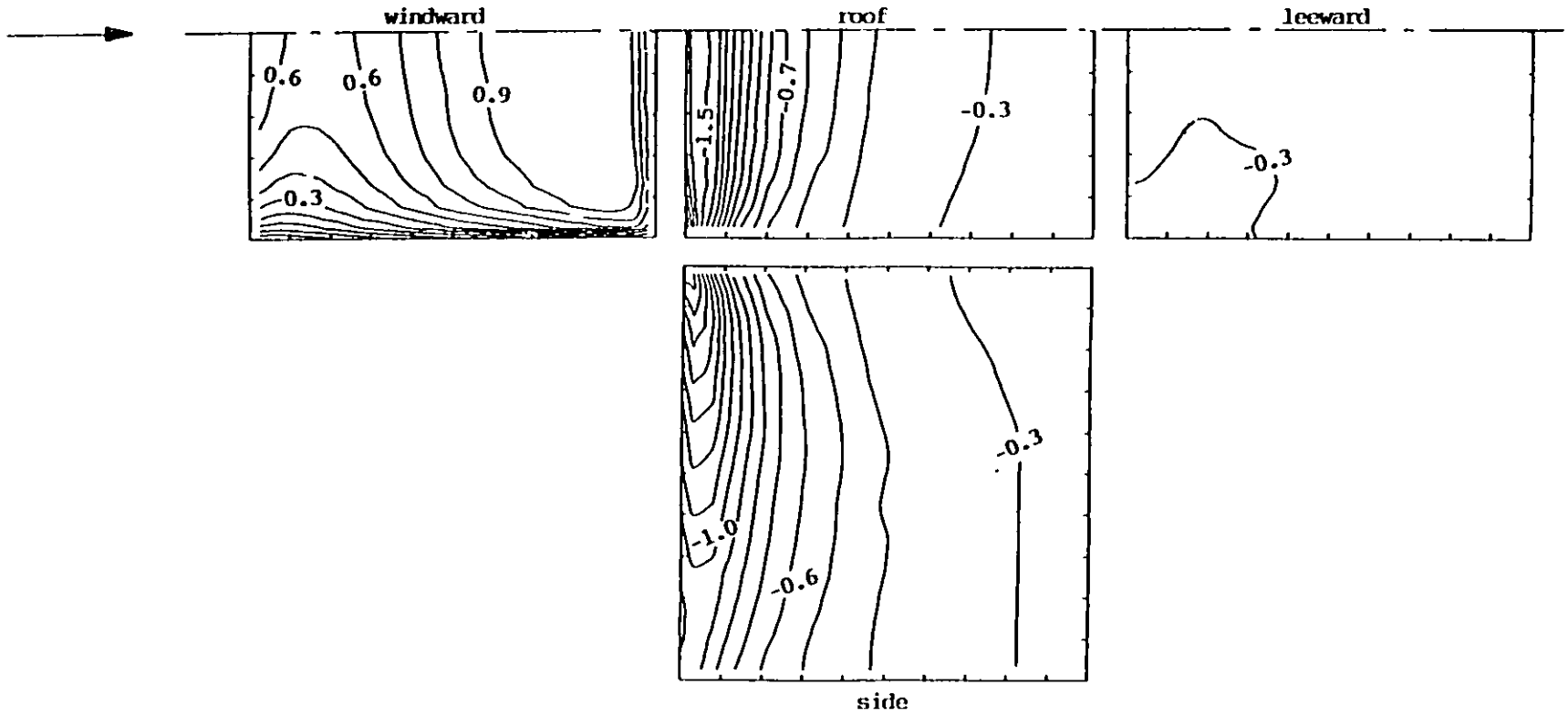

Figure 9.10 Wind pressure on the building envelope (N-R two-layer method, 0° azimuth).

highest positive pressure on front wall occurs on the vertical centre line at the level of about 80% of building height. This point corresponds also to the stagnation on this wall. Contrary to the front wall, side wall and the building roof, where pressures vary over a large range, the wind-induced mean pressure on the rear wall is very uniform due to the big vortex behind the building as has been shown in Figures 9.5 and 9.6.

The computed wind pressure coefficients obtained from both two-layer methods and the k-ε model approach along the centre lines of the building surfaces have been plotted in Fig. 9.11, and compared with the experimental data of Castro and Robins (1977) and Hunt (1982). The general agreement between numerical results and the experimental data is reasonable in most regions with the results from the N-R two-layer method showing a better agreement with the experimental data on the roof surface; in particular, the unrealistic very high suctions near the windward corner on roof surface predicted by the k-ε model method and the L-B two-layer approach have been apparently reduced. It should be reiterated that the distance from the first grid line to roof surface (d_p) is as small as 0.3 mm for the present computation with both the two-layer methods and the k-ε model approach. This distance in other studies with k-ε model approach (e.g. Paterson and Apelt, 1990, Murakami, 1990 and Baetke, Werner and Wengle, 1990) is as large as about 5 mm showing a false reduced numerical suction on the roof surface near the windward edge (see Stathopoulos and Zhou, 1992 and Chapter 8). Another fact should also be noted: the curve of pressure coefficient on roof surface from the N-R two-layer method presents a similar shape to the curves of experimental results. The curves of C_p

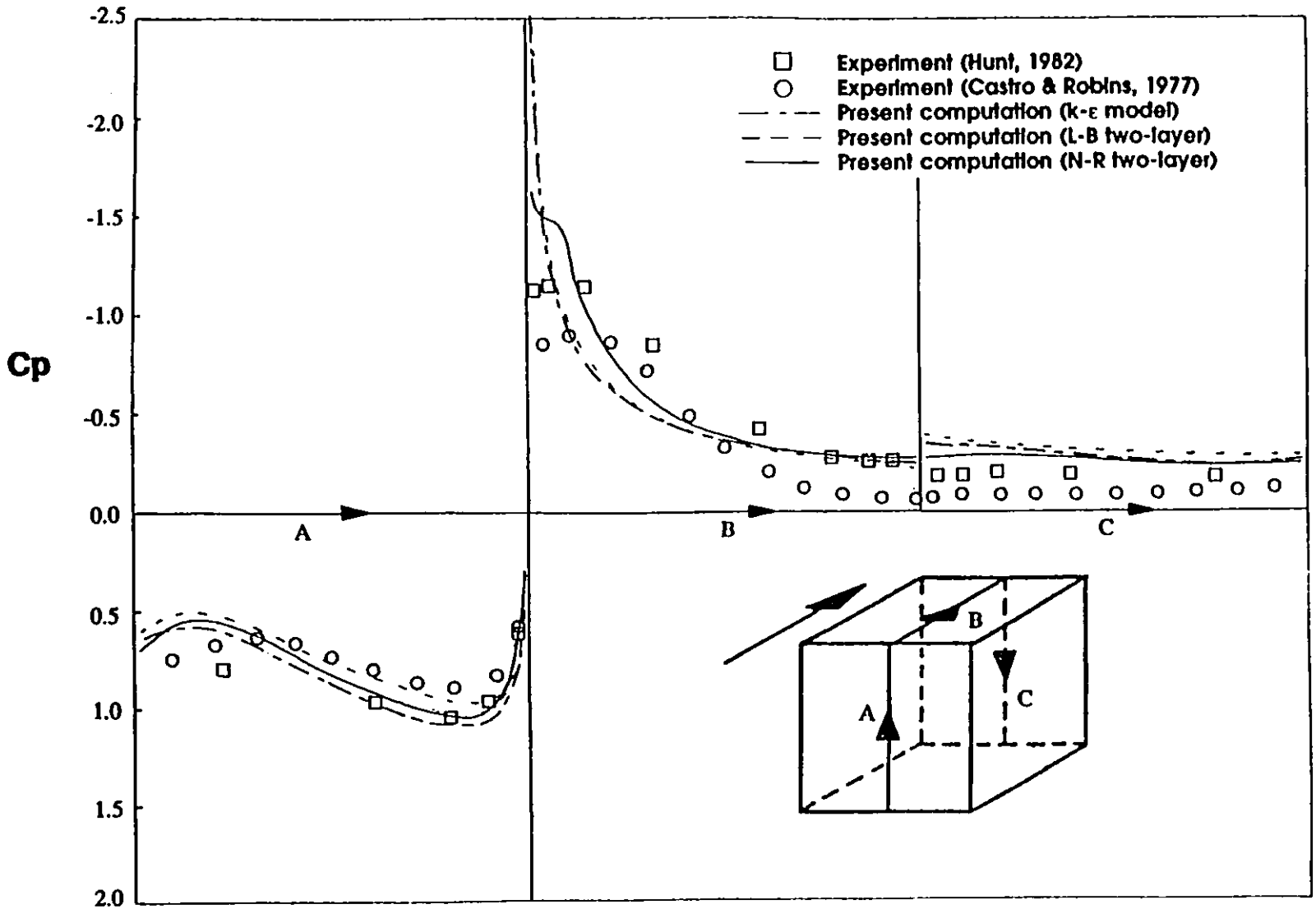

Figure 9.11 Wind pressure along the centre lines (0° azimuth).

from the L-B two-layer method and the k-ε model approach, however, follow a totally different shape. This phenomenon is relevant to the fact that the N-R two-layer method can predict the separation above roof surface while the k-ε model and the L-B two-layer approach fail to do so (see Fig. 9.5). On the lee wall, however, the results from these three methods are quite similar since the pressure is almost constant, thus the adverse pressure gradient effect is negligible.

Figure 9.12 shows the computed wind pressure coefficients on the front wall, side wall and the rear wall obtained along the horizontal line at half building height from both two-layer methods and the k-ε model approach of the current study. Results are compared with the experimental data of Castro and Robins (1977) and Hunt (1982). Apparently, phenomena similar to those discussed for Fig. 9.11 have been found in this figure. Again, the positive pressure on front wall, the negative pressure on the side and lee walls has been better predicted by the new N-R two-layer method than by the usual k-ε model approach or the L-B two-layer approach. In particular, the unrealistic high suctions near the windward edge on side wall predicted by the k-ε model method and the L-B two-layer method have been reduced by using the N-R two-layer approach. Due to the larger reverse flow regions beside the side walls (see Fig. 9.6) than above the roof surface (see Fig. 9.5), the pressure curve on the side wall near the windward corner shows a more apparent concave shape than the curve on roof surface (Fig. 9.11).

The effect of the N-R two-layer method in better predicting the wind pressure on

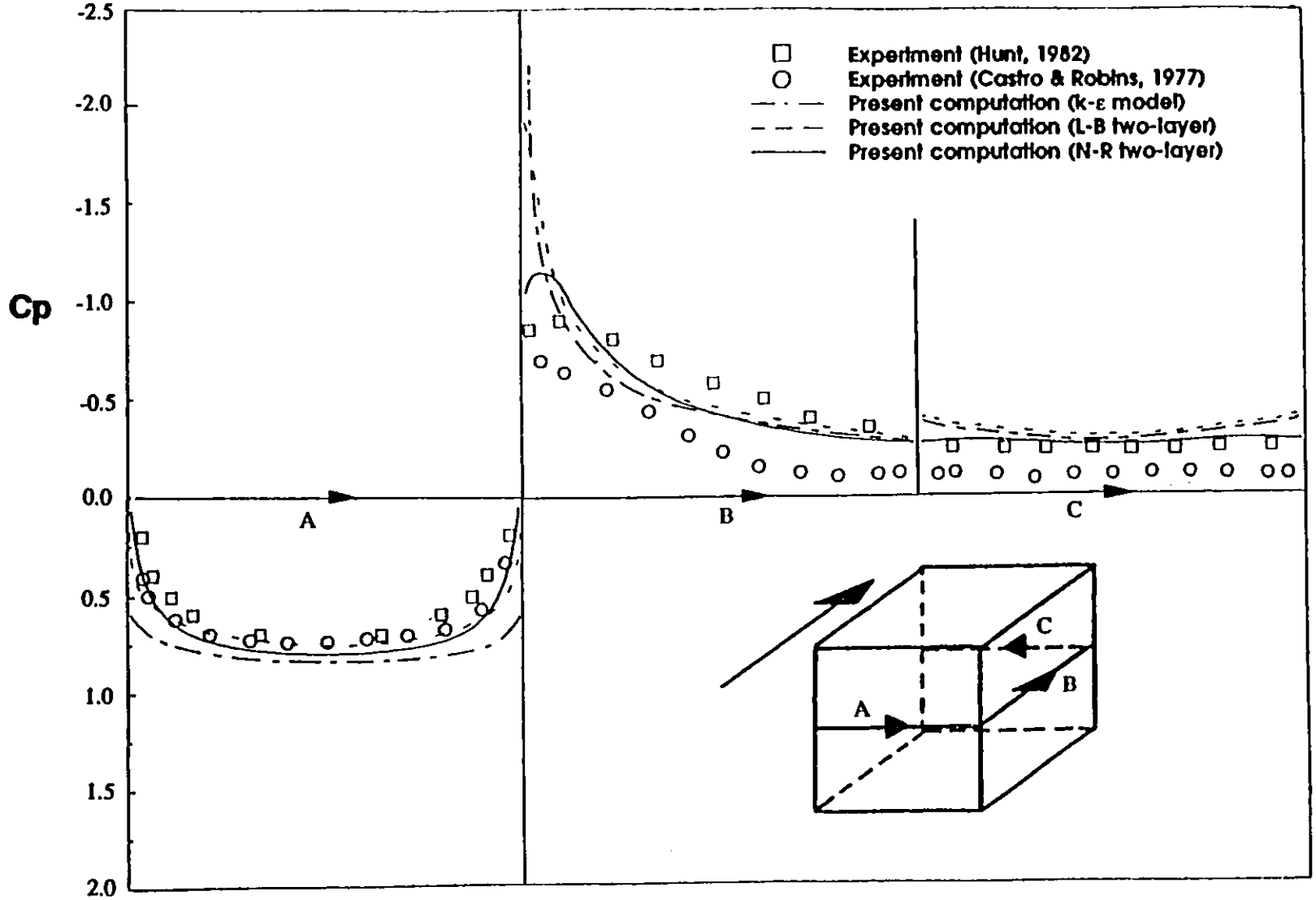

Figure 9.12 Wind pressure at half building height (0° azimuth).

roof can also be seen clearly in Figure 9.13 in which the wind-induced pressure along a line 12 mm away from the side edge of the roof has been shown. The comparison of the numerical results obtained from the two-layer methods and from the k-ε model approach with the experimental data of Hunt (1982) shows that the N-R two-layer method predicts the suctions on edge line in better agreement with the experimental data than the other two approaches. The L-B two-layer method as well as the k-ε model computation overpredicts the suction in the region very close to the windward edge and underpredicts the suctions in the region farther away from the windward edge up to the middle of the roof. These deviations, however, have been apparently improved by the N-R two-layer method.

In order to see the general distribution of pressure on the roof where the most critical suction exists, the contourlines of the computed pressure coefficients on roof surface have been presented in Fig. 9.14 and compared with the experimental results of Hunt (1982). Very dense contourlines, indicating a high pressure gradient, exist in the numerical results from the k-ε model method (Fig. 9.14b) and the L-B two-layer approach (Fig. 9.14c) near the windward corner on the roof. The experimental data (Fig. 9.14a) show a sparse contourline distribution, i.e. low pressure gradient, in this area where reverse flow exists. By reproducing the separation region (reverse flow area) on the roof (Fig. 9.5), the N-R two-layer method has clearly improved the prediction of pressure coefficients in this area as can be seen in Fig. 9.14d.

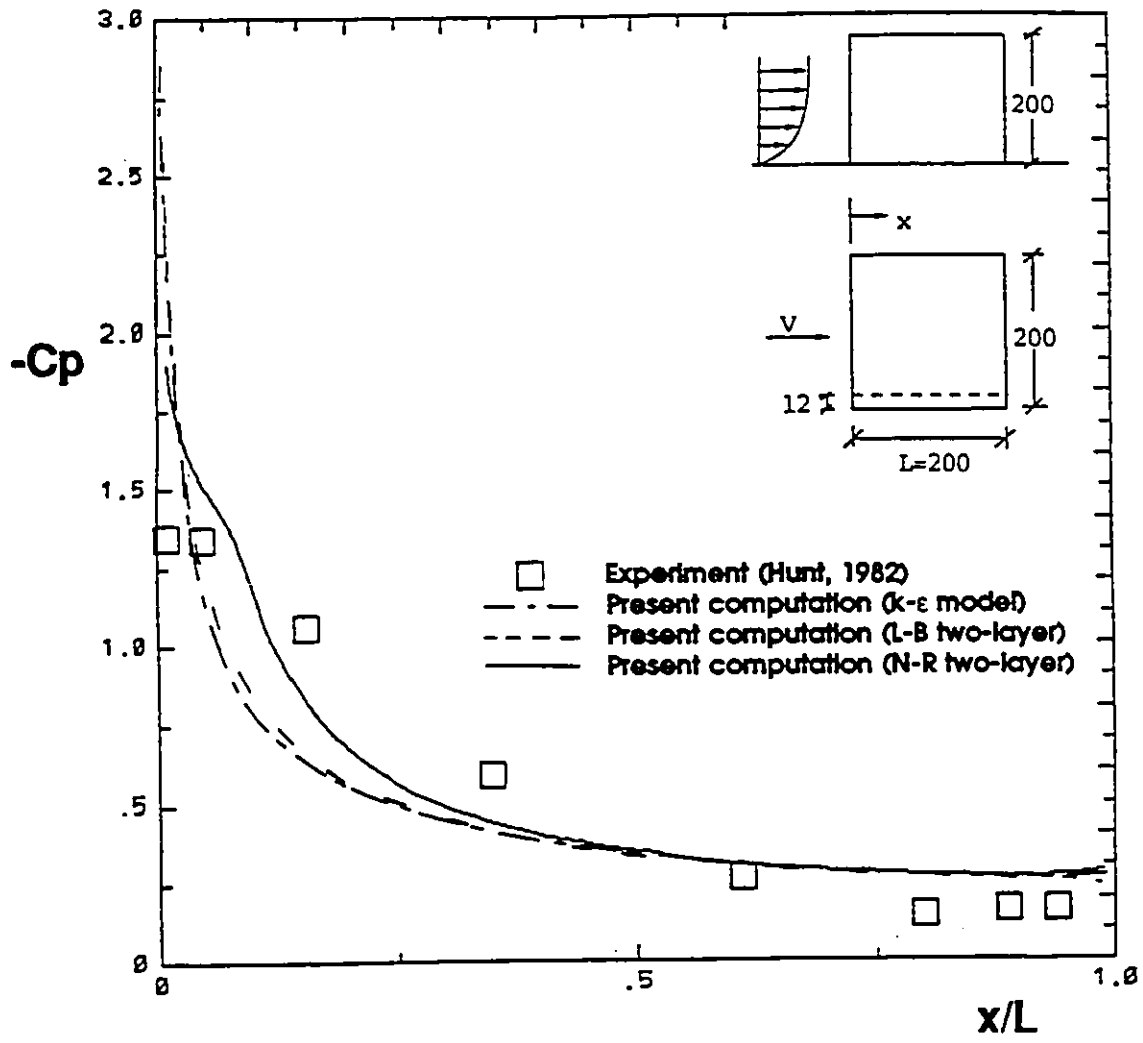

Figure 9.13 Wind pressure on the roof surface (edge line, 0° azimuth).

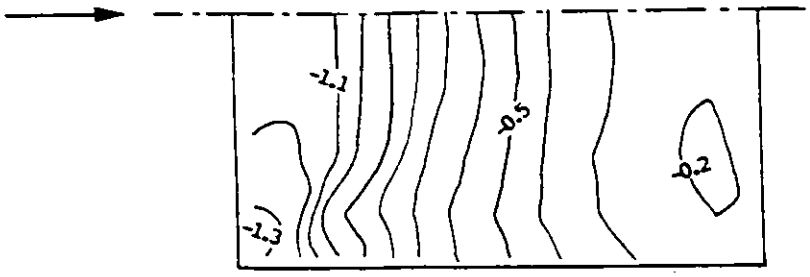

a) Experiment (Hunt, 1982)

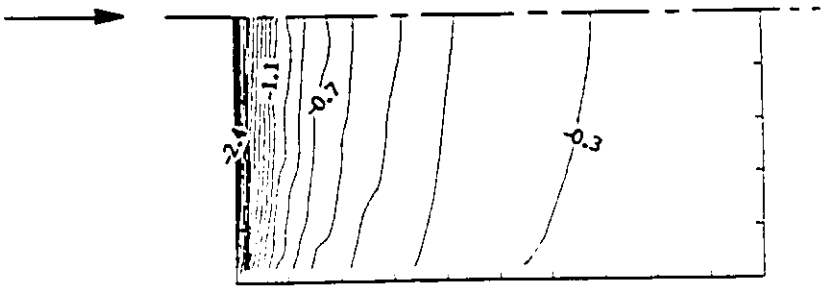

b) k-ε model computation

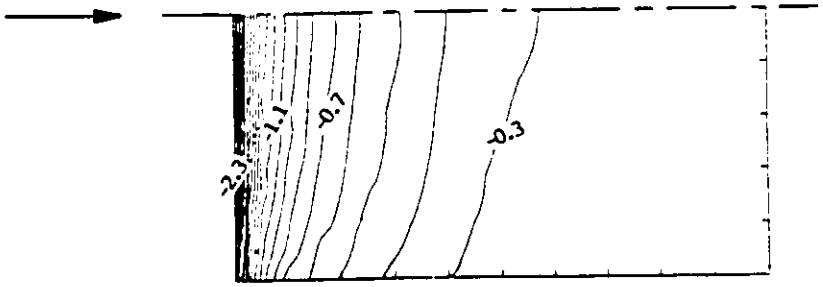

c) L-B two-layer computation

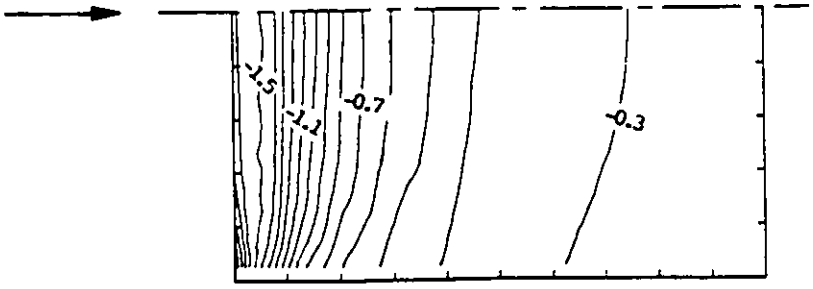

d) N-R two-layer computation

Figure 9.14 Contours of pressure coefficient on roof (0° azimuth).

The wind conditions around the cubic building model under oblique wind direction (45° azimuth) have also been evaluated in this study. The mean flow velocity vector fields and the pressure coefficients on building surfaces under oblique wind direction (45° azimuth) are presented in Figs. 9.15 to 9.19 in the same format with Fig. 9.6 and Fig. 9.10 to 9.12 and 9.14 respectively. The horizontal mean velocity vector fields at half building height under oblique wind conditions (45° azimuth) obtained from the present study with both two-layer methods and the k-ε model approach have been presented in Figure 9.15. Due to the symmetry of the flow, only half of the flow fields are presented in the figure. Results from both two-layer methods and the k-ε model approach show that the coming flow is divided at the windward corner of the building into two flows along the two front walls. These two flows pass around the two shoulder corners at opposite positions forming two big symmetrical vortices behind the building. In general, very similar flow fields were obtained from these numerical methods for this 45° oblique wind case.

The computed contourlines of pressure coefficients on the building envelope of N-R two-layer method are presented in Fig. 9.16. Since the flow is symmetrical, only the results on one side are presented. The results indicate that the highest positive pressure on front wall has moved to the upwind corner under this oblique wind condition. The highest suction on roof surface, however, does not exist on the upwind corner but adjacent to it somewhere near the side edges. The negative pressure on the back wall is rather uniform, due to the big vortex behind the building (see Fig. 9.15), at higher values than

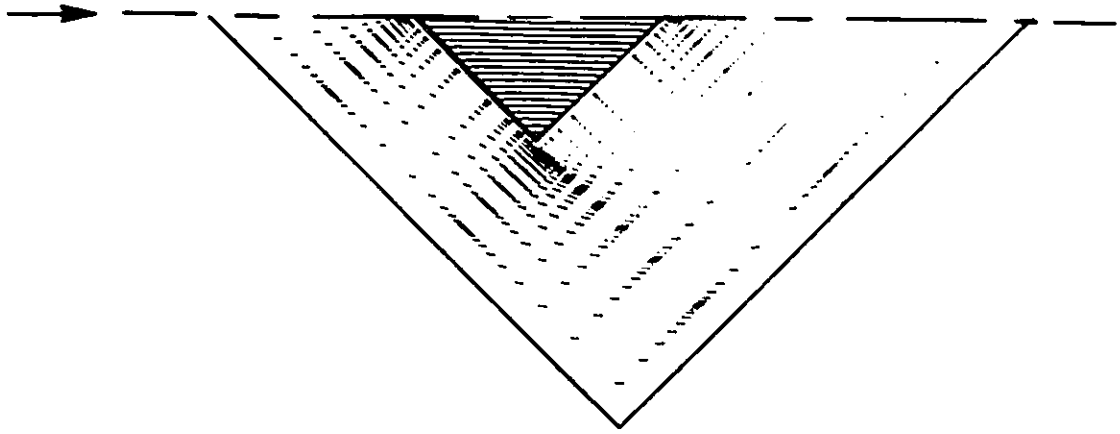

a) k-ε model computation

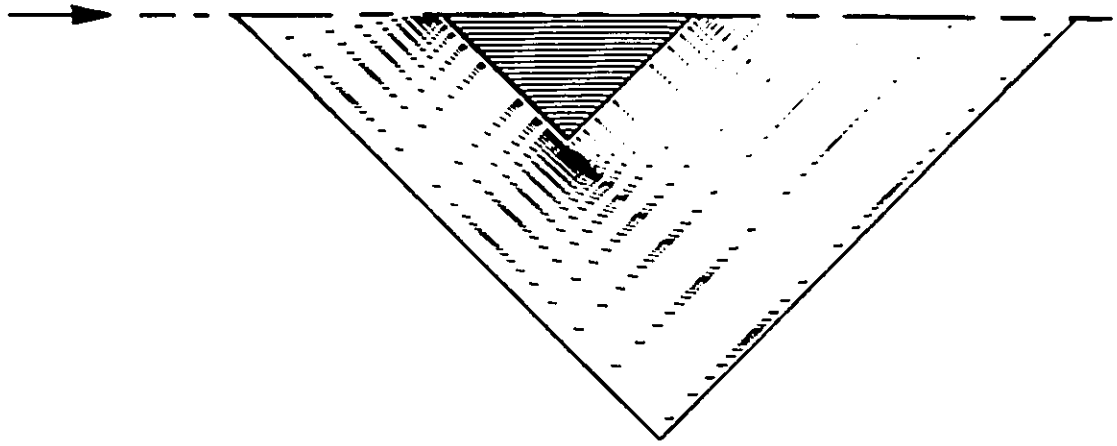

b) L-B two-layer computation

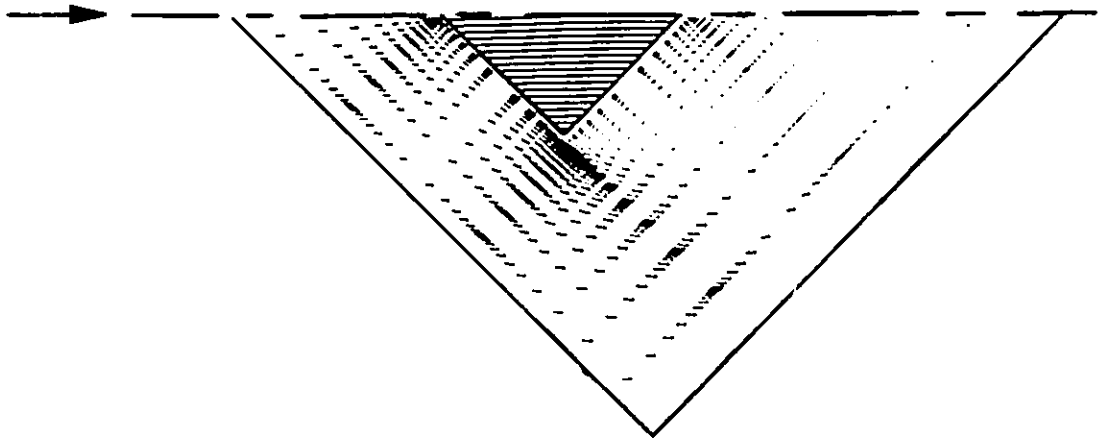

c) N-R two-layer computation

Figure 9.15 Mean velocity vector fields around the building (plan-view, 45° azimuth).

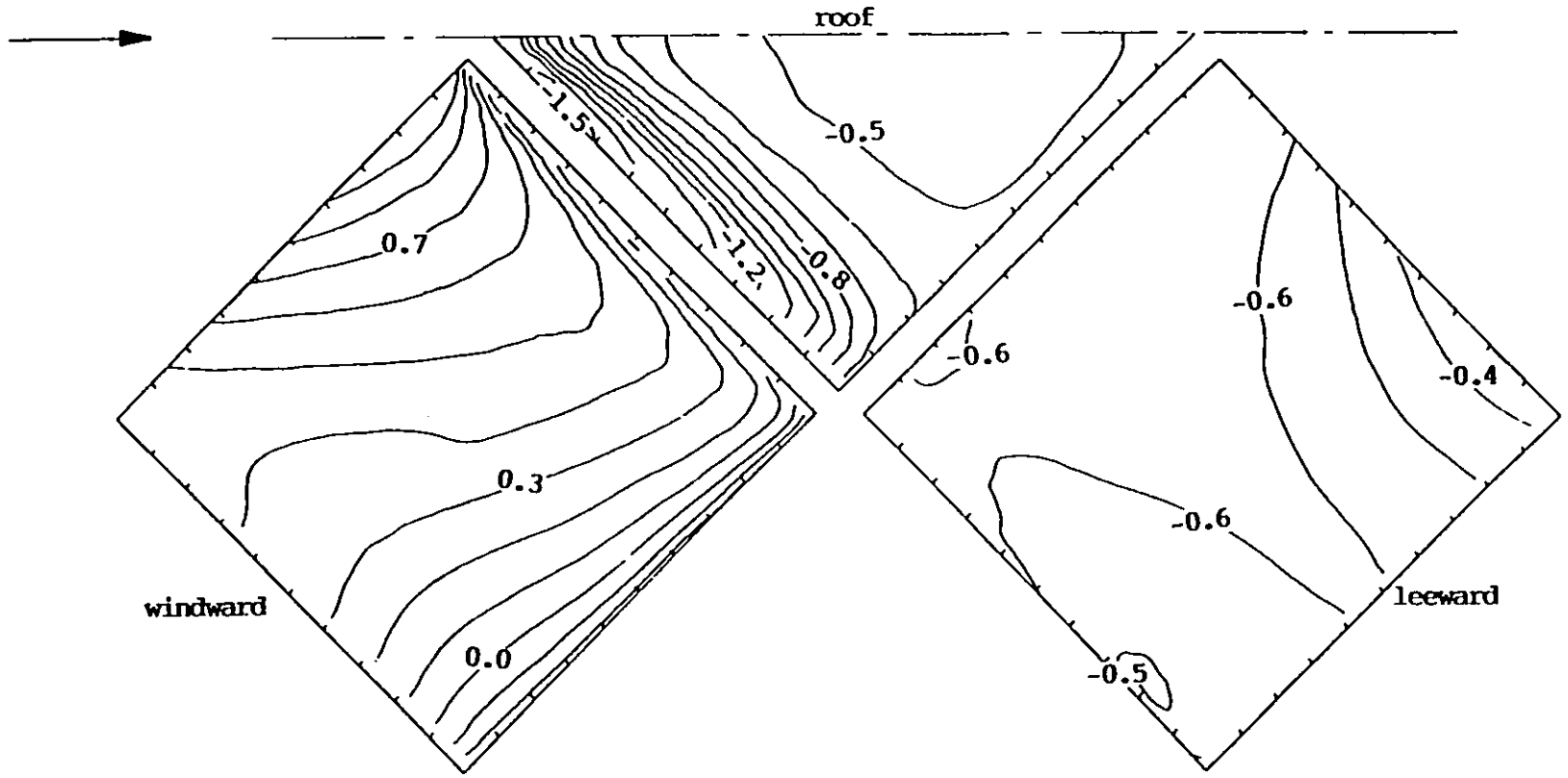

Figure 9.16 Wind pressure on the building surfaces (N-R two-layer method, 45° azimuth).

those under normal wind conditions.

A comparison of the currently computed pressures from both two-layer methods and the k-ε model approach with the experimental data of Castro and Robins (1977) can be found in Fig. 9.17 and Fig. 9.18. The results along centre lines on front wall, roof surface and back wall are shown in Fig. 9.17. Due to the symmetry of the flow, only the numerical pressure coefficients along the centre lines on one side were presented. It should be noted, however, that the experimental data on symmetrical positions have been averaged. As can be seen from the figure, the agreement between the numerical results, particularly those from the N-R two-layer method, and the experimental data is very good. In particular, the very high positive pressure on front wall and the very high suction near the windward edge on the roof surface found in the case of the k-ε model and the L-B two-layer method has been improved by the N-R two-layer method, which, overall, appears suitable to predict the wind conditions around a building even for oblique wind conditions.

The computed wind pressure coefficients on side walls at half building height from the two-layer methods and the k-ε model approach are presented and compared with experimental data in Fig. 9.18. Once again, the numerical results are presented on one side only due to the symmetry of the flow. As shown in the figure, the general agreement between the numerical results and the experimental data is good. Some discrepancies exist near the upwind corner on front wall and the downwind corner on back wall with those

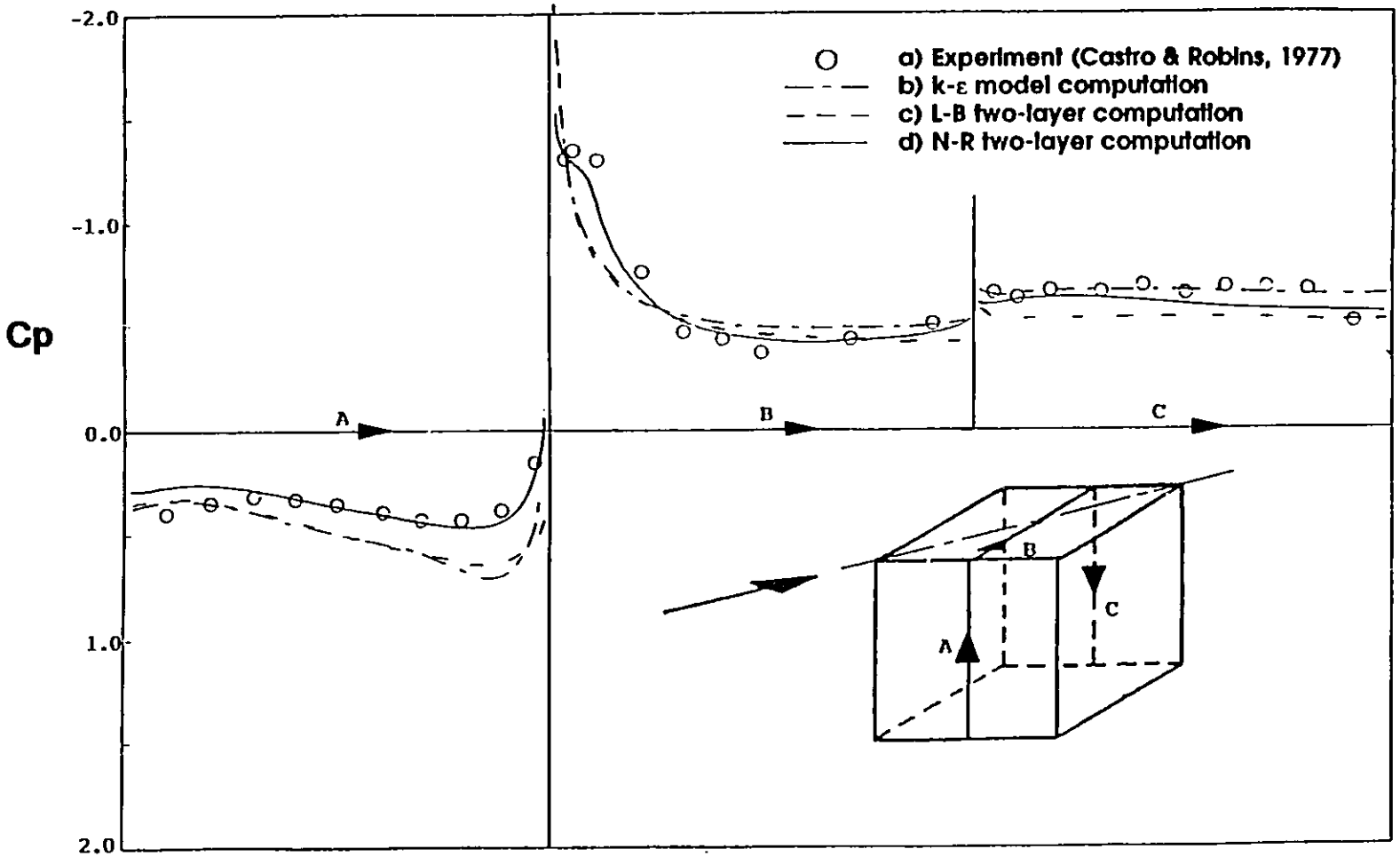

Figure 9.17 Wind pressure along the centre lines (45° azimuth).

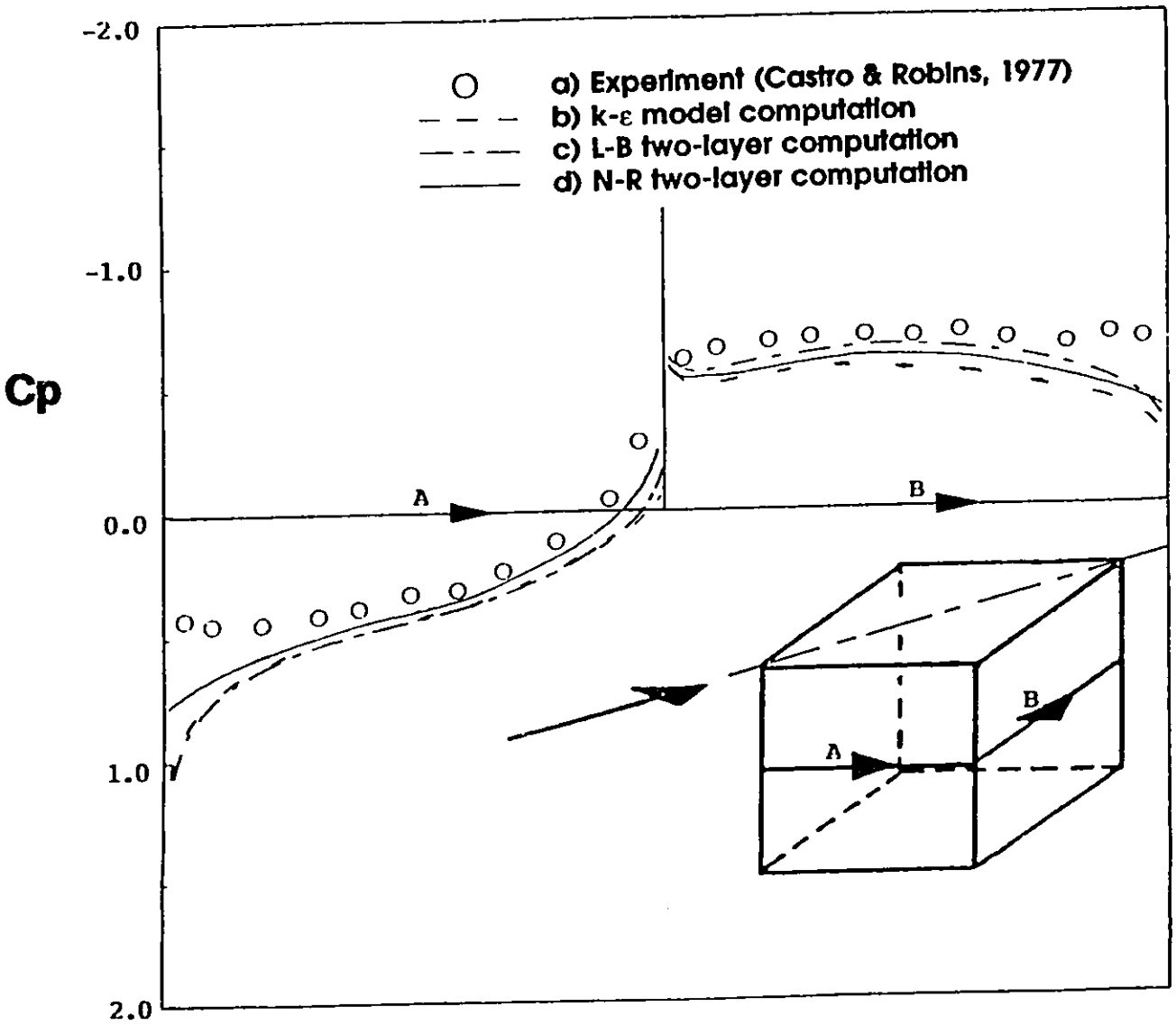

Figure 9.18 Wind pressure at half building height (45° azimuth).

from the N-R two-layer method to be somewhat smaller than the other two methods.

The contourlines of the computed pressure coefficients on roof surface are shown in Fig. 9.19. Since there is no experimental data available from either Hunt (1982) or Castro and Robins (1977), data by Stathopoulos, Surry and Davenport (1981) for slightly different building size and upstream exposure conditions are used for the current comparison. Considering these differences, the general agreement between the numerical results and the experimental data is good especially for the results by the N-R two-layer method. Most critical suctions have been found in the region near the windward corner on the roof and a relatively constant suction distribution exists in the region far from the windward edges.

In order to examine the integrated wind effects on buildings, the numerical mean drag coefficients on the cubic building have also been computed. The results are compared with the wind tunnel experimental data by Akins, Peterka and Cermak (1977). It should be noted that since the drag coefficients presented in Akins, Peterka and Cermak (1977) were defined as a drag force normalized by the dynamic force based on the averaged velocity over the building height, the current numerical results were also reorganized according to this definition. The building model tested in the wind tunnel was a cube of 25.4 cm side and the coming wind follows a power-law velocity profile with exponent 0.27. These conditions are quite similar to the cubic building model of 20 cm side and the velocity profile with a power-law exponent of 0.25 used in the current

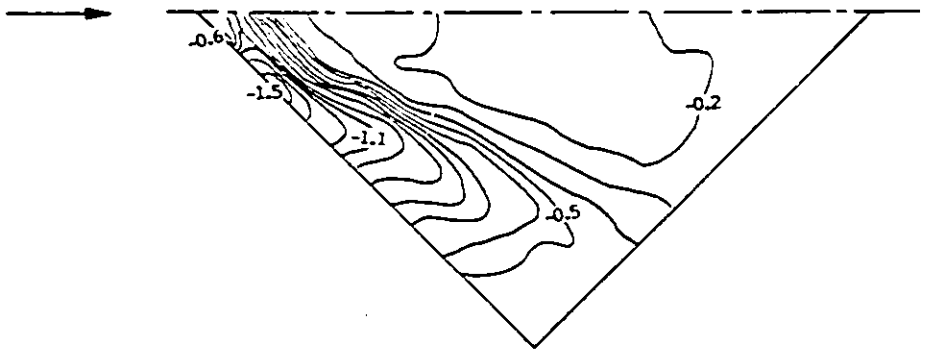

a) Experiment (Stathopoulos et al. 1981)

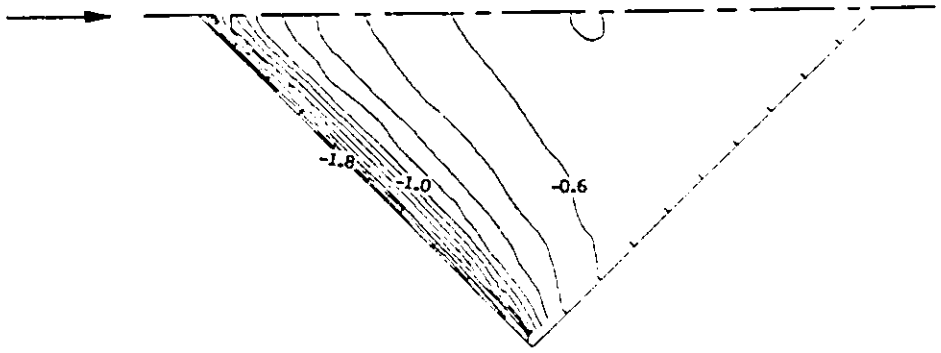

b) k-ε model computation

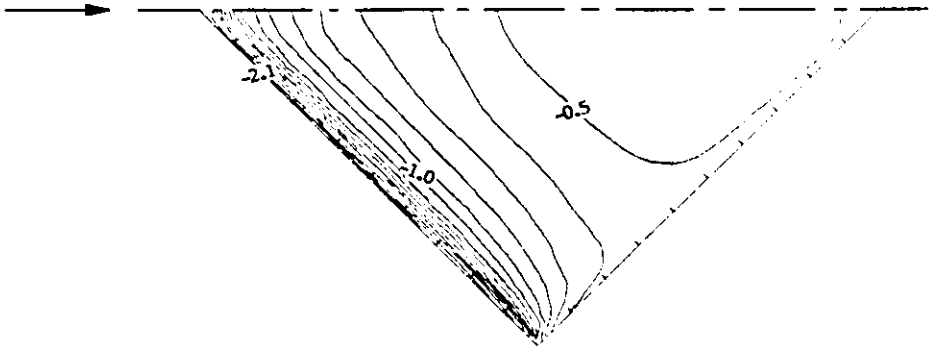

c) L-B two-layer computation

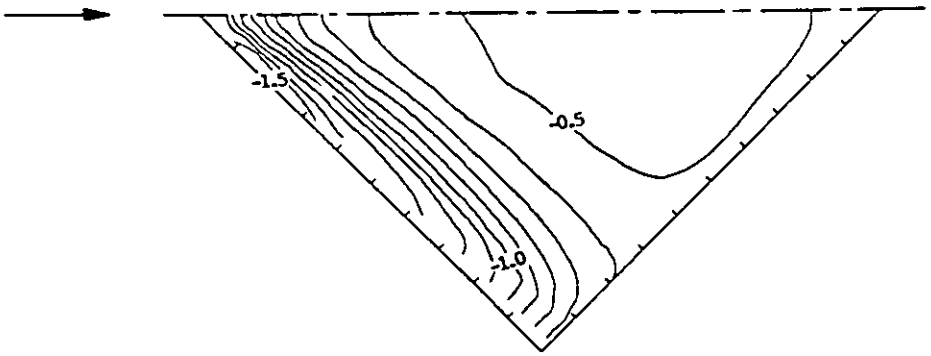

d) N-R two-layer computation

Figure 9.19 Contours of pressure coefficients on roof (45° azimuth).

Table 9.1 Drag coefficients for a cubic building.

	N-R	L-B	k-ε	experiment (Akins et al, 1977)
C_{Fx} (0°)	1.40	1.47	1.71	1.38
C_{Fx} (45°)	1.37	1.51	1.39	1.37 (40°) 1.38 (50°)

computation. The comparison has been made for both normal (0° azimuth) and oblique (45° azimuth) wind conditions. Since the experimental data do not include the results for 45° azimuth (Akins, Peterka and Cermak, 1977), the results of 40° and 50° have been presented in Table 9.1 and compared with the current numerical results. Regardless of the slight difference in the building geometry and exposure conditions, the agreement between the numerical results and the experimental data is very good with those from the N-R two-layer computation being the best.

In general, the N-R two-layer method appears significantly better than the other two approaches in reproducing the wind conditions around a cubic building, particularly for the regions on roof and side wall surfaces near the windward edge where the most critical flow properties exist.

9.6 Conclusions

The two-layer method in turbulence modelling has recently been applied in some studies in computational wind engineering (Zhou and Stathopoulos, 1995). In the current study, a k-ε model approach and two two-layer methods compiling the k-ε model for external fully turbulent flow region with either the Norris-Reynolds' one-equation model or the Lam-Bremhorst's modified k-ε model for the flow in the inner region have been adopted to numerically simulate the wind conditions on and around a cubic building model under both normal and oblique wind directions. Comparisons with experimental data for the normal wind case have shown that neither the L-B two-layer method nor the k-ε model approach can represent the flow separation above the roof and near the side walls. The N-R two-layer method, however, can effectively predict the separation. Compared with experimental data, the k-ε model method and the L-B two-layer approach overpredict the suction near the windward edge on roof and side walls and the Cp-curves computed show a different shape (concave upward) from the Cp-curve measured which is concave downward in the region near the windward edge. These discrepancies have been reduced by adopting the N-R two-layer method.

As has been indicated in Zhou and Stathopoulos (1995), the k-ε model cannot predict well the effects of adverse pressure gradient on boundary layer flows such as the turbulent flow on roof and side walls. The poor prediction in the region near the windward corner can be attributed to the fact that the length scale determined by the ε-

equation rises steeper near the wall than in the case of zero pressure gradient, whereas the experimental data suggest that the length scale is virtually independent of the pressure gradient over a wide range. This overprediction of length scale will cause over-predicted skin friction values near the walls. The Lam and Bremhorst's modified k-ε model was only derived based on zero pressure gradient boundary layer flow and therefore, does not avoid the overprediction of the skin friction values as found by Rodi and Scheuerer (1986). The one-equation model which uses an empirical length scale specification yields much better predictions for adverse pressure gradient boundary layer flows. The Norris and Reynolds' one-equation model was found to be better in representing the adverse pressure gradient effects on shear layers than the other two methods. The N-R two-layer method is also superior compared with the other two methods under oblique wind conditions.

Chapter 10

CONCLUSIONS, CONTRIBUTIONS AND RECOMMENDATIONS

10.1 Conclusions and Contributions of the Thesis

In the present study, a systematic examination of wind effects on buildings and wind flow conditions around buildings has been carried out numerically. Contrary to the usual numerical studies which were only performed on rectangular buildings, the current study evaluates the wind effects on buildings of various shapes such as L-shapes and Z-shapes. The steady state RANS equations and the k-ε model have been adopted for the numerical studies. These equations have been solved with the well known SIMPLE procedures. The numerical results for the L-shaped building in vertical cross-section agree well with the available experimental data especially for normal wind conditions. Numerical predictions for the plan-view L-shaped building and Z-shaped building have also been carried out.

The numerical evaluation of pressures on flat roofs of a rectangular building is most challenging because of the complex turbulent flow regime conditions resulting from the wind flow, particularly from oblique wind conditions. Most of the previous studies have attributed the poor prediction of wind pressure on flat roofs to the coarse grid arrangements. To investigate the effect of grid arrangement on the numerical results over flat roofs, a systematic evaluation of the k-ε model method in predicting the wind

pressure on flat roofs of a taller building and a lower building has been attempted by using grids of various densities. Wind tunnel tests for buildings of same geometries as those used in the computation have also been taken in the boundary layer wind tunnel of Centre for Building Studies, Concordia University. The numerical results show that the grid refinement cannot reproduce the flow separation on the roof and near the side walls. The numerical prediction of wind pressure on the roof however, can be improved by the grid refinement for low building and normal wind condition. This implies that the usual wall function and the k-ε model adopted cannot represent the complex flow of high vorticity in the separation regions.

To avoid applying the standard k-ε model in the near wall region, both the N-R two-layer method and the L-B two-layer approach have been adopted in the present study to evaluate the wind conditions around a cubic building. The results show that the N-R two-layer method, which is based on a one-equation model in the near wall region, can predict the flow separation on the roof and near the side walls which is not possible with the usual k-ε model method or the L-B two-layer approach. The latter is based on a modified k-ε model in the near wall area. Consequently, the prediction of the wind pressure on the flat roof and the side walls have also been significantly improved with the N-R two-layer approach. The N-R two-layer method is also superior compared with the other two methods under oblique wind conditions.

10.2 Suggestions for Future Work

This section suggests some of the possible future work under two groups. The further research sorted in the first group can be attempted by simply applying the current code RETWIST or just slightly extending the code. The second group of suggestions may need some major changes in the code by adopting additional equations or different numerical procedures.

Although the wind flow conditions around L-shaped buildings have been attempted with some success with the usual k-ε model method for low-rise buildings and normal wind direction, the numerical prediction of wind pressures on the roofs of the L-shaped buildings under oblique wind directions is still unsuccessful. By using the proposed N-R two-layer method, better prediction of wind conditions around both low and tall L-shaped buildings is expected under both normal and oblique wind directions.

The wind-building interactions become stronger when two buildings are set beside each other. Such interactions between two rectangular buildings caused by wind can be significant as explained by Khanduri, Bedard and Stathopoulos (1995), and can also be attempted numerically with the current code as well as experimentally with wind tunnel tests. Systematic studies on the effect of the distance between two buildings and their relative locations can be very efficient and inexpensive with the current computer code compared with such wind tunnel tests.

By adopting LES, the peak values of the wind-induced pressures on building surfaces can be predicted. This is because the governing equations of LES are for unsteady state so that the time history of wind conditions can be predicted numerically. Contrary to the RANS equations which are obtained by averaging the Navier-Stokes equations over a time scale, the basic equations used in LES are obtained by averaging the Navier-Stokes equations over space elements (grid volume element) as explained by Deardorff (1970). This corresponds to the taps for the wind tunnel tests which will always take a finite area. This finite area makes the wind pressures tested be the averaged values (over the tap area).

By adopting one additional equation describing the performance of pollutants or temperature transportation in the air, the diffusion of pollutants around buildings and a detailed evaluation of the heat loss of a building in cold weather can also be attempted numerically with the current code. Selvam and Huber (1995) evaluated the dispersion of pollutants from two point sources near a rectangular building by using a computed flow field. The results obtained agree with experimental data only qualitatively. Such studies can also be made with only some changes in the code RETWIST. The buildings, again, can be of L-shape, Z-shape or any other combination of two rectangular blocks.

In the k-ε turbulence model, the Reynolds stress has been assumed isotropic which is not true as confirmed by experiments (Paterson, 1986). To further improve the numerical prediction of wind conditions around buildings, a Reynolds stress model, such

as the Algebraic Stress Model (ASM) or the Differential Stress Model (DSM) avoiding the assumption of isotropy of the Reynolds stress can be adopted in the external flow region. The model in the near wall areas can still be the Norris-Reynolds one-equation model. Such a two-layer method will probably improve the quality of the prediction of wind flow conditions around buildings as also concluded by Frank and Rodi (1991) who attempted both two-layer methods, based on either the k-ε model or the algebraic stress model to predict the separation flow past a 2D rectangular prism.

With the availability of super-computers, large eddy simulation or even direct simulation can possibly be adopted to evaluate the wind conditions around buildings. The detailed transient performance of turbulent flow properties around buildings and its effect on buildings can thus be obtained.

REFERENCES

Adams, E.W. and Johnston, J.P. (1988), "Flow structure in the near-wall zone of a turbulent separated flow", *AIAA Journal*, 26, 932-939.

Akins, R.E., Peterka, J.A. and Cermak, J.E. (1977), "Mean force and moment coefficients for buildings in turbulent boundary layers", *Journal of Industrial Aerodynamics*, 2, 195-209.

Antoniou, J. and Bergeles, G. (1988), "Development of the reattached flow behind surface-mounted two-dimensional prisms", *Journal of Fluids Engineering*, 110, 127-133.

Baetke, F., Werner, H. and Wengle, H. (1990), "Numerical simulation of turbulent flow over surface-mounted obstacles with sharp edges and corners", *Journal of Wind Engineering and Industrial Aerodynamics*, 35, 129-147.

Baskaran, A. (1990), "Computer simulation of 3D turbulent wind effects on buildings", *PhD Thesis*, Concordia University, Montreal, Quebec, Canada.

Baskaran, A. and Stathopoulos, T. (1989), "Computational evaluation of wind effects on buildings", *Building and Environment*, 24(4), 325-333.

Bienkiewicz, B. and Kutz, R.F. (1990), "Applying the discrete vortex method to flow about bluff bodies", *Journal of Wind Engineering and Industrial Aerodynamics*, 36, 1011-1020.

Bradshaw, P. [ed.] (1976), *Topics in Applied Physics - Turbulence*, Springer-Verlag.

Castro, I.P. and Robins, A.G. (1977), "The flow around a surface-mounted cube in uniform and turbulent streams", *Journal of Fluid Mechanics*, 19, part 2, 307-335.

Cermak, J.E. (1975), "Application of fluid mechanics to wind engineering - a freeman scholar lecture", *Trans. ASME Journal of Fluids Engineering*, 97, 9-38.

Cermak, J.E. (1976), "Aerodynamics of buildings", *Annual Review of Fluid Mechanics*, 75-106.

Cermak, J.E. and Arya, S.P. (1970), "Problems of atmospheric shear flows and their laboratory simulation", *Boundary-Layer Meteorology*, 1, 40-60.

Chen, H.C. and Patel, V.C. (1987), "Practical near-wall turbulence models for complex flows including separation", *AIAA-87-1300*.

Chen, H.C. and Patel, V.C. (1987), "The wake of an axisymmetric body with or without

tail separation", *Sixth Symposium on Turbulent Shear Flows*, Sept. 7-9, Toulouse, France.

Chien, K.Y. (1982), "Prediction of channel and boundary-layer flows with a low-Reynolds-number turbulent model", *AIAA Journal*, 20(1), 33-38.

Choi, E.C.C. (1992), "Simulation of wind-driven-rain around a building", *Journal of Wind Engineering*, No.52, August, 60-65.

Chou, D.Y. (1945), "On velocity correlations and the solution of the equations of turbulent fluctuation", *Quart. J. Appl. Math.*, Vol.3 (1), 38-54.

Clark, J.A. (1968), "A study of incompressible turbulent boundary layers in channel flow", *Journal of Basic Engineering*, Vol.90, 455-468.

Cook, N.J. (1985), "The designer's guide to wind loading of building structures; Part 1: Background, damage survey, wind data and structural classification", *Building Research Establishment Report*, Butterworths.

Davidov, B.I. (1961), "On the statistical dynamics of an incompressible turbulent fluid", *Dokl. AN SSSR*, Vol 136, p47.

Deardorff, J.W. (1970), "A numerical study of three-dimensional turbulent channel flow

at large Reynolds numbers", *Journal of Fluid Mechanics*, 41, 453-480.

Deng, G.B., Piquet, J., Queutey, P. and Visonneau, M. (1991), "Three-dimensional full Navier-Stokes solvers for incompressible flows past arbitrary geometries", *International Journal for Numerical Methods in Engineering*, 31, 1427-1451.

Deng, G.B., Piquet, J. and Queutey, P. (1990), "Navier-Stokes computations of vortical flows", *AIAA 21st Fluid Dynamics, Plasma Dynamics and Lasers Conference*, June 18-20, 1990, Seattle, USA.

Djilali, N., Gartshore, I.S. and Salcudean, M. (1987), "An experimental and numerical study of the flow around a blunt rectangular section", *6th Symposium on Turbulent Shear Flows*, Sept. 7-9, Toulouse, France.

Djilali, N., Gartshore, I.S. and Salcudean, M. (1991), "Turbulent flow around a bluff rectangular plate. part II: numerical predictions", *Transactions of the ASME, Journal of Fluids Engineering*, 113, 60-67.

Doormaal, J.P.V. and Raithby, G.D. (1984), "Enhancements of the SIMPLE method for predicting incompressible fluid flows", *Numerical Heat Transfer*, 7, 147-163.

Durao, D.F.G., Heitor, M.V. and Pereira, J.C.F. (1987), "The turbulent flow in the

near-wake of a squared obstacle", *Forum on Turbulent Flows*, Cincinnati, Ohio, June 14-17.

Dyke, M.V. (1970), "Entry flow in a channel", *Journal of Fluid Mechanics*, 44(4), 813-823.

Fan, J. Wu, X. and Jin, J. (1989), "Numerical simulation of turbulent flow around buildings", *Recent Advances in Wind Engineering*, [ed] Sun, T.F., International Academic Publishers.

Ferziger, J.H., Bardina, J. and Allen, G. (1981), "Overview of taxonomy: morphology of the flows and computational methods", *Proc. HTTW-AFOSR Conf.*, Department of Mechanical Engineering, Stanford University, Stanford, CA, 21, 634-649.

Ferziger, J.H. (1983), "High-level simulations of turbulent flows, in J.-A. Essers", *Computational Methods for Turbulent, Transonic, and Viscous Flows*, Hemisphere, New York, 93-182.

Ferziger, J.H. (1990), "Approaches to turbulent flow computation: application to flow over obstacles", *Journal of Wind Engineering and Industrial Aerodynamics*, 35, 1-19.

Ferziger, J.H. (1993), "Simulation of complex turbulent flows: Recent advances and

prospects in wind engineering", *Journal of Wind Engineering and Industrial Aerodynamics*, Vol. 46 and 47, 195-212.

Frank, W. (1987), "Experimental and numerical study of propagation phenomena in turbulent flows around buildings", *Proceedings, 2nd International Symposium on Transport Phenomena in Turbulent Flows*, Tokyo, 425-433.

Frank, W. and Mauch, H. (1992), "Large eddy simulation of the flow around building models" *J. of Wind Engineering*, 52, 303-308.

Franke, R. and Rodi, W. (1991). "Calculation of vortex shedding past a square cylinder with various turbulence models", *Proc. 8th Symp. on Turbulent Shear Flows*, Munich, 1991.

Gadilhe, A.Y. and Fleury, B.A. (1989), "Wind pressure coefficients: a comparison between PHOENICS and wind tunnel results", *3rd International PHOENICS User Conference*, Dubrovnik, Yugoslavia, August, 183-197.

Gadilhe, A., Janvier, L. and Barnaud, G. (1992), "Numerical and experimental modelling of the tridimensional turbulent wind flow through an urban square", *J. of Wind Engineering*, 52, 231-236.

Grötzbach, G. (1978), "Direct numerical simulation of secondary currents in turbulent channel flows", *Structure and Mechanisms of Turbulence II, Lecture Notes in Physics*, [ed] Fiedler, H., Springer, 76, 308-319.

Grötzbach, G. and Schumann, U. (1979), "Direct numerical simulation of turbulent velocity, pressure and temperature fields in channel flows", *Turbulent Shear Flows 1*. Springer, 370-385.

Häggkvist, K., Svensson, U. and Taesler, R. (1989), "Numerical simulations of pressure fields around buildings", *Building and Environment*, 24(1), 65-72.

Han, T. (1989), "Computational analysis of three-dimensional turbulent flow around a bluff body in ground proximity", *AIAA Journal*, 27(9), 1213-1219.

Hanson, T., Summer, D.M. and Wilson, C.B. (1986), "A three-dimensional simulation of wind flow around buildings", *International Journal for Numerical Methods in Fluids*, 6, 113-127.

Harlow, F.H. and Nakayama, P.I. (1967), "Turbulent transport equations, the physics of fluids", Vol 10, p. 2323.

He, J. and Song, C.C.S. (1992), "Computation of turbulent shear flow over a surface-

mounted obstacle with large eddy simulation", *J. of Engineering Mechanics, ASCE*, 118, 2282-2297.

He, J. and Song, C.C.S. (1990), "Computation of wind flow around a building", *Mechanics Computing in 1990's and Beyond*, [ed] Adeli, H. and Sierakowski, R.L., 1, 468-473.

Hibi, K., Ueda, H., Wakahara, T and Shimada, K. (1992), "Use of large eddy simulation to measure fluctuating pressure fields around buildings with wall openings", *J. of Wind Engineering*, 52, 291-296.

Himeno, R. and Fujitani, K. (1993), "Numerical analysis and visualization of flow in automobile aerodynamics development", *Journal of Wind Engineering and Industrial Aerodynamics*, Vol. 46 and 47, 785-790.

Hosker, R.P. (1985), "Flow around isolated structures and building clusters: a review", *ASHRAE Transaction*, 91(26), 1671-1692.

Hoxey, R.P., Robertson, A.P. and Richards, P.J. (1989), "Full-scale, model-scale and computational comparisons of wind loads on the Silsoe Structures Building", *Recent Advances in Wind Engineering*, [ed] Sun, T. F., International Academic Publishers.

Hunt, A. (1982). "Wind-tunnel measurements of surface pressures on cubic building models at several scales", *Journal of Wind Engineering and Industrial Aerodynamics*, 10, 137-163.

Hussain, A.K.M.F. and Reynolds, W.C. (1975), "Measurements in fully developed turbulent channel flow", *Transactions of the ASME, Journal of Fluids Engineering*, December, 568-580.

Iacovides, H. and Launder, B.E. (1987), "The numerical simulation of flow and heat transfer in tubes in orthogonal-mode rotation", Proceedings 6th Symposium on Turbulent Shear Flows, Toulouse, France.

Inamuro, T. (1992), "Numerical simulations of aerodynamic instability of bluff body by the discrete vortex method", *Workshop on Prospects for Numerical Analysis of Interaction between Fluid Flow and Structural Vibration, CWE'92*, Japan.

Inamuro, T. Adachi, T. and Sakata, H. (1992), "Simulation of aerodynamic instability of bluff body", *Journal of Wind Engineering*, 52, 541-546.

Jones, W.P. and Launder, B.E. (1972), "Prediction of laminarization with a two-equation model of turbulence", International Journal of Heat and Mass Transfer, Vol. 15, 301-314.

Kanayama, H. Toshigami, K., Tashiro, Y., Tabata, M. and Fujima, S. (1993), "Finite element analysis of air flow around an automatic guided vehicle", *Journal of Wind Engineering and Industrial Aerodynamics*, 46 & 47, 801-810.

Kawai, H. (1990), "A discrete vortex analysis of flow around a vibrating cylinder with a splitter plate", *Journal of Wind Engineering and Industrial Aerodynamics*, 35, 259-273.

Kawai, H. (1992), " Vortex induced vibration of circular cylinder", *Journal of Wind Engineering*, 52, 374-379.

Kawamoto, S., Kawabata, S. and Tawahashi, T. (1992), "Numerical analysis of wind around building using high-speed GSMAC-FEM", *J. of Wind Engineering*, 52, 255-260.

Khanduri, A.C., Bedard, C. and Stathopoulos, T. (1995), "Neural network modelling of wind-induced interference effects", *9th International Conference on Wind Engineering*, New Delhi, India, 9-13 January.

Kim, J. and Moin, P. (1979), "Large eddy simulation of turbulent channel flow - Illiac IV calculation", *AGARD Symposium on Turbulent Boundary Layers.*

Klebanoff, P.S. (1954), "Characteristic of turbulence in a boundary layer with zero pressure gradient", *NACA Report*, p.237.

Kline, S.J., Ferziger, J.H. and Johnson, J.P. (1978), "Calculation of turbulent shear flows: status and ten-year outlook", *Journal of Fluids Engineering*, 100, 3-5.

Kolmogorov, A.N. (1968), "Equations of turbulent motion of an incompressible fluid", Imperial College, *Mech. Eng. Dept. Rept.* ON/6.

Kot, S.C. (1990), "Application of body-fitted coordinate and the k-ε turbulence model for wind field computation in a complex urban terrain", *Journal of Wind Engineering and Industrial Aerodynamics*, 35, 225-235.

Kot, S.C. and Yeung, P.K. (1988), "Computation of turbulent flow normal to two rows of buildings", *4th International Conference on Tall Buildings*, Hong Kong.

Latimer, B.R. and Pollard, A. (1985), "Comparison of pressure-velocity coupling solution algorithms", *Numerical Heat Transfer*, 8, 635-652.

Laufer, J. (1951), "Investigation of turbulent flow in a two-dimensional channel", *NACA Report*, 1053.

Laufer, J. (1954), "The structure of turbulence in fully developed pipe flow", *NACA Report*, 1174, 112-117.

Leonard, A. (1974), "Energy cascade in large-eddy simulation of turbulent fluid flows", *Advances in Geophysics*, 18A, 237-248.

Leschziner, M.A. (1990), "Modelling engineering flows with Reynolds stress turbulence closure", *Journal of Wind Engineering and Industrial Aerodynamics*, 35, 21-47.

Leschziner, M.A. and Rodi, W. (1981), "Calculation of annular and twin parallel jets using various discretization schemes and turbulence-model variations", *Journal of Fluids Engineering*, 103, 352-360.

Lövgren, R. (1986), "Numerical 2D airflow simulation over a backward-facing step and a block", *Numerical Simulation of Fluid Fl;ow and Heat/Mass Transfer Processes*, Springer-Verlag.

Majumdar, S. and Rodi, W. (1989), "Three-dimensional computation of flow past cylindrical structures and model cooling towers", *Building and Environment*, 24(1), 3-22.

Melbourne, W.H. and Joubert, P.N. (1971), "Problems of wind flow at the base of tall buildings", *Proceedings 3rd International Conference on Wind Effects on Buildings and Structures*, Tokyo, Japan.

Mikkelsen, A.C. and Livesey, F.M. (1993), "Evaluation of the use of the numerical k-ε

model KAMELEON II for predicting the wind velocity distribution around buildings", *7th U.S. National Conference on Wind Engineering*, June 27-30, University of California, Los Angeles, USA.

Mochida, A., Ishida, Y. and Murakami, S. (1993), "Numerical study on flowfield around structures with oblique wind angle based on composite grid system", *7th U.S. National Conference on Wind Engineering*, June 27-30, University of California, Los Angeles, USA.

Moin, P. and Kim, J. (1982), "Numerical investigation of turbulent channel flow", *Journal of Fluid Mechanics*, 118, 341-377.

Mouzakis, F.N. and Bergeles, G.C. (1991), "Numerical prediction of turbulent flow over a two-dimensional ridge", *International Journal for Numerical Methods in Fluids*, 12 287-296.

Murakami, S. (1990), "Computational wind engineering", *Journal of Wind Engineering and Industrial Aerodynamics*, 36, 517-538.

Murakami, S. (1992), "Comparison of various turbulence models applied to a bluff body", *Journal of Wind Engineering*, 52, 164-179.

Murakami, S. and Mochida, A. (1989), "Three-dimensional numerical simulation of turbulent flow around buildings using the k-ε turbulence model", *Building and Environment*, 24(1), 51-64.

Murakami, S., Hibi, K. and Mochida, A. (1990), "Three-dimensional analysis of turbulent flowfield around street blocks by means of large eddy simulation (part-1)", *Journal of Archit. Plann. Environ. Engrg., AIJ*, No.412, 1-10.

Murakami, S., Mochida, A. and Hayashi, Y. (1990), "Examining the k-ε model by means of a wind tunnel test and large-eddy simulation of the turbulence structure around a cube", *Journal of Wind Engineering and Industrial Aerodynamics*, 35, 87-100.

Nicholls, M., Peilke, R. and Meroney, R. (1992), "Large eddy simulation of microburst winds flowing around a building", *J. of Wind Engineering*, 52, 297-302.

Norris, L.H. and Reynolds, W.C. (1975), "Turbulent channel flow with a moving wavy boundary", *Report No. FM-10, Stanford University*, Department of Mechanical Engineering, Stanford, CA, USA.

Onyemelukwe, O.U., Torkamani, M.A.M. and Bosch, H.R. (1992), "Computer simulation of airflow around bridges and other bluff bodies", *10th ASCE Structures Congress*, San Antonio, April 13-15.

Onyemelukwe, O.U. and Bosch, H.R. (1993), "Numerical simulation of wind flow patterns and wind-induced forces on bridge deck section models", *7th U.S. National Conference on Wind Engineering*, June 27-30, University of California, Los Angeles, USA.

Parameswaran, S., Kiris, I., Sun, R. and Gleason, M. (1993), "Flow structure around a 3-D bluff body in ground proximity: A computational study", *Journal of Wind Engineering and Industrial Aerodynamics*, Vol. 46 and 47, 791-800.

Patankar, S.V. (1980), *Numerical Heat Transfer and Fluid Flow*, McGraw-Hill, New York, N.Y.

Paterson, D.A. (1986), "Computation of wind flows over three-dimensional buildings", *PhD Thesis*, University of Queensland, Australia.

Paterson, D.A. and Apelt, C.J. (1986), "Computation of wind flows over three-dimensional buildings", *Journal of Wind Engineering and Industrial Aerodynamics*, 24, 193-213.

Paterson, D.A. and Apelt, C.J. (1990), "Simulation of flow past a cube in a turbulent boundary layer", *Journal of Wind Engineering and Industrial Aerodynamics*, 35, 149-176.

Paterson, D.A. and Holmes, J.D. (1992), "Computation of wind pressures on low-rise structures", *Journal of Wind Engineering and Industrial Aerodynamics*, Vol. 41-44, 1629-1640.

Peric, M., Kessler, R and Scheuerer, G. (1988), "Comparison of finite volume numerical methods with staggered and collocated grids", *Computers and Fluids*, 16(4), 389-403.

Prandtle, L. (1925), "Uber die ausgebildete turbulenz", *ZAMM*, Vol. 1, p136.

Prandtle, L. (1945), "Uber ein neues formelsystem fur die ausgebildete turbulenz", *Nachr. Akad. Wiss.*, Gottingen, Math.-Phys. Klasse, P6.

Qasim, A., Maxwell, T.T. and Parameswaran, S. (1991), "Numerical predictions of the flow over a 2-D building", *Ninth ASCE Structures Congress*, Indianapolis, Indiana, April 29-May 1.

Reynolds, W. (1976). "Computation of turbulent flows", *Ann. Rev. Fluid Mechanics*, 183-208.

Reynolds, W.C. (1978), "Strategy and recent developments in turbulence", *Topics in Applied Physics*, Vol.12, Springer-Verlag, New York.

Richards, P.J. and Hoxey, R.P. (1991), "Computational and wind tunnel modelling of mean wind loads on the Silsoe Structures Building", *Eighth International Conference on Wind Engineering, BLWT*, The University of Western Ontario, London Canada, July 8-12.

Richards, P.J. and Hoxey, R.P. (1992), "Computational and wind tunnel modelling of mean wind loads on the Silsoe Structure Building", *Journal of Wind Engineering and Industrial Aerodynamics*, Vol. 41-44, 1641-1652.

Richards, P.J., Shepard, P.J. and Maharaj, P. (1989), "Pressure distributions on shade houses", *Recent Advances in Wind Engineering*, [ed] Sun, T.F., International Academic Publishers.

Robertson, A.P. and Glass, A.G. (1988), "The Silsoe Structures Building - its instrumentation and research facilities", *Div. Note DN 1482*, AFRC Institute of Engineering Research, Silsoe, Octuber.

Rodi, W. (1976), "A new algebraic relation for calculating the Reynolds stresses", *Z. Angew., Math Mech. (ZAMM)*, 56, T219-T224.

Rodi, W. (1980), *Turbulence Models and Their Application in Hydraulics*, International Association for Hydraulics Research (IAHR), Delft.

Rodi, W. (1991), "Experience with two-layer models combining the k-ε model with a one-equation model near the wall", *AIAA paper*, AIAA-91-0216.

Rodi, W. and Scheuerer, G. (1986), "Scrutinizing the k-ε turbulence model under adverse pressure gradient conditions", *Transactions of the ASME*, 108, 174-179.

Rogallo, R.S. and Moin, P. (1984), "Numerical simulation of turbulent flows", *Ann. Rev. Fluid Mech.*, 16, 99-137.

Rotta, J.C. (1968), "Statistische Theories nichthomogener turbulenz", Imperial College, *Dept. of Mech. Eng. Rept.*, Vol. 39.

Ruderich, R. and Fernholz, H.H. (1986), "An experimental investigation of a turbulent shear flow with separation, reverse flow, and reattachment", *Journal of Fluid Mechanics*, 163, 283-322.

Saffman, P.G. (1970), "A model for inhomogeneous turbulent flow", *Proc. Roy. Soc. Ser. A*, Vol. 317, P.417.

Sakamoto, S., Murakami, S., Kato, S. and Mochida, A. (1992), "Unsteady pressure field around oscillating prism predicted by LES", *Journal of Wind Engineering*, 52, 368-373.

Sarpkaya, T. and Ihrig, C.J. (1986), "Impulsively started steady flow about rectangular prisms: experiments and discrete vortex analysis", *Journal of Fluids Engineering*, 108, 47-54.

Sarpkaya, T. and Kline, S.J. (1982), "Impulsively-started flow about four types of bluff bodies", *Journal of Fluids Engineering*, 108, 47-54.

Sato, T., Uematsu, T., Nakata, T. and Kaneda, Y. (1992), "Three-dimensional numerical simulation of snowdrift", *Journal of Wind Engineering*, No.52, August, 66-71.

Schlichting, H. (1934), "Laminare kanaleinlaufströmung", *Z. Angew. Math. Mech. (ZAMM)*, 14, 368-373.

Schlichting, H. (1969), "Boundary layer theory", McGraw Hill, New York.

Schumann, U. (1973), "Results of a numerical simulation of turbulent channel flows", *International Meeting on Reactor Heat Transfer*, by Dalle-Donne, M., 230-251.

Schumann, U. (1975), "Subgrid scale model for finite difference simulations of turbulent flows in plane channels and annuli", *Journal of Computational Physics*, 18, 376-404.

Scruton, C. (1960), "The use of wind tunnels in industrial aerodynamic research", *NATO*

AGARD Report No. 309.

Scruton, C. and Rogers, E.W.E. (1971), "Wind effects on buildings and other structures", *Philos. Trans. R. Soc. London Ser.*, A269, 353-383.

Selvam, R.P. (1992a), "Computation of pressures on Texas Tech Building", *Journal of Wind Engineering and Industrial Aerodynamics*, Vol. 41-44, 1619-1627.

Selvam, R.P. (1992b), "Roof corner pressures on the Texas Tech Building: numerical and field results", *10th ASCE Structures Congress*, San Antonio, Texas, April 13-15.

Selvam, R.P. and Huber, A.H.(1995), "Computer modelling of pollutant dispersion around buildings: current status", *Proceedings, 9th International Conference on Wind Engineering*, New Delhi, India, 9-13 January, Vol.2, 594-605.

Selvam, R.P. and Paterson, D.A. (1991), "Computation of pressures on and velocities near the Texas Tech Building: using staggered and non-staggered grids", *Ninth ASCE Structures Congress*, Indianapolis, Indiana, USA, April 29 - May 1.

Shirato, H., Matsumoto, M. and Shiraishi, N. (1992), "Unsteady aerodynamics force characteristics on 2-D oscillating bluff body", *Journal of Wind Engineering*, 52, 547-552.

Simiu, E. and Scanlan, R.H. (1978), *Wind effects on buildings*, John Wiley and Sons.

Spalding, D.B. (1971), "The kW model of turbulence", *Imperial College*, Dept. Mech. Eng. Rept.

Spalding, D.B. (1981), "A general purpose computer program for multi-dimensional one- and two-phase flow", *Mathematics and Computers in Simulation*, XXIII, 267-276.

Spalding, D.B. (1989), "The PHOENICS computer code", *Computer Simulation for Fluid Flow, Heat and Mass Trasfer, and Combustion in Reciprocating Engines*, [ed] Markatos, N.C., Hemisphere Publishing Corporation.

Stanisic, M.M. (1988), *The Mathematical Theory of Turbulence*, Springer-Verlag.

Stathopoulos, T. and Baskaran, A. (1990), "Boundary treatment for the computation of three-dimensional wind flow conditions around a building", *Journal of Wind Engineering and Industrial Aerodynamics*, 35, 177-200.

Stathopoulos, T. and Dumitrescu-Brulotte, M. (1989), "Design recommendations for wind loading on buildings of intermediate height", *Canadian Journal of Civil Engineering*, 16, 910-916.

Stathopoulos, T. and Luchian, H.D. (1990), "Wind pressures on buildings with stepped roofs", *Canadian Journal of Civil Engineering*, 17, 569-577.

Stathopoulos, T, Surry, D and Davenport, A.G. (1981), "Effective wind loads on flat roofs", *ASCE Journal of the Structural Division*, 107(ST2), 281-300.

Stathopoulos, T. and Zhou, Y.S. (1993a), "Computation of wind pressures on L-shaped buildings", *Journal of Engineering Mechanics, ASCE*, 119(8), 1526-1541.

Stathopoulos, T. and Zhou, Y.S. (1993b), "Numerical simulation of wind-induced pressures on buildings of various geometries", *Journal of Wind Engineering and Industrial Aerodynamics*, 46 & 47, 419-430.

Stathopoulos, T. and Zhou, Y.S. (1992a), "Numerical evaluation of wind pressures on flat roofs", *Tenth ASCE Structures Congress*, San Antonio, Texas, USA, April 13-15.

Stathopoulos, T. and Zhou, Y.S. (1992b), "Numerical simulation of wind-induced pressures on buildings of various geometries", *Journal of Wind Engineering*, No.52, August, 477-488.

Stathopoulos, T. and Zhou, Y.S. (1992c), "Computation of wind pressures on L-shaped buildings", *ASCE Engineering Mechanics Conference*, Texas A & M University, College

Station, Texas, USA, May 24-27.

Summer, D.M., Hanson, T. and Wilson, C.B. (1986), "Validation of a computer simulation of wind flow over a building model", *Building and Environment*, 21(2), 97-111.

Sung, H.J., Kim, Y.N. and Hyun, J.M. (1992), "Discrete-vortex simulation of pulsating flow behind a normal plate", *Journal of Wind Engineering*, 52, 380-385.

Surry, D. (1989), "Pressure measurement on the Texas Tech Building-II: wind tunnel measurements and comparison with full scale", *Proceedings Eighth Colloquium on Industrial Aerodynamics*, Aachen, West Germany, September 4-7.

Svensson, U. and Häggkvist, K. (1990), "A two-equation turbulence model for canopy flows", *Journal of Wind Engineering and Industrial Aerodynamics*, 35, 201-211.

Tamura, T. (1990), "Numerical study of aerodynamic behaviour of a square cylinder", *Journal of Wind Engineering and Industrial Aerodynamics*, 33, 161-170.

Tamura, T., Krause, E., Shirayama, S., Ishii, K. and Kuwahara, K. (1988), "Three-dimensional computation of unsteady flows around a square cylinder", *11th International Conference on Numerical Methods in Fluid Dynamics*, Williamsburg.

Tennekes, H. and Lumley, J.L. (1972), *A First Course in Turbulence*, MIT-Press, Cambridge, Mass., USA.

Turkiyyah, G., Reed, D. and Yang, J.Y. (1994), "Random vortex models in wind engineering", *Proceedings of the First Congress on Computing in Civil Engineering*, Vol.1, 99-106.

Uemura, K. and Saito, T. (1992), "Automatic mesh generation for FEM simulation of wind flow around tall buildings", *J. of Wind Engineering*, 52, 327-332.

Vasilic-Melling, D. (1977), "Three-dimensional turbulent flow past rectangular bluff bodies", *Ph.D. Thesis*, University of London.

Viecelli, J.A. (1971), "A computing method for incompressible flows bounded by moving walls", *Journal of Computational Physics*, 8, 119-143.

Walther, J.H. (1993), "Numerical simulation of the unsteady flow around suspension bridge models using the discrete vortex method", *7th U.S. National Conference on Wind Engineering*, June 27-30, University of California, Los Angeles, USA.

Wang, Y.L. and Longwell, P.A. (1964), "Laminar flow in the inlet section of parallel plates", *A.I.Ch.E. Journal*, 10(3), 323-329.

Wieghardt, K. (1944), "Zum reibungswiderstand rauher platten", *Kaiser-Wilhelm-Institut für Strömunsforschung Göttingen*, UM 6612, 116-119.

Wilcox, D.C. (1993), *Turbulence Model for CFD*, DCW Industries Inc.

Wiren, B.G. (1985), "Effects of surrounding buildings on wind pressure distributions and ventilation losses for single-family houses, part 1: 1½-storey detached houses", *Meddelande M85*:19, Statens Institut för Byggnadsforskning.

Wolfshtein, M. (1969), "The velocity and temperature distribution in one-dimensional flow with turbulence augmentation and pressure gradient", *Int. J. Heat & Mass Transf.*, 12, 301-318.

Yeung, P.K. and Kot, S.C. (1985), "Computation of turbulent flows past arbitrary two-dimensional surface-mounted obstructions", *Journal of Wind Engineering and Industrial Aerodynamics*, 18, 177-190.

Yuan, M, Song, C.C.S. and He, J. (1991), "Numerical analysis of turbulent flow in a two-dimensional nonsymmetric plane-wall diffuser", *Transaction of the ASME*, 113, June, 210-215.

Zhou, Y.S. and Stathopoulos, T. (1993), "Application of CFD techniques in wind

engineering", *Conference of CFD Society of Canada*, Montreal, Quebec, June 14-15.

Zhou, Y.S. and Stathopoulos, T. (1994), "Improved computer simulation of 3D wind flow around a building", *ASCE, First Congress on Computing in Civil Engineering*, Washington, D.C., 20-22 June, 1994.

Zhou, Y.S. and Stathopoulos, T. (1995), "A new technique for the numerical simulation of wind flow around buildings", *Proceedings, Ninth International Conference on Wind Engineering*, New Delhi, India, 9-13 January, Vol. 2, 582-593.